Aus dem Institut für Radiologie
der Medizinischen Fakultät Charité – Universitätsmedizin Berlin

Dissertation

Choline Metabolism and Choline Kinase Gene Expression in Human Breast Cancer

zur Erlangung des akademischen Grades
Doctor medicinae (Dr. med.)

vorgelegt der Medizinischen Fakultät
Charité – Universitätsmedizin Berlin

von

Sebastian Herberger
aus München

Datum der Promotion: 14.02.2014

Inhaltsverzeichnis

1 Zusammenfassung

Cholinmetabolismus und Genexpression der Cholinkinasen in Humanem Brustkrebs

Sebastian Herberger

Brustkrebs ist die am häufigsten diagnostizierte Tumorerkrankung und die häufigste tumorbedingte Todesursache in der weiblichen Bevölkerung der westlichen Welt. Die diagnostische Aufarbeitung verdächtiger Läsionen der Brust erfordert die invasive Entnahme von Gewebebiopsien. Der Großteil der Biopsien liefert negative Ergebnisse und verursacht gleichzeitig signifikante Nebenwirkungen und großes Unbehagen. Neue Methoden sind nötig um die Qualität von Diagnostik und Therapie für Brustkrebspatienten zu verbessern.

Die in-vivo ^{1}H-MR Spektroskopie (^{1}H-MRS) ermöglicht einen direkten Einblick in zelluläre Aktivität durch die Messung von Gewebemetabolitenkonzentrationen. In Brustkrebsgewebe finden sich regelmäßig erhöhte Konzentrationen der Metaboliten Cholin (Cho) und Phosphocholin (PCho). Studien an Zelllinien deuten an, dass diese Veränderungen durch veränderte Genexpression der Cholinkinasen Alpha (CHKA) und Beta (CHKB) bedingt sind. Diese Studie hatte das Ziel, die zugrunde liegenden Mechanismen, welche zu Veränderungen der Gewebemetabolitenkonzentrationen in Tumoren führen, im Detail zu erforschen.

In 18 humanen Brusttumorgewebeproben und 11 gepaarten normalen gesunden Brustproben wurden die Konzentrationen von Cho und PCho mittels Ex-Vivo High-Resolution ^{1}H-Magic-Angle-Spinning-MRS quantifiziert. Benigne und karzinomatöse Epithelzellen wurden mittels Laser-Capture Mikrodissektion exzidiert und die Expressionsniveaus der CHKA und CHKB mittels real-time quantitativer PCR gemessen. Die Metabolitenkonzentrationen wurden mit den Genexpressionsniveaus in den verschiedenen Gruppen verglichen.

Tumoren zeigten signifikant höhere Konzentrationen von PCho in benignem Gewebe, wobei die höchsten Konzentrationen in niedrig gradigen, invasiv-duktalen Tumoren zu finden waren. Konzentrationen von Cho und PCho korrelierten stark. CHKA war in niedrig gradigen Tumorproben überexprimiert und korrelierte mit PCho. Die Ergebnisse zeigen dass Gewebemetabolitenkonzentrationen zwischen benignem und malignem Tumorgewebe der Brust unterscheiden können und dass Änderungen im Metabolismus mit denen der Genexpression einher gehen. Hieraus ergeben sich mögliche Ansätze für zukünftige Forschung und Entwicklung. Zukünftig werden weitreichende Untersuchungen der Tumorbiologie im Brustkrebs erforderlich sein, bis eine mögliche klinische Anwendung realisiert werden kann.

1.1 Abstract

Choline Metabolism and Choline Kinase Gene Expression in Human Breast Cancer

Sebastian Herberger

Breast cancer (BrCa) is the most frequently diagnosed malignancy and the most frequent cause of cancer death in the western female population. The diagnostic workup of suspicious breast lesions requires invasive tissue biopsies, most of which produce negative results, along with discomfort and side-effects for patients. Novel methods are needed to raise the quality of diagnostics and clinical care for BrCa patients.

In-vivo ^{1}H-MR Spectroscopy (^{1}H-MRS) allows a direct view into cellular activity by measuring tissue metabolite concentrations. ^{1}H-MRS commonly detects increased concentrations of the metabolites Choline (Cho) and Phosphocholine (PCho) in BrCa tissue. Cell-line studies suggest that these changes are caused by altered gene expression of Choline Kinases Alpha (CHKA) and Beta (CHKB). This study was undertaken to investigate in detail the underlying basic mechanisms leading to changes in tissue metabolite concentrations in BrCa.

Ex-vivo High-Resolution ^{1}H-Magic-Angle-Spinning-MRS was used to quantify Cho and PCho metabolites in 18 invasive human BrCa samples and in 11 matching normal benign breast tissue samples at high resolution. Laser-Capture Microdissection was used to microscopically isolate benign and cancerous epithelial cells, from which CHKA and CHKB expression levels were quantified by real-time quantitative PCR. Lastly, changes in metabolism were compared to changes in gene expression.

Malignant BrCa tissue contained significantly higher PCho metabolite concentrations than benign tissue. The highest concentrations of PCho were found in low-grade, invasive ductal type BrCa. Concentrations of metabolites Cho and PCho were strongly correlated. CHKA was over expressed in low-grade BrCa of all types, and CHKA expression and PCho metabolite levels were correlated. The results demonstrate the potential of metabolite measurements to distinguish benign breast tissue from BrCa, as well as between different types of BrCa. Furthermore, they indicate that changes in metabolism and in expression of underlying CHK genes are associated. While these results point to potential pathways for future research and development, more in-depth studies of BrCa tumor biology will be necessary to investigate a possible future role for metabolite quantifications in the clinical care of BrCa patients.

1.2 Abbreviations

^{1}H-MRS	Proton Magnetic Resonance Spectroscopy
BrCa	Breast Cancer
CHK	Choline Kinase
CHKA / CHKα	Choline Kinase Alpha
CHKA1	CHKA, Transcript Variant 1
CHKA2	CHKA, Transcript Variant 2
CHKB / CHKβ	Choline Kinase Beta
Cho	Choline
DCE-MRI	Dynamic Contrast Enhanced MRI
DCIS	Ductal carcinoma in situ
GPCho	Glycerophosphocholine
H&E	Hematoxylin & Eosin
HRMAS ^{1}H-MRS	High-Resolution Magic-Angle-Spinning Proton-Magnetic Resonance Spectroscopy
IDC	Invasive ductal carcinoma
ILC	Invasive lobular carcinoma
LCIS	Lobular carcinoma in situ
MR	Magnetic Resonance
MRI	Magnetic Resonance Imaging
MRS	Magnetic Resonance Spectroscopy
NMR	Nuclear magnetic resonance
PCho	Phosphocholine
PSA	Prostate Specific Antigen
PTDCho	Phosphatidylcholine
RF	Radio frequency
Rt-q-PCR	Reverse-transcriptase quantitative real-time PCR
SNR	Signal-to-noise ratio
tCho	Composite Choline resonance (total Choline)

2 Introduction

The introduction commences with a short summary, followed by an overview of the hypotheses that this work is based on. Subsequently, more in-depth background knowledge about the diagnostics of breast cancer, magnetic resonance imaging, and the anatomy and function of the breast and breast cancer is provided.

2.1 Summary

Breast Cancer (BrCa) is the most frequently diagnosed type of cancer and the second most frequent cause of cancer death among women in the US.[1] In Germany, both incidence and mortality of BrCa are the highest among all types of cancer.[2] While the incidence of BrCa has been rising for the past decades and will likely continue to rise in the future, technical advances in diagnostics are changing the face of the disease.[3] The introduction of nationwide mammography screening programs for BrCa for the female population of ages 50-69 in recent decades has led to an ongoing debate and substantial controversy about the question whether the costs justify the benefits of screening. Estimates state that screening has led to a reduction of BrCa mortality of at least 15%.[4] This achievement must be seen in the context of the related adverse effects, which are often overlooked. Until today, X-ray mammography remains the gold standard for diagnosing BrCa. Suspicious mammograms are usually followed up by invasive tissue biopsies. Yet, mammograms often yield ambiguous results, and false positive findings frequently lead to unnecessary invasive diagnostic procedures and possible overtreatment.[5, 6, 7, 8] The effort needed to diagnose one case of BrCa is large: Over 200 patients undergo mammograms, of which at least 2-3 will lead to suspicious findings; the patients will usually be further investigated, or biopsied.[9] Patients with negative diagnoses will still have been exposed to possibly harmful radiation in mammography, as well as to emotional stress-without a therapeutic benefit.[4, 6, 10] Estimates state that over the course of 10 years, 1 out of 3 women undergoing screening will receive a false positive result, usually followed by an invasive diagnostic biopsy.[11] In view of the large incidence and high relevance of the disease, more efficient and accurate diagnostic tools are needed.

Magnetic Resonance Imaging (MRI) can diagnose malignant lesions of the breast with high sensitivity and specificity, without exposing patients to radiation. Various studies have shown that the sensitivity and specificity of MRI in diagnosing BrCa is high and surpasses most other diagnostic imaging tools.[12-20] MRI is therefore a very accurate and reliable tool to diagnose

BrCa; its current role in the diagnostic process of BrCa is that of a second line examination tool, subsequent to mammography. In the USA, MRI is officially recommended for women with a number of infrequent conditions of the breast, such as pregnant women with suspected BrCa or young women with an inherited predisposition for BrCa under the age of 40.[21-23]

MRI mammography is usually performed as dynamic contrast enhanced MRI (DCE-MRI), in which an intravenous contrast agent is injected prior to imaging. While the diagnostic capabilities and limitations of conventional DCE-MRI in BrCa have been evaluated in detail, new technical possibilities to image BrCa are emerging from the continuous advancements in magnetic resonance technology.[21, 22] Among the ongoing technological innovations in the field of MR imaging is Proton Magnetic Resonance Spectroscopy (^{1}H-MRS). ^{1}H-MRS non-invasively measures metabolite concentrations within a defined tissue region of interest; the measurement can be performed on a standard MR scanner, and within the same scanning session as a regular breast exam. ^{1}H-MRS permits a direct view into the current cellular activity of a defined tissue region of interest and provides substantial additional information about regional tissue metabolite contents.

A commonly observed change in tissue metabolism of neoplastic lesions is an elevated concentration of choline (Cho) metabolites. In in-vivo ^{1}H-MRS, these changes are reflected in an increase of the characteristic resonance signal at 3.2 ppm, commonly referred to as the composite Cho resonance, or total Choline (tCho).[28] The tCho signal is the sum of the resonance signals of several individual metabolites, such as Cho, phosphocholine (PCho), and glycerophosphocholine (GPCho), which are superimposed in in-vivo ^{1}H-MRS due to low spectral resolution. TCho can be used as a diagnostic marker for BrCa itself, and has been employed to differentiate malignant lesions from normal breast tissue with both high sensitivity and specificity.[23-29] ^{1}H-MRS can potentially increase the accuracy of DCE-MRI, thereby helping to characterize suspicious lesions and to prevent unnecessary invasive procedures.[30-36]

Even though changes of tCho in BrCa tissue have been investigated previously, their exact cause and provenience remain unknown. It is generally hypothesized that elevated Cho metabolite levels in BrCa tissue are a result of accelerated metabolism of Cho, which in turn is associated with faster turnover of cell membranes in invasively growing BrCa tissue.[37] Physiologically, intracellular Cho is metabolized in the Kennedy pathway in several steps that lead up to phosphatidylcholine (PTDCho), a major building block of the cell membrane.[38] The first step in the pathway is the phosphorylation of Cho to PCho, catalyzed by the enzyme Choline Kinase (CHK); two isoforms of the enzyme exist, encoded by two separate genes: Choline

Kinase α (CHKA) and Choline Kinase β (CHKB).[38-40] Investigations in BrCa models have demonstrated that the elevation of tCho, as often found in in-vivo clinical ^{1}H-MRS, is due to a shift in concentrations of the metabolites of the Kennedy pathway: Higher concentrations of PCho were the main contributing factor to the elevation of tCho in BrCa cells. Independently, expression levels of the genes CHKA and CHKB were found elevated in different BrCa models, and a functional association between elevated CHK gene expression and corresponding increases in Cho metabolite levels has been shown.[42, 43]

To fully understand the potential of Cho metabolite levels for diagnostic and therapeutic purposes in BrCa, the underlying molecular mechanisms must be understood in more detail. Current scientific evidence from experiments on BrCa models points to a role for aberrant gene expression levels of CHK in the elevation of tCho, possibly due to an accumulation of PCho. At the same time, it is not clear whether and how these mechanisms can be translated into the human BrCa tumor environment. The goal of this study was to explore in depth how Cho and PCho metabolite concentrations and CHKA and CHKB expression levels are altered and interconnected in different types and grades of human BrCa and healthy normal breast tissue.

The limitations of in-vivo ^{1}H-MRS, which cannot quantify individual metabolite concentrations of tCho because of its limited spectral resolution, can partly be overcome by the use of ex-vivo ^{1}H-MRS. A tissue sample is first extracted, e.g. surgically removed from within the organism and then subject to ex-vivo ^{1}H-MRS metabolite quantification. A certain type of ^{1}H-MRS, High-Resolution Magic Angle Spinning ^{1}H-Magnetic Resonance Spectroscopy (HRMAS ^{1}H-MRS), can achieve particularly high spectral resolutions in metabolite quantification, as described in further detail below.[40]

The methods and design of this study used an experimental approach to investigate in detail the basic phenomena occurring in different types of BrCa. Ex-vivo HRMAS ^{1}H-MRS was used to characterize changes in Cho metabolism in different types of BrCa ex-vivo. In a second step, tissue histopathology was quantified and expression of genes involved in metabolism of Cho was quantified using real-time quantitative polymerase chain reaction (Rt-q-PCR). This experimental approach allowed us to experimentally investigate the proposed relationship between metabolite shifts and changes in gene expression in normal healthy human breast tissue and in BrCa tissue.

The following hypotheses were explored in this study.

Hypothesis 1: Choline and Phosphocholine Metabolite Concentrations

H1: BrCa tissue, benign breast tissue, and different subtypes of BrCa contain different Cho or PCho tissue metabolite concentrations.
H0: BrCa, benign breast tissue, or different types of BrCa do not differ in Cho or PCho metabolite concentration
Methods: HRMAS ^{1}H-MRS metabolite measurements of human BrCa and adjacent benign breast tissue, followed by histopathological quantification of sample pathology.

Hypothesis 2: Histopathology and Metabolite Concentrations

H1: Cho and PCho metabolite concentrations are associated with the histopathological composition of the tissue sample, i.e. the Volume% of tumor tissue within the sample.
H0: Metabolite concentrations are not associated to the sample's histopathological tissue composition.
Method: Correlation analysis of HRMAS ^{1}H-MRS metabolite measurements and specimen histopathological Volume% composition.

Hypothesis 3: Choline Kinase Gene Expression

H1: BrCa cells and benign mammary epithelial cells show different CHKA or CHKB gene expression levels.
H0: BrCa cells and benign mammary epithelial cells do not differ in CHKA or CHKB gene expression levels.
Method: LCM of cancerous and benign mammary epithelia, followed by RNA extraction and reverse-transcriptase quantitative real-time PCR of CHKA and CHKB.

Hypothesis 4: Gene Expression and Metabolite Concentrations

H1: Cho and PCho concentrations are associated with CHKA or CHKB gene expression in human BrCa and normal benign tissues.
H0: Cho and PCho concentrations are independent of CHKA or CHKB gene expression in human BrCa and normal benign tissue.
Method: Correlation analyses of metabolite concentrations (HRMAS ^{1}H-MRS) and CHKA and CHKB gene expression (rt-q-PCR) were performed.

2.2 Background

This chapter provides background information for this study. Initially, the epidemiology of BrCa is discussed in brief, followed by an overview over the current state of BrCa diagnostic practice, with an emphasis on MRI and MRS. The third part of this chapter covers the history and physical basics of NMR and MRS, followed by the fourth part, which sums up different related aspects of BrCa.

2.2.1 Epidemiology

Internationally, the reported incidence rates of BrCa vary widely.[44] The annual incidence rate in Germany has risen over the past 3 decades and is expected to continue to rise until 2020.[3] Estimates from the German Cancer Registers show that in 2010, 59500 patients will have been newly diagnosed with breast cancer in Germany, making up over 29% of all cancer diagnoses in females. At present, the age-adjusted incidence rate of BrCa is 108.8 per 100000 women in Germany. Currently, the average individual accumulated risk to be diagnosed with BrCa within a lifetime is 10.9% for the German female population. The age-adjusted risk of developing BrCa reaches its peak in the age group of 65-69 years. Concordantly, over 80% of new diagnoses can be found in patients aged 50 or higher.[2] At present, 3.5% of deaths in the female population can be attributed to BrCa. The age-adjusted mortality rate of breast cancer has slightly decreased since 1980, and is estimated at 26.8 annual deaths per 100000 women in Germany in 2004.[3] Five-year survival rates for breast cancer patients are currently between 83% and 87%.[2] Incidence of BrCa in men is about 100 times lower than in women, and will thus not be discussed in this study.[45]

2.2.2 Clinical Presentation

BrCa may present with a range of clinical symptoms, such as visible asymmetries and palpable alterations of the breast, however many cases never become clinically manifest before diagnosis. Breast lesions become palpable only at certain sizes; the precursor lesions of BrCa, DCIS and LCIS, as well as invasive BrCa at its early stages are hardly detectable in clinical examination. Up to 30% of breast tumors invade the nipple, the areola, or both, which then becomes visible on the skin surface; in these cases, the diagnosis overlaps with Paget's disease of the breast.[46, 47] Breast self-examination, a cost-efficient means against breast cancer, has produced contradicting results in terms of benefits and harms; nevertheless, a recent meta-analysis described an overall moderately positive effect in lowering mortality.[47, 48]

Numbers about how much clinical breast examination ultimately contributes to the diagnostic process vary widely. The sensitivity of clinical breast examination by a specialist for the diagnosis of BrCa has been reported to lie in a range between 40 to 69%.[49, 50] The specificity of clinical breast examination ranges from 88 to 99%, and varies with age. At the same time, its positive predictive value is lower than 5%.[51, 52] Ultimately, clinical examination is unable to detect small BrCa lesions at early stages, which requires the use of further diagnostic technologies.

Estimated New Cases*

	Males			Females	
Prostate	217,730	28%		Breast	207,090	28%
Lung & bronchus	116,750	15%		Lung & bronchus	105,770	14%
Colon & rectum	72,090	9%		Colon & rectum	70,480	10%
Urinary bladder	52,760	7%		Uterine corpus	43,470	6%
Melanoma of the skin	38,870	5%		Thyroid	33,930	5%
Non-Hodgkin lymphoma	35,380	4%		Non-Hodgkin lymphoma	30,160	4%
Kidney & renal pelvis	35,370	4%		Melanoma of the skin	29,260	4%
Oral cavity & pharynx	25,420	3%		Kidney & renal pelvis	22,870	3%
Leukemia	24,690	3%		Ovary	21,880	3%
Pancreas	21,370	3%		Pancreas	21,770	3%
All Sites	**789,620**	**100%**		**All Sites**	**739,940**	**100%**

Estimated Deaths

	Males			Females	
Lung & bronchus	86,220	29%		Lung & bronchus	71,080	26%
Prostate	32,050	11%		Breast	39,840	15%
Colon & rectum	26,580	9%		Colon & rectum	24,790	9%
Pancreas	18,770	6%		Pancreas	18,030	7%
Liver & intrahepatic bile duct	12,720	4%		Ovary	13,850	5%
Leukemia	12,660	4%		Non-Hodgkin lymphoma	9,500	4%
Esophagus	11,650	4%		Leukemia	9,180	3%
Non-Hodgkin lymphoma	10,710	4%		Uterine Corpus	7,950	3%
Urinary bladder	10,410	3%		Liver & intrahepatic bile duct	6,190	2%
Kidney & renal pelvis	8,210	3%		Brain & other nervous system	5,720	2%
All Sites	**299,200**	**100%**		**All Sites**	**270,290**	**100%**

Figure 2.1: Leading Cancer Types for the Estimated New Cancer Cases and Deaths, by Sex, United States, 2008, excluding basal and squamous cell skin cancers and in situ carcinoma except urinary bladder. Estimates are rounded to the nearest 10. (adapted from Jemal et al., 2010).

2.2.3 Preventative X-ray Mammography Screening as the Gold Standard of Diagnosis

Imaging technology for BrCa has advanced significantly during the recent decades. Today, X-ray mammography is the gold standard in diagnostic imaging for BrCa and is used for preventative diagnostic screening in many countries. Most current guidelines for BrCa screening recommend X-ray mammography for women of the age group of 50– 69 at biannual intervals. The goal of screening is to detect BrCa at the earliest possible stage, at which tumors are still small in size and have not yet metastasized to regional or distant sites, both important factors for a favorable prognosis of the individual course of disease.[53] Although widely spread and accepted in various countries, X-ray mammography is associated with a number of limitations that have caused substantial debate about benefits of screening.[54] Large efforts have been devoted to quantify its diagnostic accuracy. The results of these investigations vary and are often ambiguous, due the many different influencing factors in the diagnostic process. With regard to regional differences in mammography practices and differences in trial design, the overall sensitivity lies in the range of 77% - 95%.[52] Diagnostic specificity is influenced by several factors, such as the screening setting, technical details of the mammography unit and the skill of the individual radiologist: For example, in a larger study in a US community, X-ray mammography had an overall specificity of 93.5%. At the same time, the inter-operator performance varied strongly in specificity from 75.6% to 97.4%.[7] The positive predictive value varies accordingly: In general, the positive predictive value is higher in groups with higher prevalence of the disease, i.e. it increases with the age of the patient sample.[55] Reports range between 12% and 78%.[54-58]

While other countries have successfully implemented X-ray mammography screening decades ago, the German Bundestag decided only in 2002 to establish a nationwide screening program, the implementation of which was started in 2005.[58-61] Whether mammography screening has really led to a 35% reduction in BrCa mortality in Germany, as suggested by some authors, remains uncertain when comparing the numbers to international, large-scale randomized controlled trials.[62] 11 of these trials, carried out between 1963 and 1990, investigated the effects of preventative mammography screening in reducing BrCa mortality. The results diverged and contradicted each other heavily; as a result, an even larger number of reviews and meta-analyses of the data followed. A comprehensive overview of the original trials and the ensuing meta-analyses is provided in a Cochrane review by Goetsche et al.[4] The authors

acknowledge an overall positive effect of X-ray mammography screening in a relative risk-reduction of BrCa mortality of at least 15%. At the same time, the negative aspects of the screening practice are put into perspective: Possible harmful effects of X-ray radiation, effects of false positive mammograms and over-treatment of carcinomata that would otherwise have not become clinically manifest, among others. The conclusion "(…) it is thus not clear whether screening does more good than harm." summarizes the critics' doubts about preventative mammography screening for BrCa. When evaluating the cost and benefits of mammographic screening, it is essential to reflect on the ongoing advancement of screening practices and technology as a whole. Presently and in the future, radiologists will likely be better trained and use more advanced technology in X-ray mammography practice than before, which will lead to better diagnostic results and a higher accuracy of screening exams in comparison to past decades.

X-ray Mammography has several clear limitations: Primarily, dense breast tissue, as is often found in the breasts of young women, is often difficult to evaluate in mammograms. Furthermore, young women at elevated individual risk for BrCa cannot undergo frequent mammographic exams, because of the accumulative mutagenic effect of repeated exposure to X-ray radiation on the mammary gland. Moreover, BrCa lesions of smaller sizes, which lack characteristic diagnostic features like microcalcifications often time remain occult to mammography. In these cases, additional imaging tools like MRI mammography represent a useful and often necessary addition.[63]

X-ray mammography remains the current gold standard in BrCa screening. What follows in the course toward a diagnosis of BrCa is usually a tissue biopsy of the suspicious lesion detected in a mammogram. Different biopsy systems exist, and generally core biopsies have gained increasing popularity over the common practice of fine-needle aspiration. Biopsy material is subsequently evaluated by a pathologist; the result determines the further course of diagnostic procedures or treatment. If a biopsy of a suspicious lesion is inconclusive, the lesion is often surgically removed under on-site rapid-section evaluation or subsequent evaluation by a pathologist.[63]

2.2.4 Magnetic Resonance Mammography

The potential of MRI for diagnosing BrCa has been demonstrated repeatedly; DCE-MRI has been reported to reach an overall sensitivity of up to 100% for diagnosing BrCa. At the same time, reported specificity varies from 37% to 100%.[13-19] These values reflect the large number

of influencing factors such as differences in sample characteristics, MR protocols, hardware and individual operator characteristics. At the same time, they emphasize the high level of diagnostic performance that MRI can deliver in evaluating potential cases of BrCa.

MRI is used as first-line examination tool in screening and examination of women with a hereditary susceptibility to BrCa, as well as in certain patient groups where X-ray mammograms can be difficult to evaluate.[23, 64, 65] The European society of breast imaging has put forward clear guidelines for the use of MR mammography.[66] In the USA, DCE-MRI is officially recommended for screening of women at elevated risk of developing BrCa; it is furthermore useful in the examination of dense breast tissue, in pre-operative staging of already diagnosed BrCa lesions, and as an auxiliary imaging tool for the evaluation of inconclusive suspicious lesions of the breast.[28, 67] MR mammography can detect BrCa lesions that remain occult in conventional X-ray mammography and can help to modify surgical strategy towards less radical forms in patients in need of surgery.[68] It allows for the diagnosis of both ILC and IDC, as well as for the distinction between the two types of BrCa with high accuracy.[69] Studies have shown that ductal and lobular carcinoma in situ (DCIS and LCIS), the precursor lesions of breast cancer, often only visible as microcalcifications in X-ray mammography, which usually require surgical excision, are difficult to diagnose with DCE-MRI. Meanwhile, other findings show that even small breast lesions of sizes of 5mm or less have been well diagnosable with MR mammograms.[70] Taken together, DCE-MRI is a powerful imaging tool for the diagnosis of BrCa, whose clinical evidence base and adoption rate are growing steadily.

Besides the diagnostic performance, other aspects of MR mammography need to be considered when evaluating the diagnostic use for BrCa: One factor opposing the adoption of the diagnostic routine of MR mammograms is the associated cost: MRI is a relatively expensive diagnostic exam, and thus cannot compete with the other examination tools from an economic point of view. In conclusion, MR mammography is a very powerful diagnostic examination tool, whose high cost is the current limiting factor to a more widespread adoption in the diagnostic routine.

2.2.5 Magnetic Resonance Spectroscopy

^{1}H-MRS, which was one of the first applications of magnetic resonance technology, is now evolving into a promising diagnostic tool for BrCa. It measures tissue metabolite concentrations in-vivo, and thus provides a direct view into the cellular activity, allowing for the tracking of metabolic changes during the progression of the disease. In-vivo ^{1}H-MRS regularly

detects elevations of the composite Cho resonance signal (tCho) in BrCa lesions, which can be considered a diagnostic biomarker in ^{1}H-MRS.[24, 66] Several groups have evaluated the accuracy of these changes in BrCa tumors: The sole quantification of tCho in suspicious lesions has been reported to be able to distinguish malignant from benign breast tissue with a sensitivity of 70% - 100% and a specificity of 82% - 100%.[29] When combined with DCE-MRI, ^{1}H -MRS measurements of tCho can reportedly improve the specificity for the diagnosis of BrCa to close to 100%.[72,73] These studies, which only included small sample sizes, have to be seen in the light of their highly variable results; at the same time, they indicate the added value that ^{1}H-MRS can offer in the diagnostic workup of BrCa. Furthermore, in-vivo ^{1}H-MRS has also been useful in a number of other cases, such as monitoring neoadjuvant chemotherapy, or predicting treatment response after chemotherapy induction.[71, 74-76]

The quality of spectroscopic measurement and the resulting diagnostic accuracy strongly depend on a number of technical variables, which have been summarized by Stanwell and Mountford.[27] For example, intravenous contrast agent used in DCE-MRI, which is injected before ^{1}H-MRS, can lead to significant alterations of measured metabolite concentrations.[77] In-vivo ^{1}H-MRS performed on MRI scanners at common clinical field strengths is limited to relatively low spectral resolutions. Therefore, the subsequent metabolites of Cho in the Kennedy pathway cannot be quantified separately in in-vivo ^{1}H -MRS measurements, but only as their sum in the tCho signal.[31, 34, 78] The reason for this limitation is the broadening and overlapping of individual resonances at low magnetic field strengths. The separate quantification of the single metabolites of Cho requires a higher spectral resolution to achieve separate individual MR resonance signals. Currently, this is only possible in ex-vivo ^{1}H-MRS. In this study, tissue samples were measured ex-vivo at high magnetic field strengths, leading to increased spectral resolutions with distinguishable resonances of the single metabolites of Cho.

2.2.6 Choline Metabolism in Breast Cancer

Cho is a quaternary amine that is metabolized to become PTDCho, a major component the lipid double-layer cell membrane in the Kennedy pathway. The majority of human Cho uptake stems from the diet, making Cho an essential nutrient.[79, 80] Several membrane-bound organic cation transporters for the uptake of Cho into the cell have been identified.[81, 82] Intracellular Cho is first phosphorylated to PCho, a reaction catalyzed by the enzyme CHK. PCho, besides being a central metabolite within the Kennedy pathway, has been ascribed a role of a second messenger for growth promotion in BrCa.[40] PTDCho in turn can be broken down again and

metabolized in catabolic salvage pathways leading back to Cho and PCho.[83] Two genes encode for the two isoforms of CHK, which have likely resulted from genomic duplication: CHKA on Chromosome 11, and CHKB on Chromosome 22.[84, 85] Furthermore, two splice variants of CHKA exist, resulting in two transcript variants, CHKA1 and CHKA2.[86] Research indicates that these enzymes play a central role in the development of a variety of cancers, such as BrCa.[87] (Compare Figure 1.2)

Although several factors influencing the elevations of tCho in BrCa have been identified, the underlying molecular mechanisms are still not completely understood. Physiologically, mammary epithelial cells are able to take up large amounts of Cho, which are then concentrated and secreted as Cho-containing metabolites into milk during lactation. In-vivo ^{1}H-MRS measurements of lactating mammary glands have found significant increases in tCho, resembling the changes observed in malignancies.[88] Various techniques have been used to study Cho metabolism in BrCa: Spectroscopic analyses from BrCa tissue extracts demonstrated a relative increase of PCho over the other metabolites in the Kennedy pathway.[89, 91-93] Ex-vivo ^{1}H-MRS measurements of the tCho resonance signal in breast biopsy samples found that malignancies could be distinguished with a specificity of 92% and sensitivity of 96%.[90] De Molina et al. reported in a study of CHK in 53 ex-vivo BrCa samples that CHK activity was elevated in 38.5% and that CHK was over-expressed in 17% of tumors; these changes in activity and expression showed a correlation with tumor grade and estrogen-receptor status.[94] Taken together, while metabolite concentrations were regularly significantly elevated in BrCa, the underlying enzymatic activity and gene expression did not show regular alterations.

Cheng et al. showed that HRMAS ^{1}H-MRS, an ex-vivo high-field MRS technique, is able to measure metabolites at spectral resolutions sufficient to differentiate between the individual metabolites that make up tCho resonance. A HRMAS ^{1}H-MRS study of 19 IDC tissue specimens showed that increases in PCho occurred primarily in grades II and III carcinomata, and that the metabolite concentrations were sufficient to differentiate between histopathological tumor grades.[95] Sitter et al. published 3 studies in which HRMAS ^{1}H-MRS was used to analyze BrCa specimens ex-vivo. The results showed that high-resolution metabolite spectra can distinguish cancer from normal benign tissue specimens with high accuracy, and that PCho is the predominantly elevated metabolite in BrCa cells.[96-98]

BrCa cell line and animal xenograft models have provided insights into the mechanisms responsible for the elevation of tCho. MRS measurements of different BrCa cell lines repeatedly found significantly increased tissue concentrations of tCho, including PCho, GPCho and a

substantial acceleration of metabolic kinetics when compared to human mammary epithelial cells.[41, 42] A cell-line model of the step-wise progression of BrCa malignancy showed that higher concentrations of tCho and PCho are associated with higher malignancy; moreover, a switch in the ratios of metabolite concentrations towards increases in PCho was observed.[99] BrCa cell lines, in which key regulatory genes had been activated by artificial induction, directly showed changes in PCho concentrations: Modifications of the *ras* oncogene led to changes in CHK activity and increased PCho concentrations, while the metastasis-suppressor gene nm23 led to decreased PCho concentrations.[100, 101] Increased cellular uptake and accelerated metabolism of Cho was repeatedly found in BrCa cells evaluated with different types of MRS measurements.[98, 99]

Two studies by Glunde et al. and Eliyahu et al. compared BrCa and benign mammary epithelial cells: The results show that increases of Cho metabolite concentrations and accelerated Cho transport were accompanied by an increase in CHK gene expression (Eliyahu et al. specifically reported an elevation of CHKA over CHKB, while Glunde et al. did not distinguish between CHKA and CHKB).[42, 43] CHK activation was found to be a prerequisite for the proliferation of BrCa cells, while its depletion suppressed tumor growth and induced cellular differentiation.[100, 101] Due to their presumed central role in Cho metabolism and in BrCa carcinogenesis, CHKA and CHKB have also been proposed as potential pharmaceutical targets. Different approaches for use in treatment have been investigated, including several pharmacological compounds, as well as RNA-interference.[94, 102-111]

Together, these studies strongly suggest a role for CHK as causal agent for the observed changes in Cho metabolism in BrCa. Yet, as described above, most of these data resulted from experiments on cell culture models, from which only limited conclusions can be drawn about carcinomata inside the human organism, as reflected by the large differences in metabolism between BrCa cell lines. Moreover, only few studies of human BrCa take into account the diffuse invasive growth patterns of BrCa, which lead to mixed areas of carcinoma and benign cells; hence the question, where within the BrCa lesion alterations in Cho metabolism occur remains unanswered. Additionally, previous studies did not differentiate between the histological types of BrCa, which by definition have very different genetic and histologic properties. Subtypes of BrCa might exhibit significant differences in metabolism. In order to better understand the changes of Cho metabolism occurring in BrCa, more research about the mechanisms in human BrCa tissue is needed. These indications were the basis for this study, in which concentrations of Cho and PCho, as well as gene expression levels of CHKA and

CHKB were investigated in detail within the microenvironment of different types of human BrCa and of adjacent normal benign tissue, using HRMAS ^{1}H-MRS, followed by LCM, RNA extraction and rt-q-PCR.

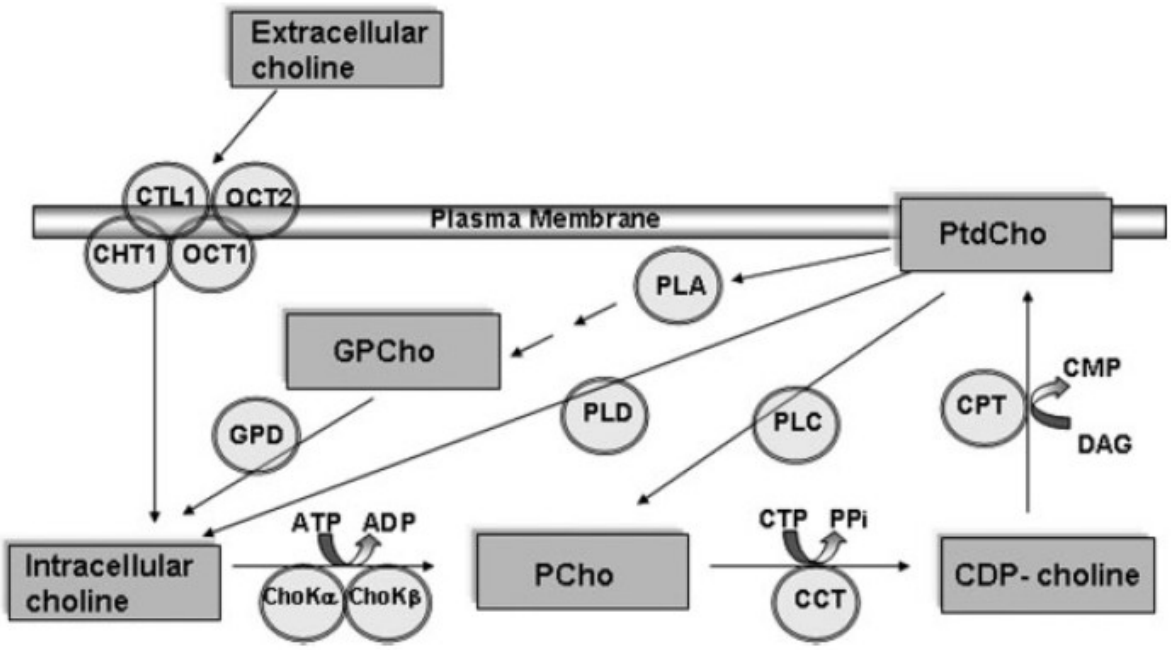

Figure 2.2: Illustration of the uptake and intracellular metabolism of Choline phospholipids in the Kennedy pathway (adapted from Eliyahu et al. 2007). CHT1: Choline high-affinity transporter 1; CTL1: Choline transport-like protein 1; OCT1 and OCT2: Organic cation transporters 1 and 2; ChoKα and ChoKβ: Choline Kinase alpha and beta; CCT: CTP-PCho Cytidylyltransferase; CDP: Cytidylylphosphocholine; CPT: Cholinephosphotransferase; PLA: Phospholipase A; PLC: Phospholipase C; PLD: Phospholipase D; GPD: Glycerophosphocholine phosphodiesterase; PtdCho: Phosphatidylcholine; GPCho: Glycerophosphocholine.

2.3 Basis of Nuclear Magnetic Resonance

The wide range of today's applications of NMR technology is the result of several key scientific discoveries made in the last century. In the following, a brief historical overview will be given, followed by technical aspects of MR.

2.3.1 Historical Development

The basic idea and principle of nuclear magnetic resonance (NMR) was first postulated by Paul Dirac in 1928; the phenomenon of the nuclear spin was subsequently discovered by Otto Stern; both were awarded a Nobel Prize in Physics for their work, in 1933 and 1943, respectively. Isidor Isaak Rabi, who was awarded the Nobel Prize in Physics in 1944, first described the measurement of magnetic properties of atomic nuclei with nuclear magnetic resonance. Edward Purcell and Felix Bloch built upon this foundation and expanded the field of NMR by performing measurements in solid and liquid matter, for which they shared the Nobel Prize in Physics in 1952. Paul Lauterbur, an American chemist, further expanded the field and built the foundation of many of today's applications of MRI in the following years. His concept of applying magnetic fields at different gradients to determine the spatial origin of the NMR signals enabled the reconstruction of two-dimensional MR images from 1973 on. Peter Mansfield of the University of Nottingham, UK expanded upon Lauterbur's discoveries and further developed the mathematical principles of image analysis. Mansfield and Lauterbur shared the 2003 Nobel Prize in Physiology and Medicine for their contributions in the development of MRI.[112] Today, NMR technology is used in a variety of applications and different scientific fields, ranging from imaging and metabolite measurements in medicine to physics, chemistry and computer science.

2.3.2 Physical Background

NMR technology is based on the atomic property called the nuclear spin, a type of angular momentum of elementary particles, composite particles and, most important in this case, of atomic nuclei. The inhomogeneous distribution of electrical charges surrounding atomic nuclei leads to a precessing spinning motion of the electrical charge of the atom, called nuclear spin. Different nuclei exhibit characteristic magnetic dipole moments, whose intensity depends on the isotope's gyromagnetic ratio, as described in the equation $\mu = \gamma \cdot I$

(μ = magnetic moment; I = angular momentum = "nuclear spin"; γ = gyromagnetic ratio)

The spatial orientation of the dipole moments can be manipulated by applying a surrounding magnetic field B_0. Spins orientate with or against the magnetic field, two possible states which are separated by the energy difference ΔE. The intensity of the spin is accelerated multiple-fold, depending on the strength of B_0. The relationship between ΔE, which is different for isotopes such as ^{1}H, ^{31}P or ^{13}C, and the surrounding magnetic field B_0 is described in the (modified) Larmor equation:

$$\Delta E = h \cdot \nu_L = \gamma \cdot B_0 / 2\pi$$

(h = Planck's constant; ν_L = Larmor frequency)

In NMR, the region of interest is located in a homogenous magnetic field B_0. A radio-frequency (RF) pulse is applied that induces B_1, a second magnetic field that usually stands at a 90° angle to B_0. Nuclear spins within B_0 absorb energy and change their orientation to align with B_1. When nuclear spins precess at 90° or lesser angles to B_0, spins radiate energy back in an electromagnetic signal: The NMR signal. The resonance frequency of the signal depends on the strength of the applied B_1 magnetic field, and is characteristic for specific quantum mechanical magnetic properties of atomic nuclei. Depending on the NMR application, the signal is then detected in the receiving antenna, usually a coil, amplified and subsequently processed. When the RF-signal stops, the nuclei gradually begin to realign with the magnetic field B_0, a process called relaxation. Each isotope is characterized by two different relaxation time constants: T1, the longitudinal or spin lattice relaxation time, and T2, the transverse or spin-spin relaxation time.[113] In MRI, an image is reconstructed based on the differences in tissue concentrations of hydrogen atoms, which give a strong resonance signal, because of the abundant tissue water content. In ^{1}H-MRS, the water resonance signal is suppressed in order to measure concentrations of the other chemical compounds contained within the tissue.[114]

2.3.3 ^{1}H-Magnetic Resonance Spectroscopy

Different types of magnetic resonance spectroscopy (MRS) are commonly used in a wide range of scientific disciplines, most notably chemistry, biochemistry and physics. In the study of organic biological tissue, ^{1}H-MRS can provide a direct snapshot of the molecular composition of a tissue sample by quantification of metabolite concentrations within tissue in the magnetic B_0 field. Measurements are based on certain physical properties that go beyond conventional MRI, and that will be explained in the following. The precessing movement of nuclear spins in complex carbon molecules not only depends on the magnetic fields B_0 and B_1, but also on the valence electrodes surrounding the nucleus. Valence electrons "shield" the

nucleus from the externally applied magnetic field by forming a small magnetic field themselves. Additionally, magnetic spins are influenced by the surrounding spins. Thus, all nuclei of the same isotope behave differently in different locations, e.g. ^{1}H nuclei exhibit slightly different physical properties when covalently bound in different organic molecules; as a result, each ^{1}H nucleus within a tissue specimen is surrounded by its own magnetic field B_{eff}:

$$B_{eff} = (1-\sigma) \cdot B_0$$

(σ = shielding constant of the electron hull)
The Larmor equation can be modified accordingly:

$$\Delta E = h \cdot \nu_L = \gamma \cdot B_0 \cdot (1-\sigma) / 2\pi$$

The Larmor frequency for Protons is 63.87MHz in a magnetic field of 1.5T. According to the equation $B_{eff} = (1-\sigma) \cdot B_0$, the same nuclei, depending on their location show slightly different resonance frequencies; based on these differences, which reflect in the MRS spectra, the reconstruction of complex molecules from their spectroscopic signatures is possible. During MRS measurements, spectral intensities are acquired continuously throughout a certain relaxation time. The intensity of the resonance signal at a given time during the acquisition period is put into relation to a known standard reference resonance frequency, and can thus be assigned to a known compound. The frequency difference between the resonance of a nucleus and the standard, relative to the standard, is defined as the chemical shift, δ, whose unit is parts per million (ppm):

$$\delta = (\nu_L - \nu_{REF} / \nu_{REF}) \cdot 10^6$$

MRS resonances can be assigned to nuclei in different molecular bonds, independent of the magnetic field strength in use. A commonly used reference standard substance in MRS is Tetramethylsilane (δ = 0 ppm). Dependent on the experimental setup, the echo time, i.e. the time between the RF pulse and the signal acquisition, and the repetition time, i.e. the time between two successive RF pulses, are chosen. The ^{1}H-MRS signal is recorded in the time domain, i.e. as a function of time elapsed since the RF pulse. Water and lipids are the most abundant molecules in the human body, whose MRS resonance signal is 4-5 magnitudes stronger than that of other molecules of interest. Consequently, different pulse sequences are used before the actual MRS measurement to stimulate and to subsequently dephase the proton resonance. The result is a suppression of the water signal, which enables the detection of the metabolites of interest, usually present in much smaller amounts.[115] Measurements are repeat-

ed multiple times and the resulting MRS spectrum is usually an average of over 100 measurements.

Several "pre-scan" procedures have to be performed prior to measurements: For example, an essential prerequisite is the adjustment of the magnetic field, called shimming, to avoid inhomogeneities that would broaden the spectra. After completion of measurements, post-acquisition processing of the data again involves a number of steps that can also have a large impact on the quality of the data. The process includes water referencing, apodization, and zero-filling, which are usually followed by Fourier transformation, a method to transform a time-series signal of various frequency components into a frequency spectrum. Phase and baseline correction are performed on the raw spectrum before spectral resonance analysis and interpretation. A comprehensive overview of the most relevant aspects of the process at the current state of in-vivo ^{1}H-MRS in BrCa is given in a review by Stanwell and Mountford.[27] In the final MRS spectrum, resonances of the different compounds are displayed as peaks over the X-axis and can be identified according to their ppm-values. The area under the curve of a peak is directly proportional to the number of atomic nuclei within the sample. The relative concentration of a metabolite can thus be quantified by calculating the integral of the peak at the respective chemical shift (ppm). Over the past three decades, substantial knowledge about spectral resonance frequencies of many different compounds in NMR measurements has been gained, which is available in reference databases for MRS metabolite quantification.[116]

The spectral resolution and quality of ^{1}H-MRS measurements depends on various factors, such as the strength and homogeneity of the magnetic field B_0, the number of measurements, and the design of the receiving coil. The sum of these technical details results in a key property, commonly referred to as the signal-to-noise ratio (SNR). In in-vivo MRS, the spectral quality is often limited by a variety of factors, such as low magnetic field strength or field inhomogeneities. Moreover, the resonance signals are broadened by chemical shift anisotropy and susceptibility-induced magnetic field distortions, altogether resulting in a low SNR.[27] In contrast, ex-vivo ^{1}H–MRS performed at higher magnetic field strengths can quantify metabolites in tissue samples at higher SNRs, allowing for higher spectral resolutions, and thus the differentiation between larger numbers of single metabolites than in-vivo MRS.

Early ex-vivo studies of BrCa metabolites using ^{1}H-MRS were based on different ways of extraction of metabolite solutions from the tissue samples and subsequent metabolite quantification. Although these spectra were high in resolution, the approach required large amounts of tissue and a time-intensive extraction process. Moreover, the processing of intact tissue sam-

ples to liquid extracts changed the molecular composition and probably led to alterations of metabolite concentrations.[89, 92, 112] Following these early approaches, other techniques, such as High-Resolution Magic Angle Spinning 1H-Magnetic Resonance Spectroscopy (HRMAS ^{1}H-MRS) were adopted for the ex-vivo measurement of intact tissue specimens.

2.3.4 High-Resolution Magic Angle Spinning ^{1}H-Magnetic Resonance Spectroscopy

HRMAS ^{1}H-MRS was originally developed as an analytical tool in solid state chemistry by Professor Raymond Andrew at Nottingham University. Its application to biological tissue for the first time allowed the ex-vivo quantification of metabolites from intact human tissue specimens at high resolutions without destroying the specimen. (Compare Figures 2.3 and 2.4) During measurement, a rotor is used to spin the sample about its own axis at an angle of -54.74° to the B_0 magnetic field, known as the magic angle. The spinning movement results in a reduction of the resonance broadening effects of chemical shift anisotropy and dipolar coupling. The spectral resolution achieved by HRMAS ^{1}H-MRS is higher than in in-vivo ^{1}H-MRS, with narrower spectral resonances, and without artifacts resulting from previous tissue processing, such as homogenization. [115] Upon completion of the measurement, the intact specimen can be recollected from the rotor head to be used for further histopathological analyses.

Cheng et. al. have previously demonstrated the potential of HRMAS ^{1}H-MRS metabolite measurements to classify a variety of neoplasia in ex-vivo measurements, such as BrCa, according to their metabolism.[95, 117-122] The use of the technique for high-resolution metabolite measurements and for the analysis of BrCa metabolism was adopted by other research groups, among them Sitter et al., who provided a detailed analysis of the metabolites occurring in the HRMAS ^{1}H-MRS spectrum.[98] Taken together, HRMAS ^{1}H-MRS allows for the separate quantification of the concentrations of Cho and PCho in intact tissue specimens ex-vivo, which are not distinguishable in in-vivo ^{1}H-MRS.

A matter of concern in HRMAS ^{1}H-MRS ex-vivo tissue metabolite quantification is the progress of tissue degradation and metabolite turnover after the tissue samples are taken from the body. Mammalian cells in tissue specimens continue with their cellular functions, and start decaying soon after resection from their natural environment. Cellular metabolite contents will therefore be significantly altered within hours after sample recollection. These effects must be prevented by proper handling and storage of tissue, which is a prerequisite for scientific investigation using this method, as described below.

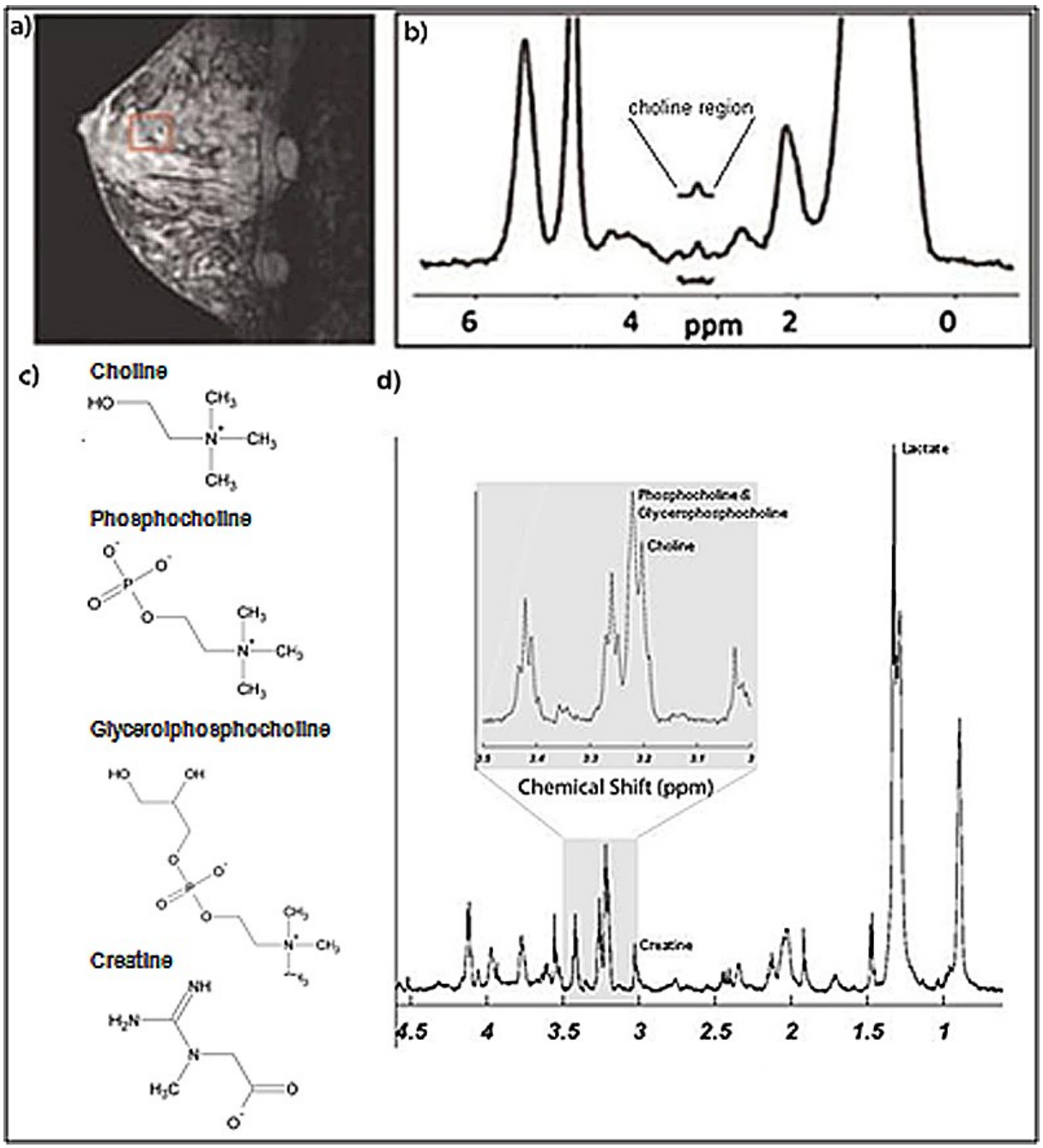

Figure 2.3: Examples of MRI and MRS of Cho metabolism in breast tissue: a) MRI of IDC. The square represents the area in which MRS is measured. b) In-vivo MR spectrum of BrCa tissue. The tCho peak is visible in the region labeled "Choline region" c) Chemical structure formulas of Cho, PCho, GPC-Cho and Creatine. Ex-vivo HRMAS ^{1}H-MR spectrum of the same BrCa tissue. d) The grey inlay shows the Cho and PCho metabolite peaks.

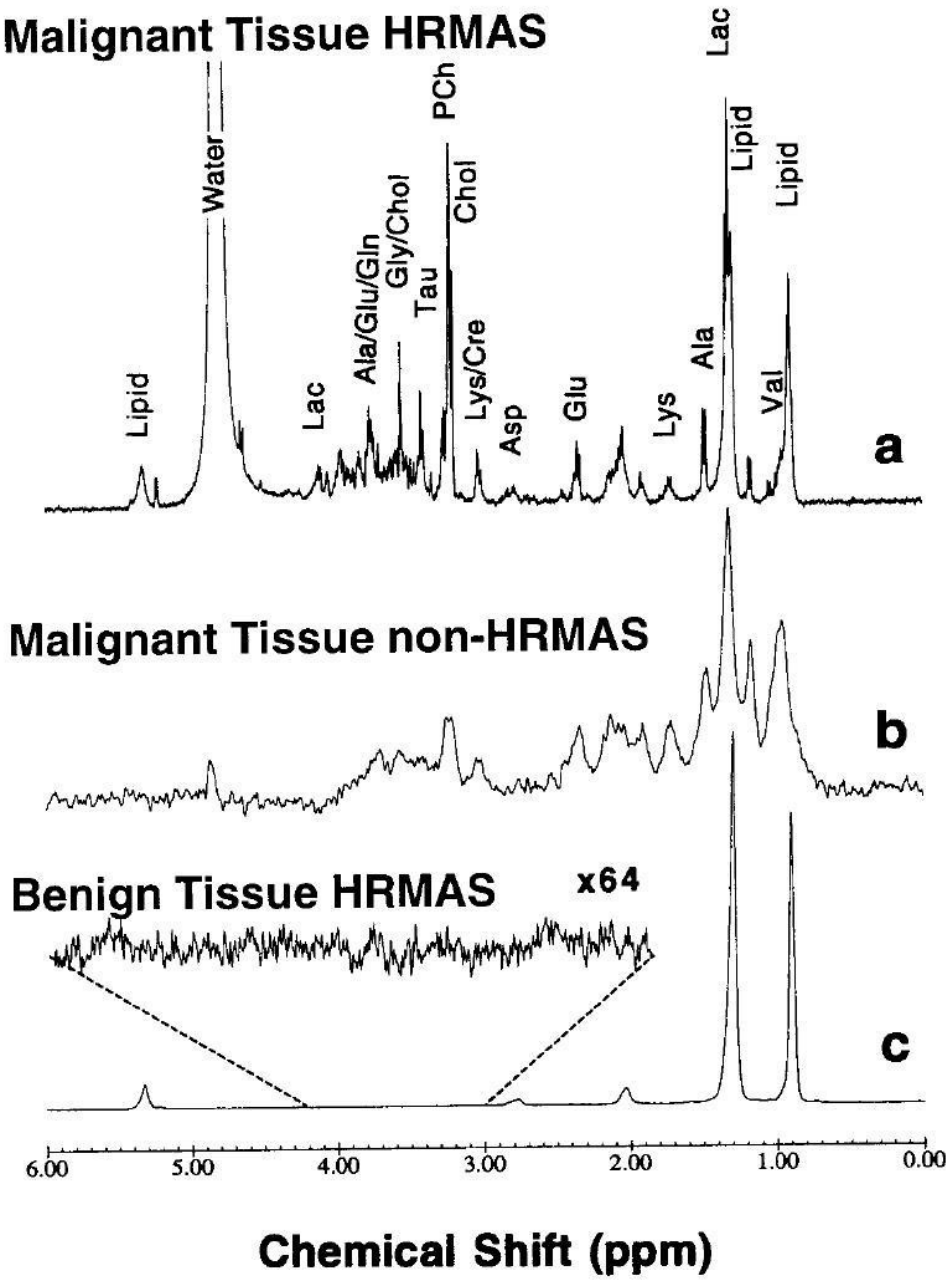

Figure 2.4: Comparison of ex-vivo ^{1}H-MRS spectra of grade II IDC breast cancer and normal benign breast tissue obtained with HRMAS ^{1}H-MRS (a,c), and normal benign breast tissue in regular ^{1}H-MRS (b). (Adapted from Cheng et al. 1998): a) T2-weighted HRMAS spectrum of BrCa tissue acquired at 2.5kHz at 20°C. Selected metabolite resonances are labeled: Val, valine; Lac, lactate; Ala, alanine; Lys, lysine; Glu, glutamate; Asp, aspartate; Cre, creatine; Chol, choline; PCh, phosphorylcholine; Tau, taurine; Gly, glycine. b) Spectrum of intact BrCa tissue, acquired under similar experimental conditions, except without HRMAS, after spinning at 2.5 kHz for more than 10 minutes. c) Spectrum of non-tumor breast tissue excised from the margin of resection. The insert shows the spectral region of 3.0 to 4.2 ppm in 64-fold expansion. Acquired under same experimental conditions of a)

2.4 Anatomy and Function of the Breast and Breast Cancer

The primary mammary ducts develop from the ventral basal cells of the epidermis of the female fetus during the second trimenon of pregnancy and form the foundation of the mammary gland. During puberty, the influence of various hormones leads to the secondary development of the breasts. The glandular body then consists of between 15 and 40 branched glands, which are embedded in fatty tissue and surrounded by fibrous stroma. Beginning from the nipple, the whole breast is categorized into lobes, which contain the branched glandular ducts; each duct ends in several lobuli, which are in turn made up of several acini, connected by smaller ducts and embedded in loose stroma. The complete glandular tree is lined by glandular epithelium on the inside, followed by a myoepithelial layer and a basal membrane on the outside. The epithelium is subject to the hormonal changes of the female menstrual cycle, with the strongest proliferation during the luteal phase, often accompanied by swelling of the breasts and followed by apoptosis of the epithelium during the days of menstruation. The final step in the functional development of the breast occurs during pregnancy and before lactation: Hormonal changes lead to proliferation of parenchyma and epithelium. Milk is produced and secreted by the epithelia of the acini, triggered by the hormonal influence of prolactin. Lactation ends after the loss of hormonal stimulation, when the epithelium is replaced by glandular progenitor cells. The breast's most sensitive part is the nipple, innervated by the fourth thoracic nerve.[123]

2.4.1 The Origin of Breast Cancer: Carcinoma in Situ

Invasive neoplasia of the breast originate from precursor lesions, carcinomata in situ, defined as neoplastic proliferations of malignant epithelial cells within the ductal and lobular parts of the mammary glands. 95% of the precursor lesions are of ductal origin, DCIS, while 5% are of lobular origin, defined as LCIS. Both are confined within the boundaries of the basal membrane of the gland. DCIS, histologically characterized by a ductal differentiation pattern of neoplastic cells, spreads within the ductal tree of the breast. LCIS tends to occur multifocally in different lobuli, and often in both breasts, i.e. bilaterally and does not spread within the ductal system. Several molecular differences are known between the two types of carcinoma in situ. LCIS exhibits a characteristic loss of functionality of the E-Cadherin-gene on Chromosome 16q, which leads to a loss of the E-Cadherin protein and resulting lack of cellular connectivity. Histological staining of E-Cadherin is hence used in pathology to differentiate between the ductal and lobular origin of breast neoplasia. Carcinomata in situ often contain

microcalcifications, which can be detected in mammography. Their final diagnosis is based on the histological evaluation of tissue biopsy material. Because DCIS and LCIS are precursor lesions for the development of invasive breast cancer, both are treated by surgical excision.[124, 125]

2.4.2 Risk Factors for Breast Cancer

The exact cause of BrCa remains unclear; a multi-factorial, sequential process of cellular alterations, resulting from genetic disposition, as well as behavioral and environmental risk seems likely. Age can be considered the most important risk factor for BrCa. The relative risk in the age group of 65-69 year old females is almost 17 times higher than in 30-34 year olds. A family history of BrCa puts first-degree relatives of BrCa patients at a risk several times higher than that of the average population. Menarche before the age of 12, first pregnancy after age 35, menopause after the age of 55 or nulliparous patient history additionally increase the risk of developing BrCa several fold. Further risk factors for BrCa are alcohol consumption, smoking, hormonal imbalances, such as increased estrogen levels due to post-menopausal hormone replacement therapy, previous benign and malignant diseases of the breast, as well as obesity, body height or exposure to ionizing radiation.[126]

The identification of the "breast cancer genes" BRCA1 and BRCA2 in the 1990s has attracted major public attention. The abbreviation "BRCA" was in this context used as an acronym for Berkeley, California, where the discovery was made, at the same time forming a double entendre with the disease itself. Both genes encode for proteins that play a role in DNA repair mechanisms; their mutated alleles, which highly increase the risk for BrCa, occur as inherited or as somatic mutations. Nevertheless, mutations of BRCA genes are only found in 5-10% of all BrCa cases. Carriers of BRCA1, which is localized on 17q21, are at an accumulated relative risk of 80% for developing BrCa until the age of 70 and the majority of the cancers already develop before the age of 50. BRCA2 is located on Chromosome 13q12-13 and puts people at a 70% risk of developing BrCa until age 70.[127,128]

2.4.3 Molecular Carcinogenesis

Genetic and molecular biological analyses of the different stages and types of BrCa have shown that neoplastic development follows a series of genetic changes, often corresponding to the histological features and different grades of malignancy. Repeated mutations and resulting dysfunction of tumor-suppressor-genes, amplification of oncogenes or higher expression and

activity levels of other regulatory genes are among the complex mechanisms involved in the development of the disease.[129] The following genes, whose function is in cellular growth and homeostasis regulation and DNA repair, are among the most thoroughly investigated. Mutations of their sequence and changes in expression levels influence the prognosis; the proteins encoded by these genes are already, or could be future therapeutic targets:

ERB-B2 (Her-2/neu) is a gene located on chromosome 17q12, which is amplified to up to 100 times in BrCa, thereby becoming an oncogene. It encodes for a growth receptor of the tyrosine kinase type that stimulates cell growth and is overexpressed in around 20% of BrCa. It has an influence on the prognosis of the disease, and is used as a therapeutic target.[129-131] EGFR (7p13), another member of the same ErbB receptor family, also encodes for an epidermal growth factor; it is amplified in about 3% of BrCa tumors, which is also associated with a poor prognosis. Like Her-2/Neu, it is a tyrosine kinase growth receptor and is also a target in tumor chemotherapy.[132] A different central oncogene is MYC (8q24), which encodes for c-myc a central transcription factor in the regulation of the expression of hundreds of genes. It influences the progression of BrCa, and an amplification of MYC is associated with a poor prognosis.[133] The majority of BrCa tissue shows alterations of CDH-1 (16q22), a tumor-suppressor gene that encodes for the adhesion molecule E-cadherin, and is altered and inactivated by point mutations, deletions and hypermethylation. The resulting loss of adhesive function enables infiltrative growth of tumor cells.[134,135] As in many other types of cancer, the tumor suppressor gene p53 (17p13) is inactivated by mutation or deletion in around 20% of BrCa. Its central and complex function in cellular proliferation and growth has been thoroughly investigated.[136] Moreover, several hormone receptors occur in altered fashion in BrCa: Estrogen receptors, along with progesterone receptors, regulate cell growth after hormonal stimulation. Over expression of either, or of both can be found in the majority of BrCa and seem to play a central role in BrCa carcinogenesis. Their expression levels directly influence the prognosis of the disease.[137]

2.4.4 Pathology of Breast Cancer

More than half of the cases of BrCa develop in the lateral, upper quadrant of the breast. Roughly another 15% occur in the upper medial quadrant, 15% in the area of the nipple and the areola, 5% in the lower median and 10% in the lower lateral quadrants. BrCa is categorized into various histological subspecies, which can be classified according to three systems- the WHO classification is the most common and widely used of these three.[138, 139] The prima-

ry pathological distinction between ILC and IDC is based on the histological presentation of the tumor. Therefore, BrCa tissue is evaluated by microscopy of stained tissue sections: Histological grading is made according to pathological grading schemes, a good overview of which is given by Singletary et al.[140] Factors like the formation of tubuli, the degree of nuclear aberrations and the mitotic frequency of the tumors are summed up and the result is a classification as low, intermediate or high grade tumors. In addition, different subtypes of IDC can be distinguished. In this study, the focus was on the general forms of IDC and ILC, which make up 85% and 5-15% of the cases, respectively. IDC is characterized by mostly coherent invasive growth of cancer cell populations in tubular, trabecular or solid patterns. The malignancy originates from the ductal part of the mammary gland and usually coincides with intra-ductal spread of carcinoma. By contrast, ILC spreads in a dissociated fashion, with groups of tumor cells occurring separately throughout benign tissue; common characteristic growth patterns are rows or circles around the lobules.[141]

The clinical stage of the disease is categorized according to the TNM system, which takes into account the size of the primary tumor, the presence, number and size of lymph node metastases and the presence of distant metastases. Advances in research are bringing forth more and more prognostic factors in BrCa, which allow for an increasingly accurate prognosis of the future course of the disease. Nevertheless, the prognosis is still often highly unpredictable and 10-year survival rates deviate greatly among different types of BrCa. Despite the development of several molecular prognostic marker systems, the TNM system and the histological tumor grade remain the most important prognostic factors.[125,142] The prognosis for the individual patient is a result of a combination of these and other factors. An example of one of the leading systems for prognosis of life expectancy is the Nottingham Prognostic Index, which incorporates several prognostic factors and aims to provide a broad orientation about the statistically most probable course of disease.[143]

2.4.5 Metastases and Tumor Markers in Breast Cancer

BrCa can metastasize early in the course of disease through the vascular and lymphatic systems. Lymphatic metastases occur primarily along the lymphatic drainage vessels of the ipsilateral axilla, while hematogenous metastases occur throughout the body. Metastasized tumor cells can remain dormant for up to 5-10 years before becoming manifest as carcinoma; then, metastases occur most frequently in the skeletal system, lung and pleura, liver and brain.[144] Unlike in prostate cancer, where the serological marker Prostate Specific Antigen

(PSA) is used for diagnostic purposes and screening in high-risk population groups, no serological tumor markers for the screening of breast cancer exist. The currently established serological tumor markers CEA, CA 15-3, CA 27.29 and Ki-67 are thus used only in follow-up and monitoring of the course of disease after the initial diagnosis, or throughout and beyond the completion of treatment.[145]

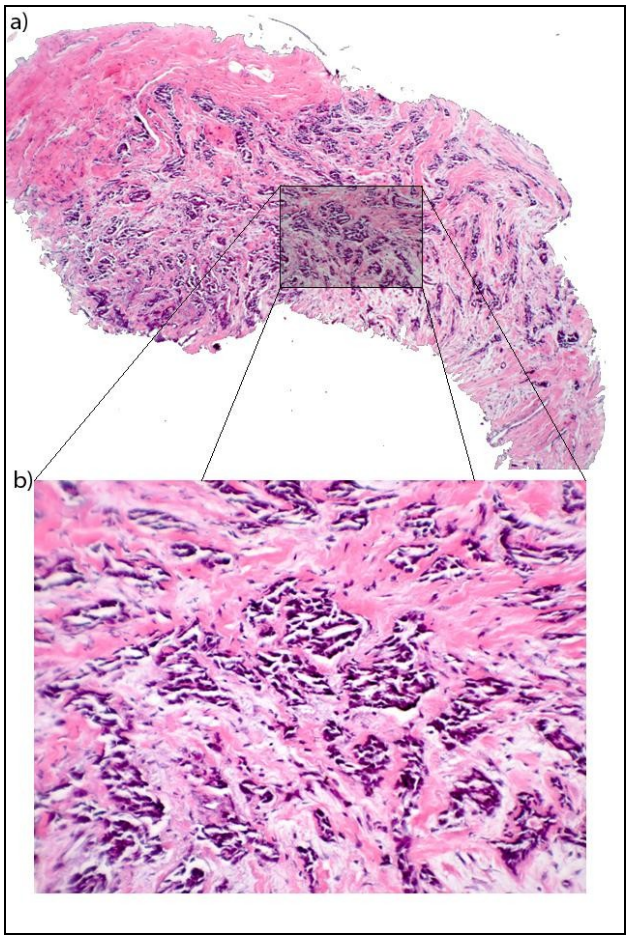

Figure 2.5: H&E stained serial section of an IDC tissue specimen after metabolite measurement in HRMAS MRS. a) x5 magnification, b) x20 magnification.

2.4.6 Treatment

Therapeutic protocols for BrCa can include any combination of surgery, adjuvant radiation or adjuvant systemic chemotherapy. Several studies have compared radical mastectomy, breast-conserving modified mastectomy and lumpectomy, in combination with adjuvant radiation or chemotherapy. The results showed very similar survival rates for the radical and less radical

therapeutic approaches. Therefore, modern surgical strategies favor modified, less radical surgical therapy in combination with radiation and/or chemotherapy over radical mastectomy.[146,147] During surgical treatment of BrCa, the first lymph node in the lymphatic drainage pathway, the sentinel lymph node, is usually identified and checked for the presence of cancer cells. Depending on the findings of BrCa cells in the sentinel lymph node, axillary lymph node dissection is performed subsequently.[148-150] Systemic chemotherapy with commonly used chemotherapeutics, as well as novel therapeutics against cell receptors are used as neo-adjuvant and adjuvant therapies in addition to surgery.[151]

3 Materials and Methods

3.1 Study Design and Protocol

This study was conducted with the approval of the institutional review board at Massachusetts General Hospital, USA. Benign and cancerous human breast tissue samples were collected from patients undergoing breast surgery who had given informed consent about the use for research purposes. Tissue specimens were snap-frozen in liquid nitrogen within less than 10 minutes after surgical resection and stored in the BrCa tumor bank at -80°C for a maximum duration of 18 months until further processing in the radio-pathology tissue bank.

Previous studies by Cheng et al. have shown that storage at -80°C for up to several years is adequate to ensure metabolite and RNA integrity of human tissue. [152] It has been suggested that freezing and thawing of samples are more likely to alter tissue metabolite levels than the duration of frozen storage. As previously demonstrated, breast tissue specimens were frozen without addition of any storage buffer, in order to avoid metabolite leakage to buffer solution.[153, 154]

Each specimen was initially bisected using sterile surgical equipment over dry ice. One half was used for HRMAS ^{1}H-MRS metabolite measurements, followed by evaluation of the histopathological tissue composition of the specimen. The other half was used for the quantification of CHKA and CHKB gene expression in the tumor microenvironment: It was serial sectioned on a cryostat microtome as preparation for the ensuing LCM, in which tumor and benign cell populations were excised individually. RNA was extracted from excised cells, transcribed to cDNA, and rt-q-PCR was performed to quantify gene expression of CHKA and CHKB.

The accuracy of metabolite and gene expression measurements in human tissue is highly dependent on the specimen integrity and susceptible to contaminations. At room temperature, metabolites and RNA degrade rapidly after tissue is removed from the organism. Tissue samples and extracts must therefore be frozen immediately, kept in sterile containers, transported on dry ice and stored at -80°C without interruption. All materials, surfaces and staining solutions must be free of contaminants and RNases. Regular cleaning of surfaces and all tools with RNase-AWAY and 70% Ethanol before experimental procedures is essential. Additionally, when working with tissue, the use of disposable gloves is necessary at all times.

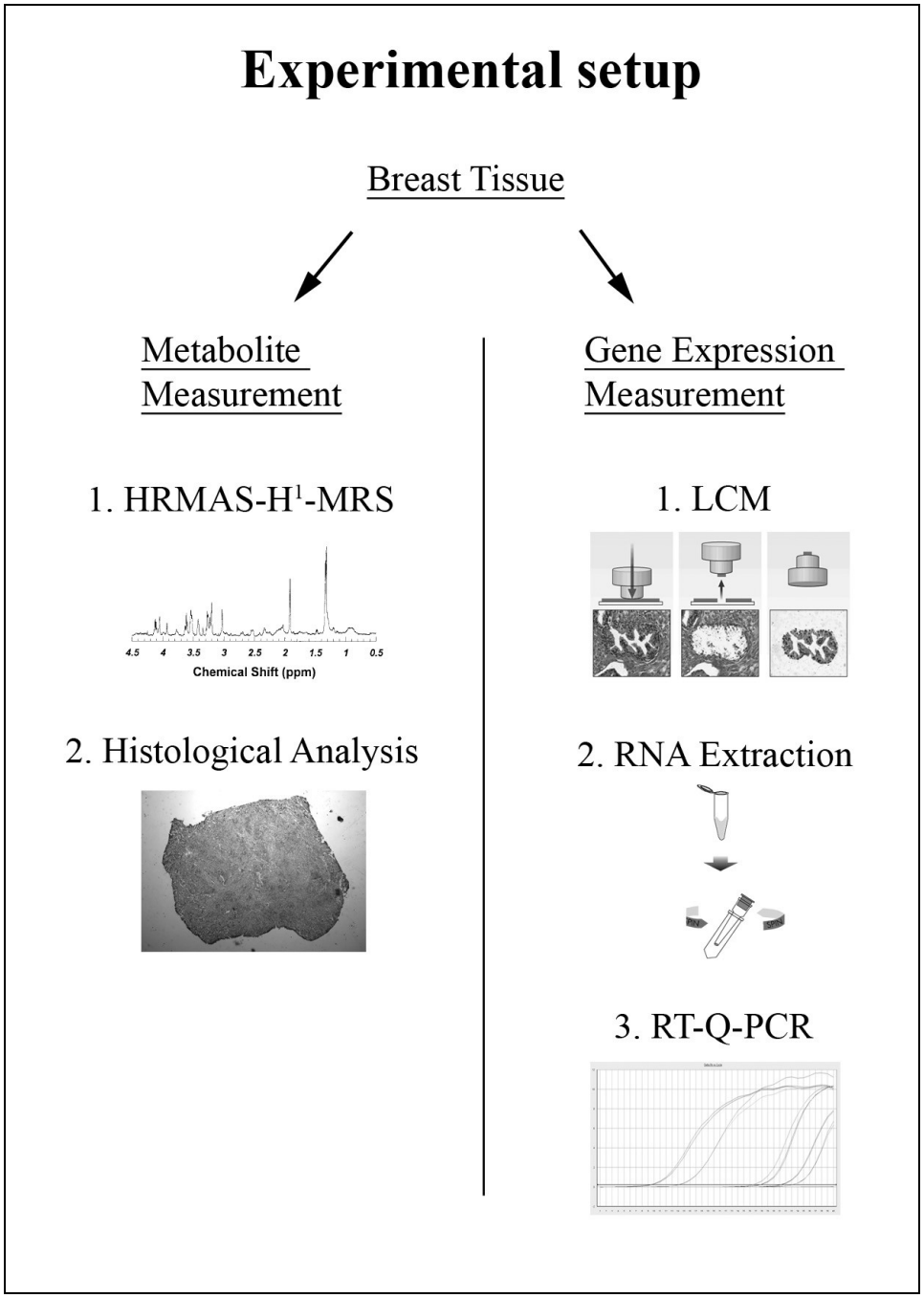

Figure 3.1: Schematic illustration of experimental study design.

3.2 Patient Sample Overview

Inclusion criteria for the study were a complete clinical case record and continuous documentation of the specimen's provenience and storage. 18 BrCa samples from 18 patients of an approximate average diameter of 5 mm were randomly selected from over 250 specimens in the radio-pathology tumor tissue bank without knowledge of patient clinical records. 11 matching adjacent normal glandular tissue samples from the same cases were selected as benign comparisons. Patient clinical and pathology data were later obtained through the clinical application suite patient record system at Massachusetts General Hospital.

Patient	Diagnosis	Tumor Size (cm)	Stage	Nodes	Grade	HER-2/ neu	Estro- gen	Progeste- rone
1	ILC	9x5x2.5	T3N3M1	22/22	2	-	+	+
2	ILC	2.2x1.5x1.0	T2N0M0	0/3	2	++	+	+
3	IDC	4.2x2.6x2.4	T2N0M0	0/2	3	+++	+	+
4	ILC	3.2x2.4x1.7	T2N1MX	1/30	3	-	+	+
5	ILC	3.7x2.5x2	T3N2M0	9/21	2	-	-	+
6	IDC	7x5.5x2.2	T3N1M0	1/17	1	++	+	+
7	IDC	2.5x2x1.3	T2N1M0	1/4	2	-	+	-
8	IDC	0.4x0.2x0.5	T1N1M0	2/2	3	-	-	-
9	ILC	3.4x2.3x1.5	T3N3M0	23/23	2	-	+	-
10	IDC	2.5x2.5x2.5	T2N1MX	1/8	3	-	+	+
11	IDC	6x3.2x2	T3N0M0	1/10	3	-	+	+
12	ILC	5x4.7x2.5	T2N1MX	2/4	2	-	+	+
13	IDC	2.1x2.0x1.4	T2N1M0	1/2	2	-	+	+
14	ILC	3.0x2.0x2.0	T2N0M0	0/2	2	-	+	+
15	ILC	3.6x1.0x1.0	T1N1M0	3/13	2	-	+	+
16	IDC	2.5x2.1x1.7	T2N1M0	2/13	3	+	-	-
17	ILC	3.8x2.5x2	T2N1M0	2/4	2	-	+	+
18	ILC	1.8x1.6x1.5	T1N1M0	1/3	2	-	+	+

Tab. 3.1: Patients included in this study. Nodes = Lymphatic node involvement; HER-2/neu = HER-2/neu receptor over expression; Estrogen = Estrogen receptor overexpression; Progesterone = Progesterone receptor over expression

3.3 Metabolite Measurements

3.3.1 High-Resolution Magic Angle Spinning ^{1}H-Magnetic Resonance Spectroscopy

Tissue concentrations of Cho and PCho were quantified by High-Resolution Magic Angle Spinning ^{1}H Magnetic Resonance Spectroscopy (HRMAS ^{1}H-MRS) on a Bruker AVANCE spectrometer operating at 600MHz (14.1 Tesla). A 4mm MRS rotor with plastic inserts forming a spherical sample space of ~10 µl was used as probe head. A silicone rubber sample of ~0.1mg inside one of the rubber spacers without contact to the sample itself was used as external control. Immediately before scanning, previously frozen samples were thawed for less than 10 minutes and scanned at an operating temperature of 4°C. The B_0 magnetic field was shimmed before each scan to avoid field inhomogeneities. During spectral acquisition, the rotor-spinning rate was kept at 2.5 (±0.001) kHz, regulated by a Bruker MAS controller. A rotor-synchronized Carr-Purcell-Meibom-Gill (CPMG) pulse sequence [90-(τ-180-τ)$_n$-acquisition] was used as a T2-Filter to minimize spectral broadening due to lipids. [155] The inter-pulse delay of 400 µs was synchronized to the rotor rotation. The value of n was 500 ($2n\tau$ = 500 ms). The 90° pulse length was adjusted for each sample individually and varied between 9.6 to 10.6 µs. The number of transients was 512 with a repetition time of 3s. The acquisition time of 1016 ms (16K complex points) resulted in a spectral width of 8 kHz (20 ppm). After completion of data acquisition, tissue was recovered from the rotor head and stored at -80°C until subsequent processing.

3.3.2 Data Processing

Spectroscopic data were processed and analyzed manually using NUTS software after previous blinding of information about specimen quality or case history. Free induction decays were subject to 1 Hz apodization. Fourier transformation was carried out, followed by baseline correction and phase adjustment of zero and first order according to common reference peaks. The resonance from the rubber inserts within the HRMAS rotor was used as reference for the assignment of spectral peaks to known metabolites within the spectrum. Metabolite concentrations were quantified by curve fitting of Lorentian-Gaussian-line-shapes to the corresponding peaks of the resonance spectrum and integration of the areas under the curve. The Creatin peak was used to set the baseline reference ppm for each sample individually, with a resulting Cho frequency at roughly 3.204 ppm, and PCho at roughly 3.225 ppm.[89]

3.3.3 Histopathological Tissue Analysis

Samples were recovered from the HRMAS probe and fixed in 10% formalin solution for 8-12 hours, dehydrated in increasing concentrations of alcohol (80%, 90%, 95%, 100%) for a minimum of 30 minutes each, cleared with Xylene and embedded in paraffin wax blocks. Embedded tissue samples were serial sectioned at 5 μm. Consecutive serial-sections of 100 μm distance were collected from each sample and mounted onto charged glass slides. Serial sections were stained with hematoxilin and eosin according to the H&E protocol shown in table 3.1. An Olympus BX41 Microscope Imaging System was used to quantify the histopathological composition of the serial sections of scant samples. The relative amount of cancer cells, normal epithelial cells, stroma and fat in each cross section was estimated to the nearest 5% using the image analyzer software MicroSuite without any knowledge of the spectroscopy results. The amount of the different tissue entities within each specimen was calculated as the average of the amounts contained in the serial sections at intervals of 100 μm throughout each sample.

3.3.4 Hematoxylin and Eosin Staining Protocols

The following staining protocols were used to stain benign and malignant breast tissue serial sections with H&E.

Standard H&E staining protocol for formalin-fixed, paraffin embedded tissue sections		H&E quick-staining protocol for OCT-embedded tissue sections, RNA-preserving, adapted for LCM	
Xylene	10 min	70% Ethanol	1 min
Xylene	10 min	RNase free H20	10 dips
100% Ethanol	4 min	Hematoxylin	3 dips
95% Ethanol	2 min	RNase H20	10 dips
dH2O	Rinse	Bluing Reagent	3 dips
Hematoxylin	5 min	70% Ethanol	10 dips
dH2O	Rinse	95% Ethanol	10 dips
Bluing Reagent	10 dips	Eosin	5 dips
dH2O	Rinse	95% Ethanol	10 dips
95% Ethanol	10 dips	95% Ethanol	10 dips
Eosin	10 min	100% Ethanol	1 min
95% Ethanol	10 dips	Xylene	1 min
95% Ethanol	10 dips		
100% Ethanol	10 dips		
100% Ethanol	10 dips		
Xylene	5 min	(500:1 ProtectRNA RNase Inhibitor was added to all staining solutions except Xylene)	
Xylene	5 min		

Tab. 3.2: Staining protocols used for Hematoxylin and Eosin staining of tissue serial sections

3.4 Gene Expression Measurements

The remaining second halves of the tissue specimens were used to measure gene expression levels according to the procedures described in the following.

3.4.1 Laser-Capture Microdissection

Tissue specimens were embedded in Tissue-Tek O.C.T. compound, cooled down to the optimum cryostat operating temperature (-24°C) for 30 minutes before cutting, and serial sectioned at 10µm intervals at -20° C under RNase-free conditions on a Leica CM3050 cryostat microtome. Sections were dry mounted onto uncharged glass slides, which were placed in airtight sealed slide boxes on dry ice and subsequently stored at -80°C for up to 3 days. Every tenth section was stained using a regular H&E staining protocol and evaluated in blinded reading with an experienced breast pathologist to assess presence, histopathological grade and extent of BrCa or benign breast glandular tissue, or both within the section. H&E stained sections later served as reference for orientation during the microdissection. Directly before LCM, each serial section was H&E quick-stained under RNA preserving conditions (cp. Tab. 2.1). LCM was performed on an Arcturus PixCell II LCM System. The glass slide holding the specimen was placed on the LCM microscope table and the Laser beam was tested before the actual capturing was started. The laser operating settings were set to duration of 2 ms, spot size of 7.5µm, and a laser power of initially 50mV, which was increased up to 70 mV, if necessary.[156] Tumor and benign breast epithelial cells were collected separately. Microdissection was limited to a maximum time-frame of 30 minutes per serial section in order to guarantee RNA integrity. Microdissected cells were transferred into a microcentrifuge tube containing 100 µl of Stratagene Absolutely RNA Microprep Lysis Buffer and 0.7µl of β-Mercaptoethanol. A minimum of 5000 cells were collected per case and tissue entity (benign or cancer), which required the subsequent use of between 2 to 10 subsequent serial sections. A new LCM cap was used for each serial section and entity (Compare figures 3.1 and 3.2)

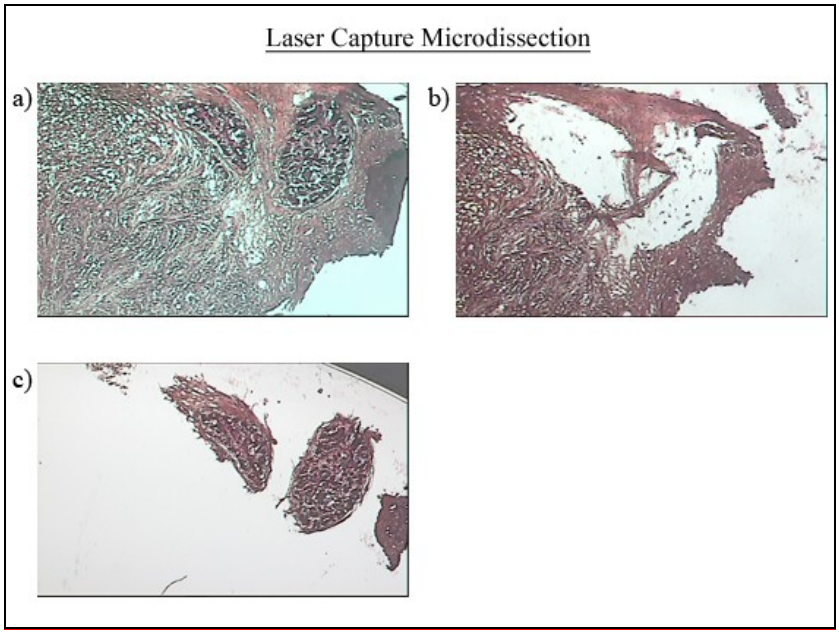

Figure 3.2: Illustration of Laser-Capture Microdissection: a) intact serial section of benign hyperplastic epithelia; b) remaining surrounding tissue after excision of epithelia; c) epithelial cells attached to LCM cap after microdissection.

3.4.2 RNA Extraction and Reverse Transcription

RNA was extracted from LCM samples with the Stratagene Absolutely RNA Microprep Kit according to the manufacturer's manual, including the DNAse step. DNAse was subsequently cleared in purification steps on spin columns according to the manual; purified RNA from captured and lysed cells was eluted in 30 µl of buffer solution and stored at -80°C.

The quality of extracted RNA was assessed by measuring the photometric absorption of 1 µl of RNA on a Nanodrop ND1000 spectrophotometer. The ratio of 260/280 nm photospectrometric absorption was used to assess RNA integrity, 1.8 being the minimum threshold for RNA integrity. Before each measurement, the Spectrophotometer was calibrated with the Stratagene Elution buffer, containing the same amount of added ß-Mercaptoethanol as the buffer in which the RNA was dissolved. RNA was reversely transcribed into complementary DNA (cDNA) by combining 15µl of extracted RNA, 0.5 µl DTT, 0.5 µl RNase inhibitor, 1.5 µl random hexamers, 1.5 µl of deoxynucleotide triphosphates, 5 µl of reverse transcriptase buffer and 1.5 µl of reverse transcriptase in a 1.5 ml microcentrifuge tube. The

reaction was incubated at 37°C for one hour, interrupted by cooling to -4°C for 15 minutes and finally heated up to 95°C for 5 minutes to denaturate the newly formed cDNA strands. The newly synthesized cDNA was stored at -80°C until further processing.

3.4.3 Reverse-Transcriptase Quantitative Real-Time PCR

Primer design according to standard criteria is necessary in order to achieve optimal molecular properties for successful rt-q-PCR measurements. Custom oligonucleotide primers for 12 of the known enzymes involved in Cho metabolism were designed in accordance with the NCBI reference database using the Primer3Plus freeware primer design tool (compare Tab. 2.5 and 2.6).[157, 158] As expected, the amount of extracted RNA from laser-capture microdissected cells was relatively small. The number of genes, whose expression could be quantified in rt-q-PCR, was therefore limited. In this study, the focus was put on the measurement of the expression levels of the two isoforms of CHK, CHKA and CHKB in the RNA extracts. Primer pairs for the target genes CHKA and CHKB were designed according to the NCBI reference database transcript sequences.[84, 85] Design was according to standard primer design criteria and included an exon-exon-boundary within the amplicon to ensure mRNA specificity. Primer pairs were dissolved in RNase free water to a 20µM solution, and were tested in rt-q-PCR on cDNA, which had previously been transcribed from commercially available breast RNA with the identical settings used in later measurements.

Prior to processing of specimens, PCR standard curves were established on cDNA from transcribed commercial human breast cancer RNA to localize the limits of the linear range of rt-q-PCR amplification. The linear range represents the minimal and maximal initial concentration of DNA that can be reliably quantified using the rt-q-PCR assay.[159] It is demarcated by quantification of 10-fold dilutions of an initial amount of DNA, which appear at intervals of √10 (=3.1622) amplification cycles in the rt-q-PCR fluorescence results plot, indicating that measurements can be reliably performed within this range (compare figure 3.4). Amplification products were sequenced to ensure correct selectivity of amplification. Contaminations were ruled out by running positive and negative controls in the 96-well plate, as well as by control of the dissociation curves after completion of measurements.

Results were additionally controlled according to the dissociation curves of the measurements. The curves are acquired after the last cycle of rt-q-PCR amplification, in which the amplified PCR product is heated to a temperature maximum. DNA double strands of the same length and sequence dissociate at a specific temperature, resulting in a burst of fluorescence of

the SYBR green dye. The result is a characteristic peak in fluorescence, known as dissociation curve, which reoccurs in identical shape and at the same temperature if the amplification was successful and uncontaminated (compare figure 3.5).

Amplification products were confirmed by agarose gel electrophoresis. Agarose gel was prepared by combining 1,5g of agarose and 100ml of 0.5xTAE buffer in a 2l Erlenmeyer flask and heating for 1 minute at 90W in a microwave oven, followed by cooling, adding 50 µg of ethidium bromide and pouring into the electrophoresis mold. After solidification, the gel was submerged in 0.5x TAE buffer. 5 µl of loading dye was added to 25µl of PCR product, of which 15 µl was loaded into the gel pockets. 5µl of a 100 basepair DNA reference ladder was added as a reference next to the PCR products and run on the same gel. Electrophoresis was carried out at 60V for 2 hours. Additionally, quality of amplification products was assured by sequencing according to the Sanger Method, carried out by the MGH sequencing core facility, where an Applied Biosystems Taq Dye Deoxy Terminator Cycle Sequencing Kit was used.

Rt-q-PCR reactions were performed using the fluorescent dye SYBR Green, whose fluorescent activity is activated in the presence of DNA double strands.[160] The ribosomal gene 18s was used as housekeeping (reference) gene to normalize the amount of loaded DNA in every PCR reaction.[161] Reactions were prepared in 96 well-plates and run on an ABI PRISM 7000 Fast Lightcycler. Each well contained 2 µl of cDNA, 12,5 µl of RT^2 SYBR Green/ ROX Mastermix, 9,5µl of RNase free water and 1 µl of 20 µM target gene primer solution or 1µl of 10µM 18s primer solution, respectively. An optical adhesive cover foil was used to seal the plate. The housekeeping gene 18s was measured in duplicates and the target genes CHKA and CHKB in triplicates. Negative and positive template controls were included on each plate to rule out sample and reagent contamination.

The following temperature cycling protocol was used in all rt-q-PCR reactions: 15 initial minutes of incubation at 95°C to denaturate DNA double strands and to activate the TAQ polymerase, followed by 40 cycles of 1 minute at 60°C for annealing and DNA translation, and 15 seconds at 95°C for denaturation of DNA and primers. In a last step, the PCR reaction was heated in order to obtain the melting curve, representing the last quality control gate in the rt-q-PCR experiment. (Compare Fig. 3.5)

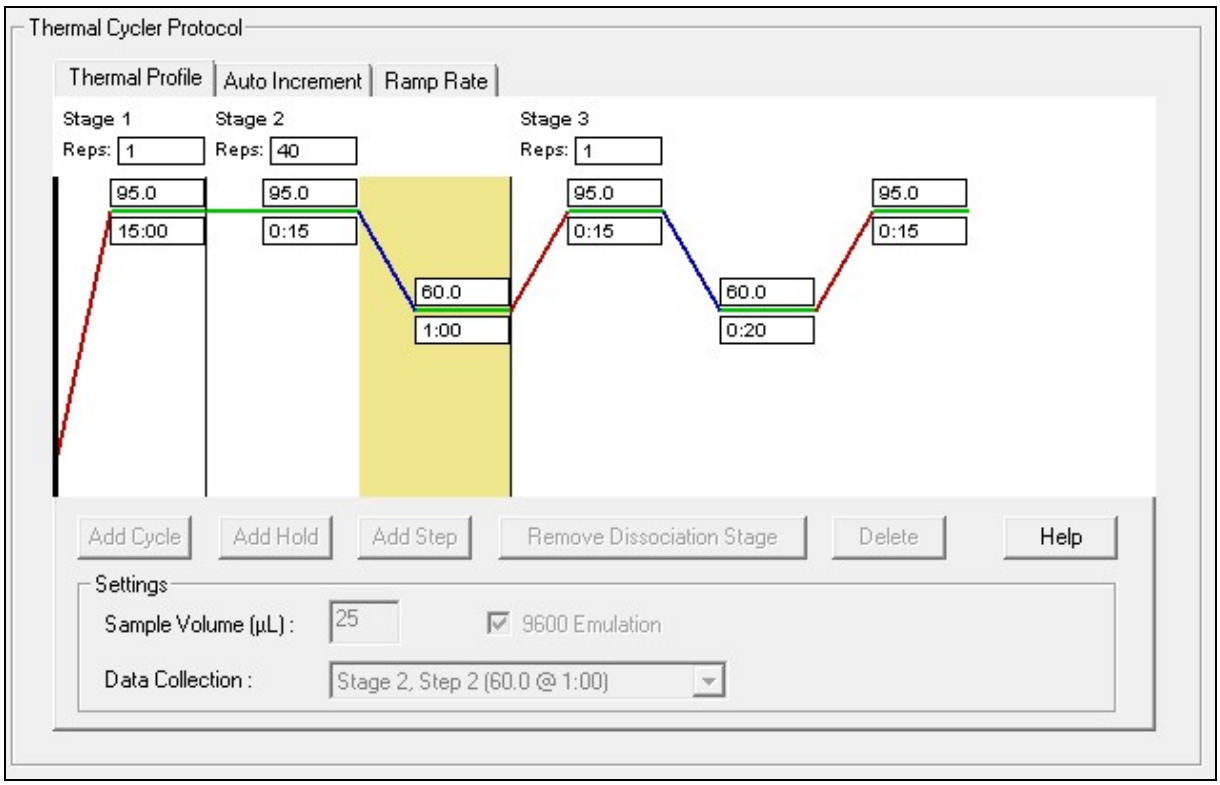

Figure 3.3: Temperature cycling protocol for rt-q-PCR .

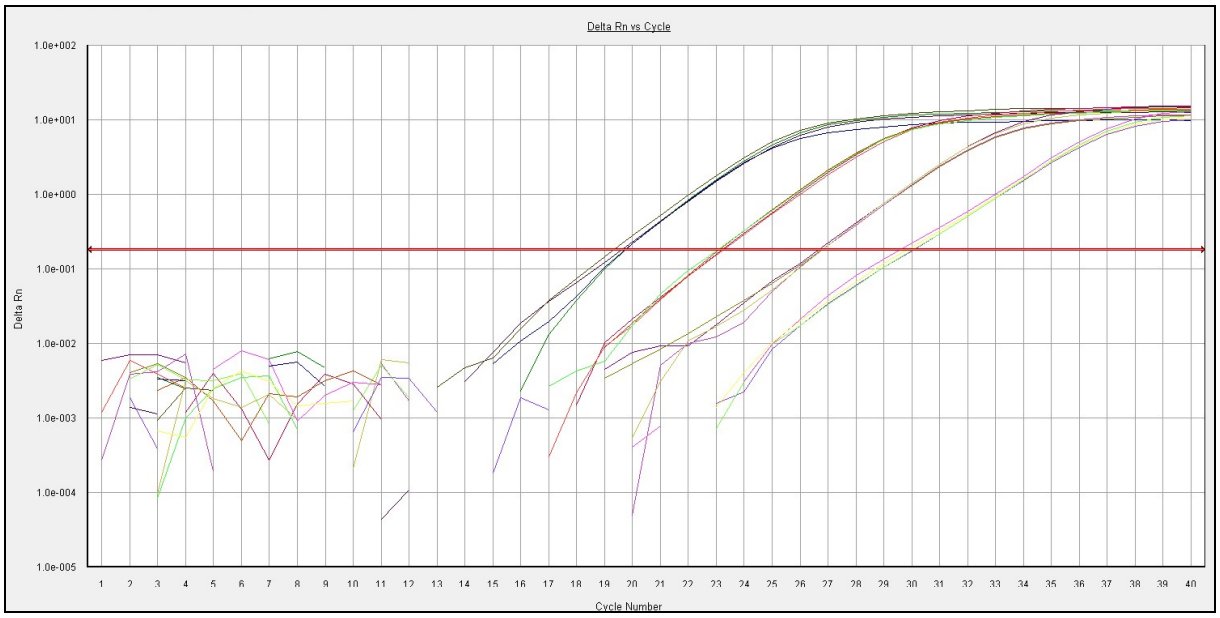

Figure 3.4: Example of amplification of 1-, 10-, 100- and 1000-fold dilutions of cDNA, transcribed from commercial breast tissue total RNA. The Ct-values are within the linear range of amplification.

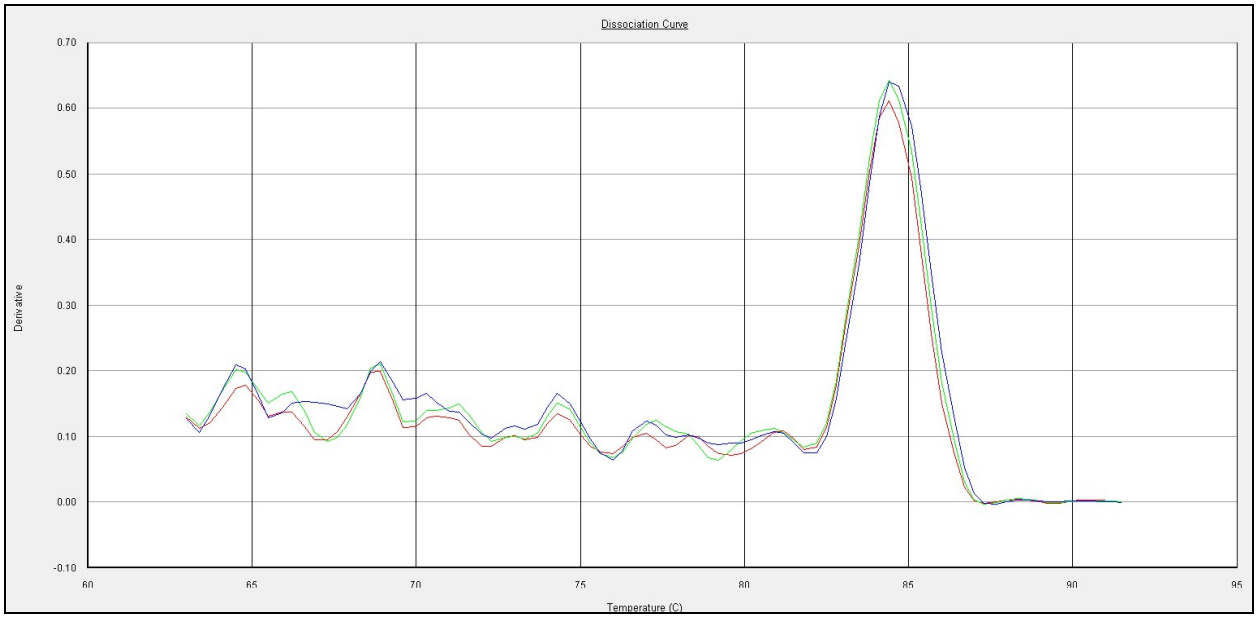

Figure 3.5: Example of a rt-q-PCR dissociation curves of a triplicate measurement of gene expression levels of CHKA in a benign breast tissue specimen. Overlapping, symmetrical peaks indicate successful amplification.

3.4.4 PCR Amplification Efficiency Correction and Relative Quantification

In theory, the amount of DNA in a PCR reaction doubles after every reaction cycle until fluorescence reaches a plateau phase. Thus, the ideal reaction, in which the amount of DNA grows exponentially by the factor of 2, would by definition exhibit 100% amplification efficiency. In practice, the amplification efficiency of a PCR reaction is influenced by numerous factors within the reaction and usually varies slightly between reactions; it is rarely 100%. When using the $2^{-\Delta\Delta Ct}$ method in rt-q-PCR, differences in gene expression are quantified by normalizing levels of target genes to a reference ("housekeeping") gene.[159] Relatively small differences in amplification efficiency can, thanks to the nature of exponential growth in PCR amplification, ultimately lead to substantial deviations of the results. Thus, equal amplification efficiencies for all rt-q-PCR measurements are essential for obtaining valid results.[159, 160] One way to ensure an amplification efficiency of 100% is to post-process the rt-q-PCR fluorescence data according to the principle of sigmoidal curve fitting, initially described by Liu and Saint, and further developed by Rutledge.[162, 163] A custom software tool was developed for this purpose, which enables processing of rt-q-PCR data to 100% efficiency. The program

was written in MATLAB R2009b (Version 7.9). All acquired rt-q-PCR data were corrected for 100% amplification efficiency. After correction of amplification efficiency, results were calculated according to the $2^{-\Delta\Delta Ct}$ method. Means of duplicate and triplicate measurements were used as final Ct-values. ΔCt was calculated for each sample as the difference between the Ct of the target gene and that of the housekeeping gene 18s.

3.4.5 Statistical Analysis

Statistical analysis was performed using JMP statistical software (Version 8.0.2.2). Descriptive statistical data, such as means, standard deviations, standard error of the means, 95% confidence intervals, as well as medians, quantiles and maximum-minimum spans were calculated and are reported in the following figures.

Student t-tests were used to compare significant differences in metabolite concentrations among groups. An alpha-level of $p<0.05$ was applied as threshold for statistical significance in the comparison of two groups.

Linear regression analyses were used to investigate correlations between two variables.

3.5 Materials

3.5.1 Instruments and Software

Bruker AVANCE spectrometer	Bruker BioSpin Corporation, Billerica, MA, USA
HRMAS probe	Bruker BioSpin Corporation, Billerica, MA, USA
HRMAS rotor	Bruker BioSpin Corporation, Billerica, MA, USA
NUTS software	Acorn NMR Inc. Livermore, CA, USA
Olympus BX41 Microscope Imaging System	Olympus American, Inc., Melville, NY, USA
MicroSuite image analysis software	Soft Imaging System Corp., Lakewood, CO, USA
Leica CM3050 cryostat microtome	Leica Microsystems, Bannockburn, IL, USA
PixCell IIc Laser-Capture Microdissection System	Arcturus Engineering, Mountain View, CA, USA
Nanodrop ND 1000 Spectrophotometer	Thermo Fisher Scientific, Waltham, MA, USA
ABI Prism 7000 Sequence Detection System Rt-q-PCR cycler	Applied Biosystems, Foster City, CA, USA
ABI Prism 7000 SDS software, Version 1.2.3	Applied Biosystems, Foster City, CA, USA
MATLAB R2009b (Version 7.9)	The Mathworks, Natick, MA, USA
Horizontal gel electrophoresis system	No name brand manufacturer
Gel Doc 2000 Gel Documentation System	BioRad, Hercules, CA, USA
JMP, Version 8.0.2.2	SAS Institute, NC, USA
Microsoft Excel 2007	MS Office 2007, Microsoft Corp., USA

Origin, Version 8.1	OriginLab Corporation, Northampton, MA, USA

Tab. 3.3: Instruments and Software used in this study

3.5.2 Disposable Materials and Laboratory Equipment

MicroAmp Optical 96-Well Reaction Plates	Applied Biosystems, Carlsbad, CA, USA
Positively charged and uncharged microscope glass slides, cover glasses	No name brand manufacturer
Accu-Edge Disposable Microtome Blades	Sakura Finetek USA, Torrance, CA, USA
Capsure HS LCM Caps	Arcturus Engineering, Mountain View, CA, USA
Standard Laboratory equipment: Latex and nitrile gloves, pipettes and pipette tips from 0,5µl to 20ml, 1,5ml and 5ml microcentrifuge tubes, falcon tubes, glassware, tabletop vortex, incubation block and centrifuges, refrigerators of 4°-, -8°, -80°, fumehood, dry ice, etc.	

Tab. 3.4: Disposable Materials and Laboratory Equipment used in this study

3.5.3 Reagents, Buffers and Kits

RNase AWAY	Sigma-Aldrich., St. Louis, MO, USA
95% Ethanol (190 proof)	Sigma-Aldrich., St. Louis, MO, USA
99,5% Ethanol (199 proof)	Sigma-Aldrich., St. Louis, MO, USA
RNase-free water	Qiagen, Valencia, CA, USA
Distilled H_20	Sigma-Aldrich., St. Louis, MO, USA
Mayer's Hematoxylin	Sigma-Aldrich., St. Louis, MO, USA
Aqueous Eosin Y	Sigma-Aldrich., St. Louis, MO, USA
Bluing Reagent	Thermo Fisher Scientific, Waltham, MA, USA
10% Formalin solution, neutral buffered	Sigma-Aldrich., St. Louis, MO, USA
Paraffin wax	Sigma-Aldrich., St. Louis, MO, USA
Xylene	Sigma-Aldrich., St. Louis, MO, USA
Tissue-Tek O.C.T. Compound	Sakura Finetek, Torrance, CA, USA
ProtectRNA RNase-Inhibitor 500x	Sigma-Aldrich., St. Louis, MO, USA
M-MLV (Moloney-Murine Leukemia Virus) Reverse Transcriptase	Promega, Madison, WI, USA
RNase-Inhibitor	Promega, Madison, WI, USA
Deoxynucleotide-Triphosphates	New England Biolabs, Ipswich, MA, USA
Random Oligo-deoxyribonucleotide Hexamers	Roche Diagnostics, Indianapolis, IN, USA
DTT, molecular grade	Promega, Madison, WI, USA
SYBR Green PCR Master-Mix	Applied Biosystems, Carlsbad, CA, USA
Agarose	Sigma-Aldrich., St. Louis, MO, USA
DirectLoad DNA 100 basepair Step Ladder	Sigma-Aldrich., St. Louis, MO, USA
Ethidiumbromide 10mg/ml	Sigma-Aldrich., St. Louis, MO, USA
Electrophoresis Gel loading buffer II	Applied Biosystems, Carlsbad, CA, USA
Total Human Breast Tumor DNA	Clontech Laboratories, Mountainview, CA, USA

Stratagene Absolutely RNA Microprep Kit	Stratagene, La Jolla, CA, USA
0,5x TAE buffer prepared with 40x TRIS-Acetate-EDTA Buffer Mix	Promega, Madison, WI, USA
Deuterated H_20 (D2O) used for deuterated phosphate buffered saline (D2O/PBS) solution	Cambridge Isotope Laboratories, Andover, MA, USA
Custom oligonucleotides (Primers)	SABiosciences, Frederick, MD, USA
Ribosomal 18s RNA Primer Assay	SABiosciences, Frederick, MD, USA

Tab. 3.5: Reagents, Buffers and Kits used in this study

Gene name/ Gene/ NCBI RefSeq (NM_*)	Primer sequence	pre-mRNA length (basepair)	Amplicon length (basepair)
Choline Kinase Alpha, transcript variant I CHKA; 001277.2	For: TGCTCAGTTACAATCTGCCCTTGG	3720	134
	Rev: AGAATTCTCTCGGCCTTCCAGCAA		
Choline Kinase Beta CHKB; 005198.3	For: AAGCGTGATGTTCGCCATACTTGC	298	104
	Rev: TCAATGGCCGACTTGGGATGTACT		

Tab. 3.6: PCR primers for Choline Kinases

Gene	Variant	Oligonucleotide sequence	pre-mRNA length (basep)	Amplicon length (bp)
Phosphate cytidylyltransferase 1, Cho-specific, alpha	1	For: GCAACCAGCTCCTTTTTCTG	9567	105
		Rev: ACAGGTCGCTCACAAGGAGT		
PCYT1A	2	For: ACTCCTTGTGAGCGACCTGT	10280	129
005017.2		Rev: GCAAACTCCCACAATGAGGT		
Phosphate cytidylyltransferase 1, Cho-specific, beta	1	For: ACATTCCGTATTCCTCTGCTGGCT	7876	95
		Rev: TGAGATGCCTTCTGTTCTCTGCGT		
PCYT1B	2	For: CCTCAGAAACCATGGAGGAA	28022	118
004845.3		Rev: AGTTTTTCATGGGGTGCTTG		
Choline phosphotransferase 1	1	For: CACCGAAGAGGCACCATACT	16048	92
CHPT1		Rev: CTGGCTTGTTTCCCATCAAT		
020244.2	2	For: GCGCTCATTGGCAGACTTAT	2200	118
		Rev: ATTGTTGCTCCTCCAAATGC		
Phospholipase A2, group IVA (cytosolic, calcium-dependent)	1	For: ACTGCACAATGCCCTTTACC	6656	115
PLA2G4A		Rev: ATTTAGCCATGCCAATTTCG		

024420.2	2	For: TGCAGCTGTAGCAGATCCTGATGA	9159	96
		Rev: AATGTGAGCCCACTGTCCACTACA		
Phospholipase D1, PTDCho-specific	1	For: CAGTGGTTGAGGGAAATCGT	7405	105
PLD1		Rev: GAGCGAGTTCCACCTCTTTG		
002662.2	2	For: GAGGACTTCGGCTACAGTGC	6970	109
		Rev: GAAACCCACACCTCCTTGAA		
Phospholipase D2	1	For: GCTCGATTTGCCGTTGCCTATTCT	887	113
PLD2		Rev: TTCTGTTTGCTGGCTGCATGTCTG		
002663.3	2	For: CAGACATGCAGCCAGCAAACAGAA	313	93
		Rev: TCTGTCATGGCATGGTAGTTGCGA		
Solute carrier family 44, member 1	1	For: ACCGTAGCTGCACAGACATACCAT	10513	100
SLC44A1 (CTL1)		Rev: GCTGCTGCACCTGTTGCTATTGAA		
080546.3	2	For: TCTTGCATTTGTTGCCTTTG	8264	96
		Rev: GCAGAAGTTGGTGCTGTTGA		
Solute carrier family 22, member 1	1	For: CCCTTCATTTGCAGACCTGT	3099	98
SLC22A1 (OCT1)		Rev: GCCCCTGATAGAGCACAGAG		
003057.2	2	For: TCGTCACTGAGTTCAACCTGGTGT	7865	110
		Rev: TGCAAAGTAGCCAACACCGAGAGA		
Solute carrier family 22, member 2	1	For: TCGAGGAAGCCGAAAATATG	7318	114
SLC22A2 (OCT2)		Rev: ACAGCAGCAACGGTCTCTCT		
003058.2	2	For: TGAGCTGTACCCCACATTCA	800	93
		Rev: TAGACCAGGAATGGCGTGAT		
Solute carrier family 5, member 7	1	For: CCTGCACTGATGGGAGAAAT	4830	120
SLC5A7 (CHT1)		Rev: GGCAATGAGTGCAGAGATGA		
021815.2	2	For: GCTCAAGTGCTGTCCTTCCT	2376	120
		Rev: ATCTGGAAGCCCATATGCAG		

Tab. 3.7: Additional rt-q-PCR primer pairs designed for genes in the Kennedy cycle of Choline metabolism; Var. = Primer Design Variant

4 Results

4.1 Metabolite Measurements

4.1.1 High-Resolution Magic-Angle-Spinning ^{1}H-Magnetic Resonance Spectroscopy

HRMAS ^{1}H-MRS metabolite measurements were performed on 18 BrCa tissue specimens and 11 adjacent normal benign specimens. Twenty-three out of twenty-nine HRMAS ^{1}H-MRS measurements were successful, six measurements failed due to technical difficulties with the MAS rotor, problems in data acquisition or in tissue recollection, and were not included in the metabolite dataset. Successfully acquired spectra were processed manually using NUTS software. (Compare Fig. 4.1)

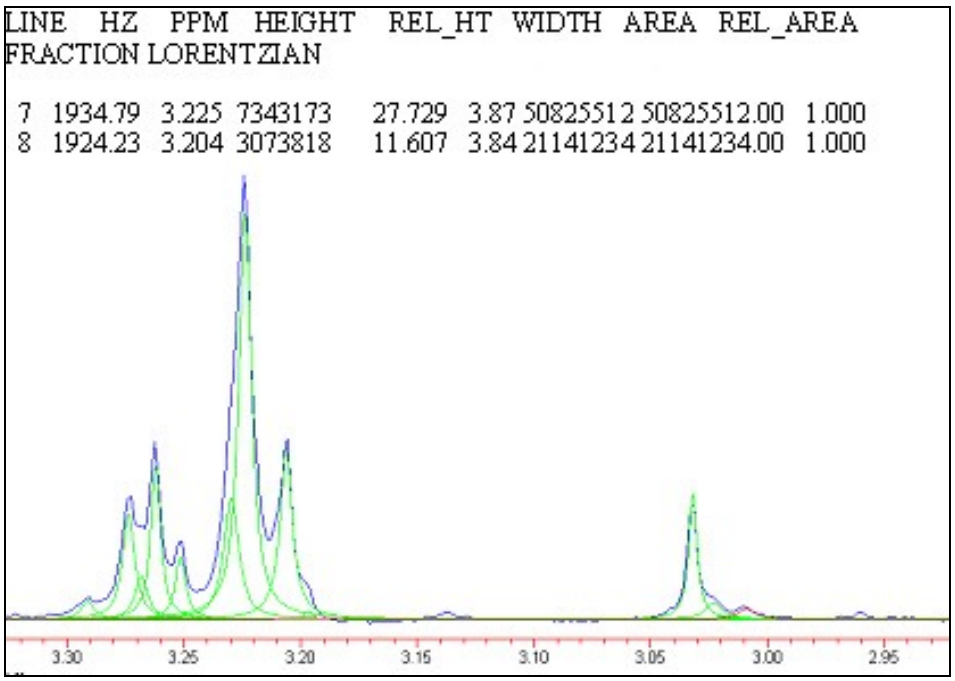

Figure 4.1: Example of line-fitting of spectral peaks in MRS data analysis, magnified image of NUTS software data report.

4.1.2 Histopathological evaluation of MRS specimens

Histopathological analysis of scant samples revealed that tissue pathology assigned upon surgical resection, i.e. tumor or benign as classified by the surgeon in the operating room, in fact was relatively inaccurate. One of the 10 presumed benign specimens from adjacent to the tumor margin in fact contained 45.9% tumor tissue, while three of the 13 presumed carcinoma tissue samples contained no tumor cells. The results of the evaluation are summarized in Tab. 4.1.

Patient	Histopathology					
	LCM/ PCR sample	HRMAS ^{1}H-MRS sample	Volume % tissue composit. of HRMAS ^{1}H-MRS sample			
			tumor	fat	benign stroma	benign epithelium
1	ILC	-				
	benign	benign	0.0	14.8	85.2	0.0
2	ILC	ILC	52.2	13.0	34.8	0.0
	benign	benign	0.0	12.5	82.5	5.0
3	IDC	-				
	benign	-				
4	ILC	ILC	66.6	0.0	33.4	0.0
	benign	benign	0.0	2.6	92.9	4.5
5	ILC	benign	0.0	98.4	1.6	0.0
	benign	benign	0.0	31.3	63.7	5.0
6	IDC	IDC	61.9	6.4	31.7	0.0
	benign	benign	0.0	47.3	44.2	8.5
7	IDC	IDC	45.9	0.0	54.1	0.0
	benign	IDC	100.0	0.0	0.0	0.0
8	IDC	-				
	benign	benign	0.0	10.0	80.0	10.0
9	ILC	-				
	benign	benign	0.0	4.3	95.7	0.0
10	IDC	IDC	23.4	17.3	59.3	0.0
	benign	benign	0.0	5.0	83.2	11.8
11	IDC	IDC	55.7	0.0	44.3	0.0
	benign	benign	0.0	0.0	100.0	0.0
12	ILC	benign	0.0	8.0	92.0	0.0
13	IDC	IDC	71.3	0.7	28.0	0.0
14	ILC	ILC	46.7	11.7	41.6	0.0
15	ILC	benign	0.7	50.7	48.5	0.0
16	IDC	benign	0.0	0.0	100.0	0.0
17	ILC	-				
18	ILC	ILC	65.1	12.5	22.3	0.0

Tab. 4.1: Results of histopathological analysis of HRMAS samples

4.2 Gene Expression Measurements

The aim of the second part of this study was to examine differences in gene expression of CHKA and CHKB within the tissue microenvironment of benign tissue, IDC and ILC. 29 tissue specimens were processed according to the protocol described in section 3.3.

4.2.1 Laser-Capture Microdissection

LCM serial sectioned tissue samples contained highly variable amounts of tumor and benign epithelial cells, ranging from a few hundred to several thousand such cells per section. Initial test runs of the PCR protocol with cDNA from different numbers of microdissected cells had shown that a minimal number of approximately 5000 cells (5000 LCM laser pulses, assuming that each pulse yields one cell on average) were sufficient for measurements in the desired range. LCM was performed on sets of between 2 and 10 adjacent serial sections per sample, depending on the amount of cells within the sections, until the necessary quantity of cells was captured. Figure 3.2 illustrates the LCM process.

4.2.2 RNA Isolation and Quality Control

RNA from microdissected cells was isolated with the Stratagene Absolutely RNA Microprep Kit, and transcribed to cDNA as described in section 2.3.2. Initially, 5 samples did not reach the spectrophotometric quality control threshold, the reason for which could be protein contamination or RNA degradation. In these 5 cases, the protocol was started over, beginning with laser capturing, until a satisfactory amount of intact RNA was obtained.

4.2.3 Quantitative Real-Time PCR

Gene expression levels of CHKA and CHKB were measured in 29 tissue samples, 18 of which contained BrCa cells, and 11 contained solely benign cells.

4.2.4 Data Analysis

Cho and PCho metabolite concentrations, as well as CHKA and CHKB gene expression levels were compared among benign breast tissue, and BrCa specimens were grouped according to histopathological tumor type (benign tissue, ILC, and IDC) and grade (grade 1-3); owing to the small sample size of grade 1 tumors (n=1), tumor tissue specimens of grades 1 and 2 (n=6) were grouped as low-grade tumors (n=7), and compared to high-grade (grade 3) tumors (n=3).

In the following figures of metabolite analyses, means and standard deviations are graphed as lines in blue color; medians, quantiles, and minimum-maximum spans are displayed in red box plots.

4.3 Metabolite Concentrations

4.3.1 Benign Tissue, Low-Grade and High-Grade Invasive Carcinoma

When compared to normal benign breast tissue, PCho metabolite concentrations were significantly increased by 279% ($p<0.05$) in low-grade BrCa, and by 152% in high grade BrCa ($p<0.02$).

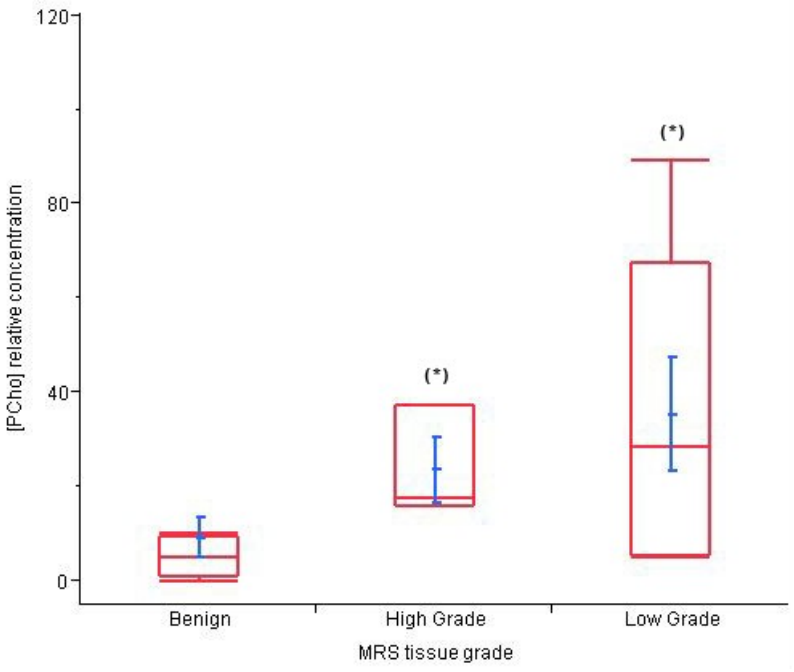

Figure 4.2: Metabolite concentrations of PCho in benign breast tissue, low-grade and high-grade BrCa.

Quantiles							
Tissue type	**Minimum**	**10%**	**25%**	**Median**	**75%**	**90%**	**Maximum**
Benign	0	0.123685	1.214061	5.022025	9.719767	3.991034	5.964109
High Grade	16.00376	16.00376	16.00376	17.66602	37.34669	37.34669	37.34669
Low Grade	5.20367	5.20367	5.536351	28.60188	67.68566	89.48103	89.48103
Means and Standard Deviations							
Tissue type	**Count**	**Mean**	**St Deviation**	**St Error of Mean**	**Lower 95% KI**	**Upper 95% KI**	
Benign	13	9.3573	15.6095	4.329	-0.576	18.790	
High Grade	3	23.6722	11.8716	6.854	-5.819	53.163	
Low Grade	7	35.4203	31.9776	12.086	5.846	64.995	

Tab. 4.2: Descriptive Statistics of Figure 4.2

Cho tissue metabolite concentrations exhibited no statistically significant changes when compared to normal benign specimens.

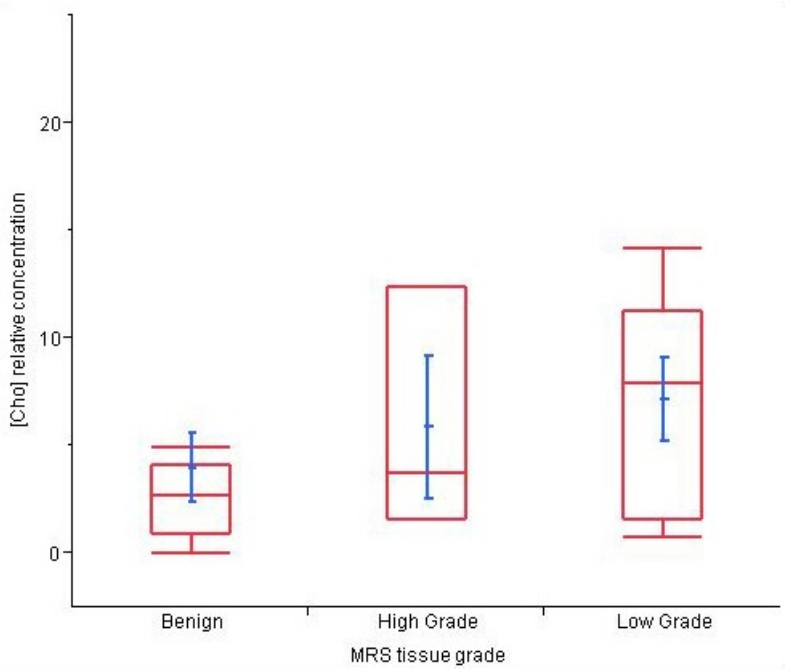

Figure 4.3: Metabolite concentrations of Cho in benign breast tissue, low-grade BrCa, and high-grade BrCa.

Quantiles							
Tissue type	**Minimum**	**0,1**	**0,25**	**Median**	**0,75**	**0,9**	**Maximum**
Benign	0	0	0.93465	2.73704	4.128351	15.40821	22.37778
High Grade	1.566872	1.566872	1.566872	3.75153	12.41474	12.41474	12.41474
Low Grade	0.766464	0.766464	1.562058	7.960365	11.25529	14.20304	14.20304
Means and Standard Deviations							
Tissue type	**Count**	**Mean**	**St Deviation**	**St Error of Mean**	**Lower 95% KI**	**Upper 95% KI**	
Benign	13	4.01133	5.76408	1.5987	0.528	7.495	
High Grade	7	5.91105	5.73731	3.3124	-8.341	20.163	
Low Grade	7	7.19122	5.06693	1.9151	2.505	11.877	

Tab. 4.3: Descriptive statistics of data presented in figure 4.3

4.3.2 Benign Tissue, Invasive Ductal and Invasive Lobular Carcinoma

In IDC PCho metabolite concentrations were elevated by 315% over normal benign tissue on average ($p<0.01$). In ILC, the PCho concentration average showed a trend towards elevation by 129% over normal benign tissue ($p=0.0617$).

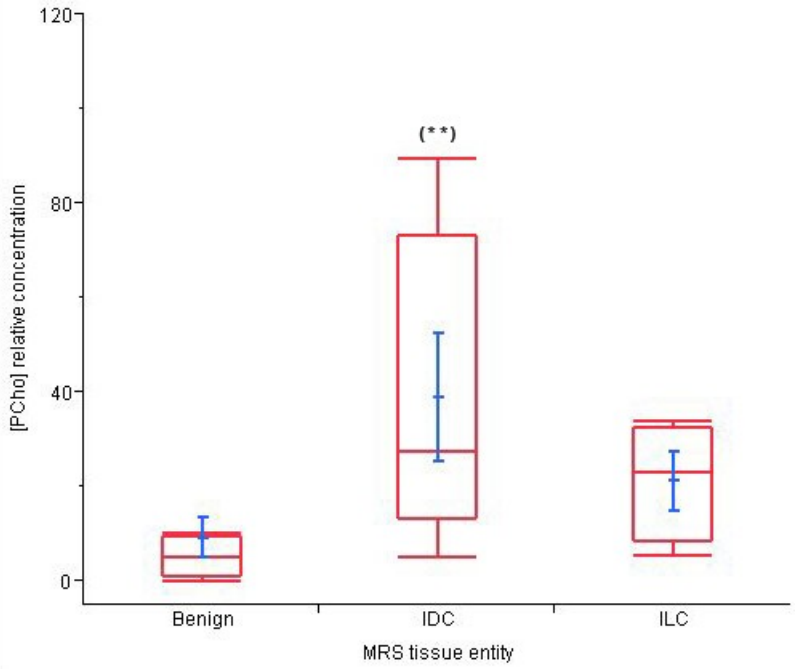

Figure 4.4: Relative metabolite concentrations of PCho in benign breast tissue, invasive ductal carcinoma (IDC) and invasive lobular carcinoma (ILC).

Quantiles							
Tissue type	**Minimum**	**0,1**	**0,25**	**Median**	**0,75**	**0,9**	**Maximum**
Benign	0	0.123895	1.214061	5.022025	9.719767	39.91034	59.64109
IDC	5.20367	5.20367	13.30374	27.48698	73.1345	89.48103	89.48103
ILC	5.536351	5.536351	8.568768	23.13395	32.50515	33.80624	33.80624
Means and Standard Deviations							
Tissue type	**Count**	**Mean**	**St Deviation**	**St Error of Mean**	**Lower 95% KI**	**Upper 95% KI**	
Benign	13	9.3573	15.6095	4.329	-0.075	18.790	
IDC	6	38.8913	33.1713	13.542	4.080	73.702	
ILC	4	21.4026	12.3503	6.268	1.457	41.349	

Tab. 4.4: Descriptive statistics of data presented in figure 4.4.

Cho concentrations in BrCa were not statistically elevated when compared to normal benign specimens.

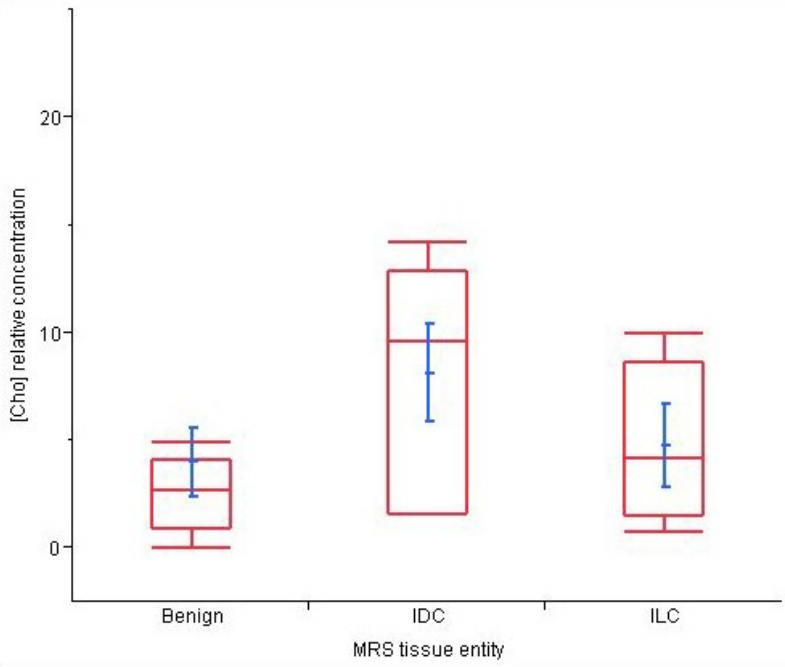

Figure 4.5: Relative metabolite concentrations of Cho in benign breast tissue, invasive ductal carcinoma (IDC) and invasive lobular carcinoma (ILC).

Quantiles							
Tissue type	**Minimum**	**0,1**	**0,25**	**Median**	**0,75**	**0,9**	**Maximum**
Benign	0	0	0.93465	2.73704	4.128351	15.40821	22.37778
IDC	1.562058	1.562058	1.565669	9.60783	12.86181	14.20304	14.20304
ILC	0.766464	0.766464	1.51273	4.164272	8.654971	10.01429	10.01429
Means and Standard Deviations							
Tissue type	**Count**	**Mean**	**St Deviation**	**St Error of Mean**	**Lower 95% KI**	**Upper 95% KI**	
Benign	13	4.01133	5.76408	1.5987	0.528	7.495	
IDC	6	8.16039	5.49989	2.2453	2.389	13.932	
ILC	4	4.77732	3.85596	1.9280	-1.358	10.931	

Tab. 4.5: Descriptive statistics of data presented in figure 4.5.

4.4 Choline Kinase Gene Expression

Means of gene expression levels in microdissected normal benign epithelia (graphed in black) were used as baseline, while expression levels in tumors were calculated relative to the benign baseline according to the $2^{-\Delta\Delta Ct}$ method as described by Schmittgen in 2001. [159]

4.4.1 Benign Tissue, Low-Grade and High-Grade Invasive Carcinoma

CHKA expression was elevated by 142,5% in low grade BrCa samples, and by 5,2% in high grade BrCa when compared to baseline benign samples. CHKB was lower in BrCa than in benign tissue: Low grade BrCa showed 41,9% lower expression levels, while high grade BrCa contained 37,2% lower levels.

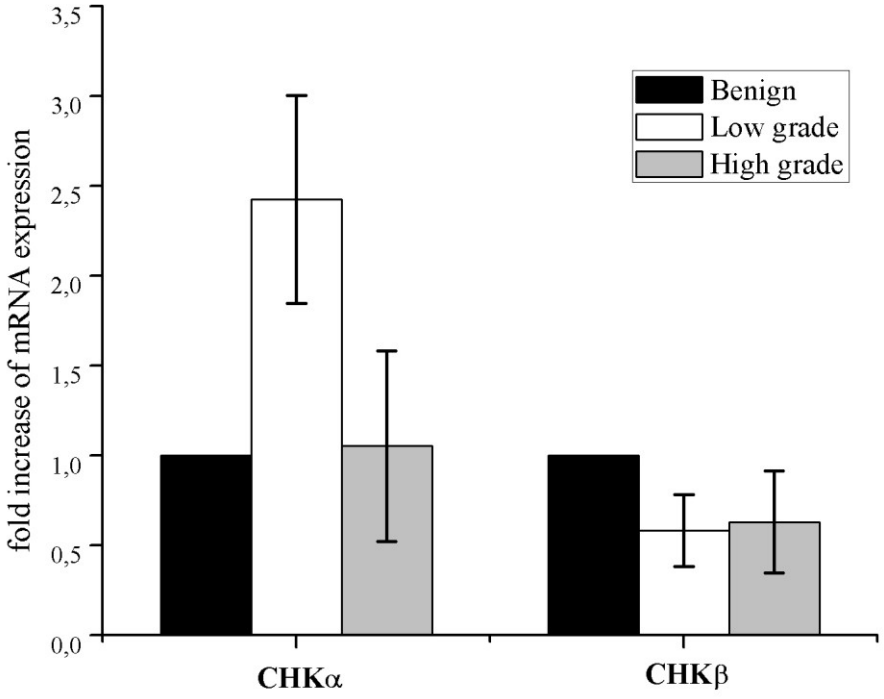

Figure 4.6: Expression levels of CHKA and CHKB in benign breast tissue, low grade and high grade carcinomata.

4.4.2 Benign Tissue, Invasive Ductal and Invasive Lobular Carcinoma

Expression levels of CHKA were elevated by 92,4% in IDC and by 85,9% in ILC when compared to the benign baseline. CHKB was 44,4% lower in ILC, and 14,7% lower in IDC than the benign baseline.

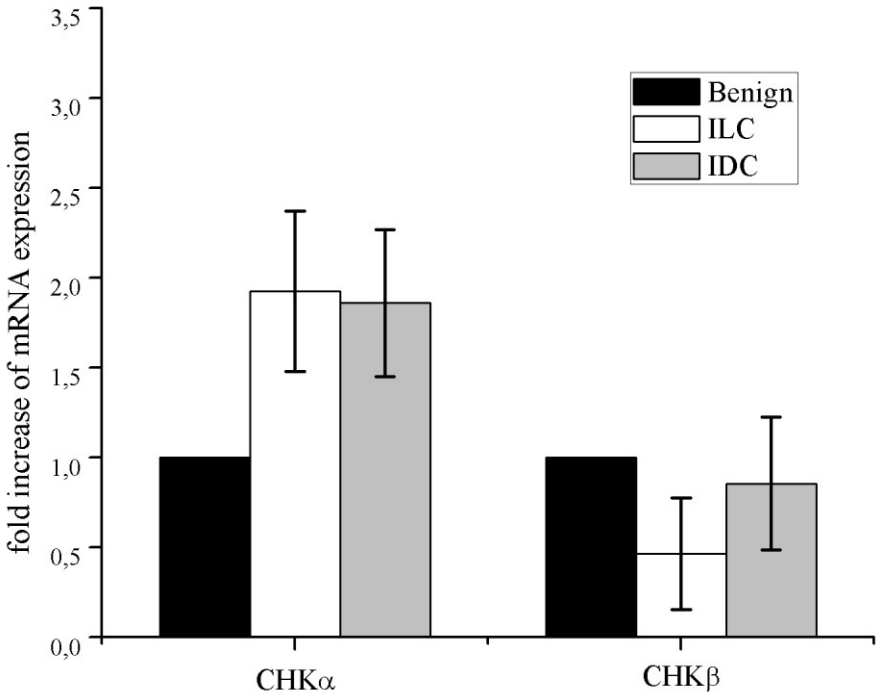

Figure 4.7: Expression levels of CHKα and CHKβ in benign breast tissue, invasive ductal carcinoma (IDC) and invasive lobular carcinoma (ILC).

4.5 Correlation Analyses

4.5.1 Correlation of Choline and Phosphocholine Metabolite Concentration

A correlation was found between Cho and PCho metabolite concentrations in all specimens (r^2= 0.701, p<0.001).

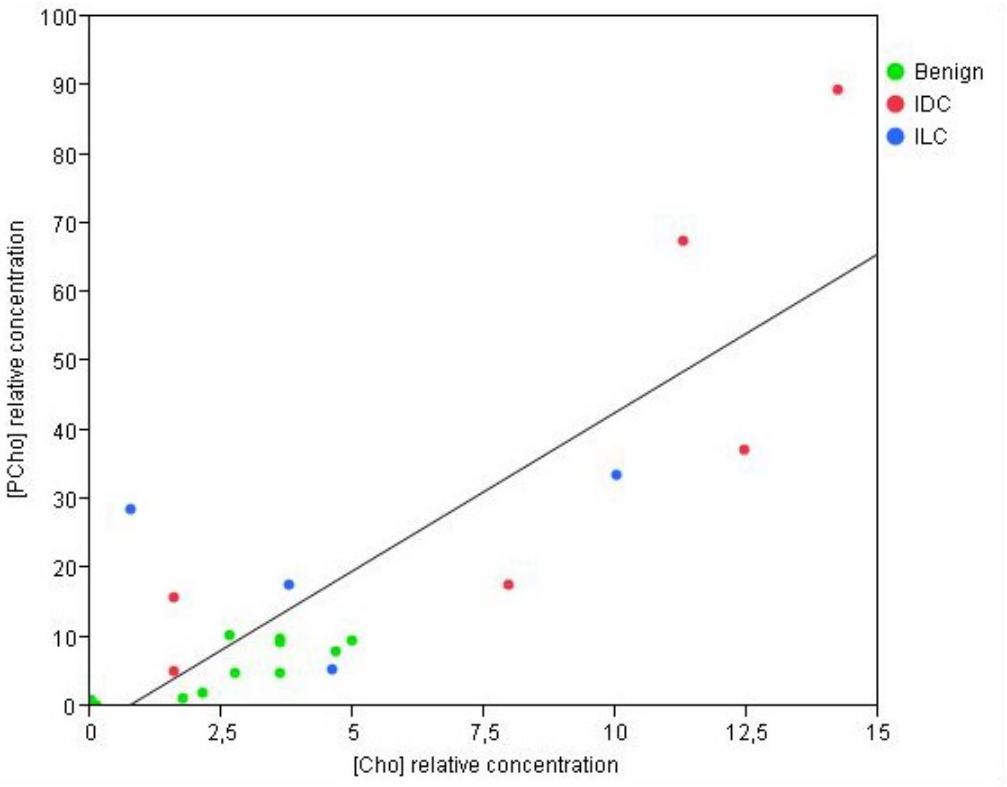

Figure 4.8: Correlation analysis of Cho and PCho tissue metabolite concentrations. Sample tissue entity is indicated by color (benign, IDC and ILC).

Summary of Fit				
3,225 = 3,110887 + 4,5931815 * 3,204				
r^2	**0.701382**	Root mean square error		12.69193
r^2 corrected	**0.686451**	Mean value		17.31649
Analysis of Variance				
	Degrees of freedom	Sum of squares	Mean squares	F-value
Model	1	7567.012	7567.01	46.9752
Error	20	3221.703	161.09	
K. sum	21	10788.715		
Prob > F	**<0.0001**			
Parameter Estimate				
	Estimate	Std. error	T-value	**Prob > |t|**
Intercept	-3.110887	4.025542	-0.77	**0.4487**
[Cho]	4.5931815	0.670161	6.85	**<0.0001**

Tab. 4.6: Descriptive statistics of data presented in figure 4.8.

4.5.2 Correlation of Choline Kinase Alpha Expression and Phosphocholine Metabolite Concentration

CHKA gene expression was correlated to PCho metabolite concentration (r^2= 0.532; p=0.04).

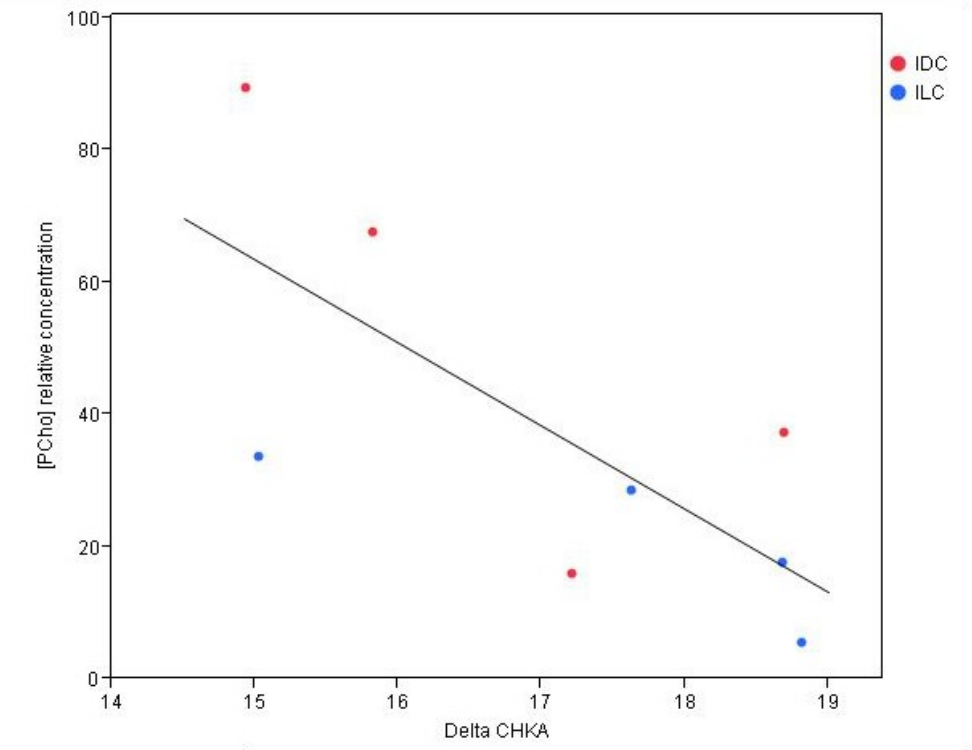

Figure 4.9: Correlation analysis of CHKA expression and PCho concentration in BrCa. CHKA expression is displayed as Delta CT, i.e. difference to the rt-q-PCR "reference housekeeping gene"; the scale is an inverse logarithmic scale of RNA concentration. BrCa subtypes IDC and ILC are indicated by color.

Summary of Fit				
3,225 = 251.30866 + 12.532692 * Delta CHKA				
r^2	**0.531968**	Root mean square error		20.86559
r^2 corrected	**0.453963**	Mean value		37.01595
Analysis of Variance				
Source	Degrees of Freedom	Sum of Squares	Mean Squares	F-value
Model	1	2969.0844	2969.08	6.8196
Error	6	2612.2360	435.37	
K. sum	7	5581.3204		
Prob > F	**0.0400**			
Parameter Estimate				
	Estimate	Std. error	T-value	**prob > |t|**
Intercept	251.30866	82.39002	3.05	**0.0225**
Delta CHKA	-12.53269	4.799143	-2.61	**0.0400**

Tab. 4.7: Descriptive statistics of data presented in figure 4.9

4.5.3 Correlation of Breast Cancer Histopathological Composition and Metabolite Concentrations

The histopathological composition of the tumor specimen, i.e. the amount of benign and malignant tissue within the specimen, did not show any association to either Cho or PCho metabolite concentrations.

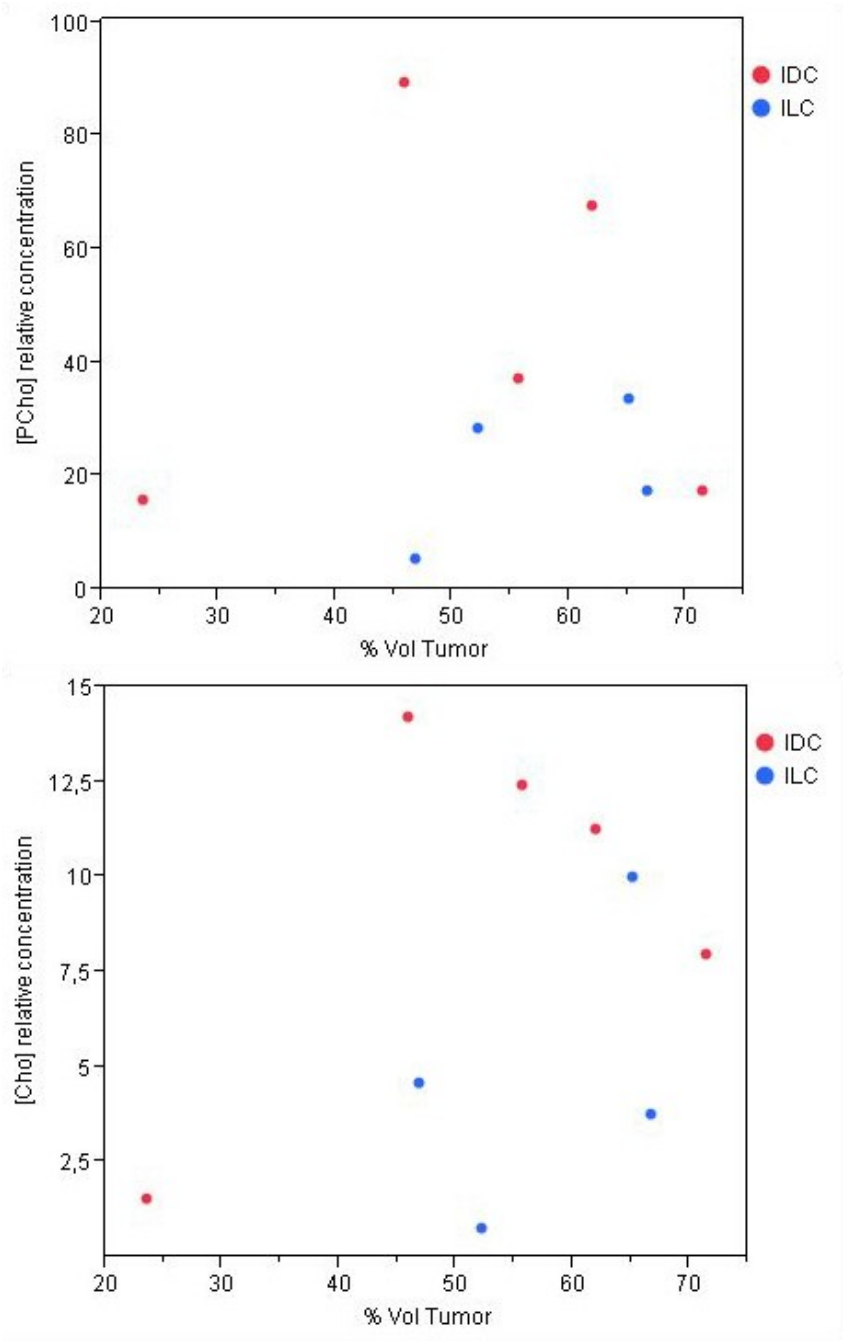

Figure 4.10: The Volume% content of tumor cells within BrCa tissue samples is not associated with metabolite concentrations of Cho or PCho. BrCa type is indicated by color.

5 Discussion

This section will discuss the following aspects of this work: Initially, a brief review of what was done, together with a synopsis of the most important results will be provided. Secondly, previous studies on the subject will be reviewed, followed by an evaluation of the study design and the methods used in this study. After that, the results of this study will be discussed in detail in the order of their appearance in section 3. Finally, limitations to the results will be pointed out, and an outlook on the future of 1H-MRS and the relevance of the results of this study will be given.

5.1 What Was Done and What Was Found

This study was undertaken to explore human BrCa Cho metabolism in detail, and to compare normal benign human breast tissue with IDC and ILC BrCa tissue. Individual metabolite concentrations of Cho and PCho were quantified ex-vivo at high resolutions by using HRMAS ^{1}H-MRS.

CHKA and CHKB, the genes encoding for the enzymes that catalyze the intracellular phosphorylation of Cho to PCho, have repeatedly been found to be over-expressed, and seem to play a central role in altered Cho metabolism in BrCa. CHKA and CHKB gene expression was measured in LCM-dissected normal benign glandular epithelia and tumor cells by using rt-q-PCR.

When compared to benign breast tissue, PCho metabolite concentrations were increased by 279% in low-grade BrCa ($p<0.05$), and by 152% in high grade BrCa ($p<0.02$). When comparing benign breast tissue to BrCa grouped by histological type, PCho metabolite concentrations were elevated by 315% ($p<0.01$) in IDC, and concentrations in ILC showed a trend towards elevation (129%; $p=0.0617$). Changes in Cho metabolite concentrations were not statistically significant.

Compared to normal benign samples, expression levels of CHKA were pronouncedly increased in BrCa samples of IDC (92.4%) and ILC (85.9%) types. Grouped by histological grade, expression was elevated in low grade tumors (142.5%). CHKB expression was not elevated in any tumor group.

Correlation analysis between the measured variables showed a strong correlation between Cho and PCho metabolite concentrations ($p<0.0001$; $r^2= 0.701$). Furthermore, CHKA expression and PCho concentration levels were correlated ($p<0,0079$;$r^2= 0.316$.).

5.1 Previous Studies

Previous studies of Cho metabolism in BrCa can mostly be grouped into two categories: The first group of studies quantified Cho concentrations in BrCa lesions using in-vivo 1H-MRS, and some of the studies evaluated tissue histopathology after removal of biopsies or of larger tissue sections. In so doing, changes in Cho metabolism were correlated to tissue pathology and assessed as diagnostic markers. While these studies fulfilled the purpose of relating changes of Cho metabolite concentrations to the underlying tissue pathologies, they could not address the question of the microscopic origin of the changes, or more specifically, which cells within the tumor contained altered concentrations of metabolites. Furthermore, most of the in-vivo metabolite measurements were limited in spectral resolution, and could not quantify Cho and PCho separately, but only tCho as a whole.[27-29,164,165]

The second group of studies aimed at evaluating changes of Cho metabolism on the molecular level; to the author's knowledge, all except one study were based on BrCa cell-cultures. They succeeded in demonstrating several mechanisms involved in the alterations of Cho metabolism in BrCa. Higher expression levels of CHKA were repeatedly found to strongly influence metabolism of Cho, and had a direct influence of BrCa proliferation. Yet, the conclusions that can be drawn from cell cultures are only limited, as they are only a reductionist representation of the complex tumor environment of human BrCa.[39, 87,100,101,105,107,166]

Sitter et al. published a study in 2006, resembling the first part of this study. Ex-vivo high resolution ^{1}H-MRS was used to quantify Cho and PCho metabolite levels in BrCa and in adjacent normal benign specimens, and tissue was subsequently analyzed microscopically. The study showed that histopathological tissue type and sample composition are directly correlated to metabolite concentrations. The results showed that metabolite concentration is directly correlated to the presence or absence of cancer cells.[97]

5.2 Study Design

This study was designed to overcome the limitations identified in cited previous works: Human tissue specimens of BrCa and adjacent normal benign tissue were used; one half of each

specimen was used for metabolite measurement, the other half for measurements of gene expression. Both parts of the study accounted for the complex and often diffuse invasive growth patterns of BrCa, which lead to largely mixed areas of benign and cancer cells within the tumor.

Firstly, Cho and PCho metabolite concentrations were quantified and compared to the histopathological specimen composition; in doing so, the question of whether metabolite concentrations were associated with increased amounts of tumor in the area of interest, i.e. whether changes in metabolite concentrations indicated invasive tumor growth, or whether they occurred similarly in adjacent normal benign tissue, was addressed.

Analogous to this, gene expression levels were measured in BrCa and normal benign epithelial cells: Because of the diffusely invasive BrCa growth, and the common mixed areas of benign and cancer cells, BrCa and normal benign epithelia were separated using LCM. Microdissected cells were subsequently processed and prepared for further analysis using rt-q-PCR; the use of LCM allowed for posing the question if the changes in gene expression of CHK occurred in cancer epithelia only, or if this was the case in normal benign cells as well.

Various forms and subtypes of BrCa exist, each of them with distinct features, such as characteristic macroscopic and microscopic growth patterns, genetic aberrations and varying prognoses. So far, these subtypes have not been investigated for differences in their Cho metabolism. Therefore, this study included and differentiated between the most frequently occurring types of BrCa, according to their histopathological entity (IDC and ILC) and histological tumor grade (grades 1-3).

During surgery, the distinction between tumor margins and adjacent normal benign tissue can be difficult. In this study, surgical sample characteristics were controlled by histological evaluation. Moreover, diffuse invasive growth of BrCa can often lead to invasive tumor tissue intermixed with benign cells and stroma. This was taken into account by careful evaluation of the sample tissue composition. The tissue entity in several samples turned out to be erroneously classified, and had to be reclassified according to the histopathological results.

5.3 Methods

5.3.1 HRMAS ^{1}H-MRS Metabolite measurements

HRMAS ^{1}H-MRS is an ex-vivo technique that allows for the measurement of high resolution metabolite spectra in tissue samples. It allows for the differentiation of individual metabolites that would not be possible in-vivo ^{1}H-MRS, where spectral resolution is lower. In-vivo ^{1}H-MRS cannot resolve the metabolites that make up the composite resonance signal tCho. HRMAS ^{1}H-MRS on the other hand, can individually quantify Cho and PCho in tissue samples ex-vivo. Owing to the nature of the experiment, HRMAS ^{1}H-MRS metabolite measurements can only be performed once per biological sample. Repeated or extended measurements on the same sample lead to tissue degradation and alterations of metabolite concentrations. Several previous studies have employed the method for high resolution metabolite measurements in intact BrCa and other human tissue specimens.[95,96,98,168] Cheng et al. have previously shown that the storage of human prostate tissue samples at -80°C for up to 3 years only had a small effect on metabolite concentrations.[152] Furthermore, Cheng et al. have previously demonstrated the feasibility of a combination of HRMAS 1H-MRS metabolite measurements with subsequent recovery of the specimens for histopathological evaluation of the composition on a number of different human tissue types.[41,119,121,122]

5.3.2 Reverse-Transcriptase Quantitative Real-Time PCR

In the second part of the study, LCM was used to dissect, and to separately collect BrCa cells and normal benign epithelia. In the last decade, LCM has been developed as a tool to separate cells from other surrounding tissue at microscopic resolution and at the scale of a single cell. It enables the excision of one or more cells or cellular structures from within a tissue serial section; excised cells can be subject to further analyses to determine where within a tumor which molecular processes are taking place.[169]

Rt-q-PCR is a widely established method for the quantification of gene expression levels. Previous investigations have analyzed CHK gene expression in BrCa cell cultures using rt-q-PCR, and have shown that either CHK expression levels or enzymatic activity, or both, were elevated in numerous different types of BrCa cells.[42, 88, 103] In this study, the fluorescent dye SYBR green was used to visualize and measure the amplification process.[160] The evaluation of the resulting fluorescence data is an area of ongoing development. Traditional methods used quantitative or semi-quantitative approaches; among them, the $2^{-\Delta\Delta Ct}$-method, originally

developed by Schmittgen et al. is among the most widely used to date.[159] In this study, a custom software tool based on the model originally proposed by Liu et al. was used to account for 100% amplification efficiency of rt-q-PCR reactions and measurements.[162,163,170]

5.4 Results

5.4.1 Hypothesis 1: Metabolite Concentration

PCho levels were significantly elevated in low-grade and high-grade BrCa, as well as in IDC and ILC, when compared to adjacent normal benign breast tissue, confirming our first hypothesis. Elevations of PCho were more pronounced in IDC, and in low-grade tumors, when compared to normal benign tissue. Meanwhile, changes in Cho metabolite concentrations, which were generally increased in tumor specimens, did not reach statistical significance when comparing cancerous and normal specimens.

Metabolite concentrations in BrCa specimens exhibited a relatively large variance (compare figures 4.2 – 4.5), as has been reported in previous studies of Cho and PCho metabolite concentrations in different cell culture-, and human tissue-based comparisons of BrCa and normal benign breast tissue.[88, 90, 91] PCho concentrations fluctuated between different BrCa cases. In theory, only ceratin BrCa lesions, or even only areas within a BrCa lesion, might exhibit elevated PCho concentrations when compared to adjacent normal benign tissue. At the same time, other malignant lesions of the breast, or parts of them, might not show any elevation of PCho concentrations. The factors influencing these metabolic distributions remain to be defined.

In-vivo 1H-MRS has been reported to be able to diagnose BrCa at a specificity and sensitivity of up to 100%.[13, 34] The results of this study raise doubt about this notion: Although mean metabolite concentrations of BrCa specimens were elevated in comparison to normal benign breast tissue, some BrCa specimens exhibited metabolite concentrations in the range of benign tissue; for these cases metabolic information would not have helped in the diagnosis.

A major difference between in-vivo and ex-vivo MRS is resolution, both spectral and spatial. In-vivo MRS at currently common clinical magnetic field strengths of 1.5T is limited to the measurement of metabolites in tissue voxels of a minimal volume of 1 cm^3; in this study, metabolites were quantified in ex-vivo specimens smaller than 50 mm^3. Relatively large voxel sizes in in-vivo 1H-MRS, along with lower SNR, might be the reason that fluctuations of individual Cho metabolites within a voxel, or within a tumor, are averaged out. The question

arises, whether higher spectral and spatial resolution can lead to better results in the diagnostic procedure, or whether there is an optimal voxel size and SNR at which to perform metabolite measurements.

Metabolite concentrations of Cho and PCho in both BrCa and normal benign specimens showed a strong correlation: On average, increases of Cho were accompanied by almost 4.6-fold increases of PCho ($r^2 = 0.701$) (compare figure 4.8 and table 4.6). This result is in line with previous research, showing that while PCho is the main accumulating metabolite in BrCa, Cho also increases.[42, 43, 99]

5.4.2 Hypothesis 2: Histopathology and Metabolite Concentration

As to the second hypothesis, which states that histopathological composition of the tissue sample (Volume% of tumor cells in BrCa) is associated with elevated metabolite concentrations of Cho and PCho, no such association was found (compare figure 4.10). This implies that PCho and Cho concentrations are not only highly variable, but also independent of tissue histopathology. It has previously been proposed that metabolite concentrations in different tissues frequently undergo changes, even before a change in tissue differentiation becomes visible, a notion which requires more in-depth research of tissue metabolism.[96]

In 2010, Sitter et al. published a study, of which the authors had no knowledge at the time of investigation, using a similar design as the first part of this study. Ex-vivo metabolite measurements showed that PCho and tCho metabolite concentrations were strongly and directly correlated to the Volume% of tumor within the tissue specimen.[98] These findings would very well support our second hypothesis. In comparing the two studies, it seems noteworthy to compare one methodic difference: In the present study, the whole specimen was serial sectioned at 100 μm intervals, in order to reconstruct its complete composition. For the same step, Sitter et al. analyzed only a single serial section from the middle of the tissue specimen and took it as representative of the rest of the specimen. Despite this possible confounder, Sitter et al. have shown what we had hypothesized, but did not find. Further research will be necessary to substantiate these results.

Analysis of the histological tissue composition revealed that not all specimens contained what was expected according to labels made in surgical resection: 1 of the 10 presumed normal benign specimens collected from the surgical margin adjacent to the tumor in fact contained 45.9% tumor tissue, while 3 of the 13 samples which had been labeled as carcinoma tissue contained no tumor cells whatsoever. The rest of the BrCa specimens contained mixed

amounts of tumor, normal benign epithelia and stroma. As invasive BrCa tends to grow diffusely, nests of tumor cells can often be found intertwined with areas of benign breast tissue. Specimens taken from close to the margins of resection are especially prone to contain mixtures of different tissue types, as has been reported previously.[97] These apparent inaccuracies in macroscopic tissue evaluation demonstrate that it is essential to perform a thorough histopathological analysis of tissue specimens.

5.4.3 Hypothesis 3: Choline Kinase Gene Expression

CHKA expression levels were significantly higher in IDC and ILC of low histological tumor grade (grade 1 and grade 2) when compared to normal breast tissue, while high grade tumors showed no increase of CHKA over normal tissue specimens. At the same time, CHKB expression was lower in all tumors in comparison to normal samples. These results confirm our hypothesis, stating that gene expression differs between normal benign breast tissue and different types of BrCa tumors. (Compare figures 4.6 and 4.7)

CHKA and CHKB gene expression was quantified in microdissected human BrCa cells and adjacent normal breast tissue glandular epithelia, while distinguishing between the histological grades and subtypes of BrCa. The results show differences in CHKA expression in comparison of benign normal breast tissue to IDC and ILC BrCa tissue, as well as between benign and low grade BrCa tissue. At the same time, CHKA expression levels did not differ significantly between IDC and ILC subtypes. CHKB, which had previously also been described as less relevant in metabolic alterations in BrCa, was under expressed when compared to normal benign tissue, representing another novel finding.

Ramirez de Molina et al. measured expression and activity levels of CHK in 53 BrCa specimens without further differentiation of CHKA and CHKB: CHK was over expressed in 17.5% of the specimens, and CHK activity was increased in 38.5% of BrCa specimens. In the study, expression levels of CHK activity increased stepwise with increasing malignancy, and correlated highly with histological tumor grade.[94] This finding is contrasted by our results, in which CHKA was over expressed in low-grade tumors, whereas high grade tumors exhibited equal expression levels to the benign baseline. In 2004, Glunde et al. found significantly elevated concentrations of PCho and tCho in combination with a 4,27-fold increase in CHK expression in cultured BrCa cells. These findings are congruent with the results of this study, which also found increased concentrations of CHKA and PCho in BrCa specimens. In 2007, Eliyahu et al. published a comparison of Cho metabolism and CHK activity in 5 BrCa cell

lines with a normal benign human mammary epithelial cell line. BrCa cells exhibited between 8 - 13 fold higher expression levels of CHKA, while CHKB was only moderately elevated in 2 out of 5 cell lines. These results underline the central role of an elevated expression of CHKA, associated with altered metabolism in the Kennedy cycle, which is mostly in line with the results of this study.[42, 43]

Cell culture models and results based on these models are not only a limited representation of the tumor environment within the human organism, but also do not allow for any correlation of clinical information. Overall, the changes in gene expression measured by Glunde et al. and Eliyahu et al. in cultured BrCa cells are several fold higher than the changes found in real human BrCa and in normal benign breast tissue in the present study. This relatively large variation of gene expression levels between cell lines can occur in a similarly large range in different human BrCa tumors, or possibly even within a single tumor itself.

5.4.4 Hypothesis 4: Gene Expression and Metabolite Concentration

Tumor specimens exhibited a strong positive correlation between PCho and CHKA ($r^2 = 0.32$, compare figure 4.9). This association was herein demonstrated for the first time in human BrCa tissue and supports what had previously been shown in cell culture models of BrCa: Increased expression levels of CHKA are associated with increased tissue metabolite concentrations of PCho, consistent with the fourth hypothesis of this study.[104] Meanwhile, no correlation was found between CHKB and metabolite concentrations, or between gene expression levels and concentrations of Cho. In addition to the lack of other previous supporting evidence, this further points to a role for CHKA as regulatory agent in Cho metabolism in BrCa.

5.5 Limitations

When interpreting the results of this study, several limitations should be considered: Firstly, because of the large amount of time required to process each sample, this study was limited to 29 samples in total. Of those, only 3 cases were high-grade BrCa, and 4 were ILC BrCa. Because of the small sample size, these results can only be seen as an indication of how a larger sample might be distributed. Larger studies of CHKA gene expression and Cho metabolism in BrCa will be necessary to verify the results.

Several authors have suggested a direct causal relationship between the cellular metabolism and homeostasis of Cho and PCho and expression levels of CHKA, which are in turn known to be regulated by other proteins, such as the Ras family of GTPases.[171] Efforts to develop

CHKA as a molecular target for the treatment of BrCa in various research groups are under way; these studies are based on the premise that a causal connection exists between CHKA gene expression and metabolite concentrations in the real tumor environment.[167] The results of this study, in which human BrCa and normal benign breast tissue was used match with this hypothesis, and could be seen as indicative of such a relationship. Yet, considering the high variance of the results in this and in previous studies, significant uncertainty remains regarding the degree to which CHK expression and metabolism are altered in BrCa. Larger studies of human tumor samples are needed to reach a deeper understanding of the distribution across the population, and to identify factors influencing the changes.

5.6 ^{1}H-MRS Metabolite Measurements in the Current Diagnostic Evaluation of Breast Cancer

In recent years, in-vivo ^{1}H-MRS has been thoroughly investigated and has become a diagnostic tool that is used in combination with DCE-MRI in the diagnosis of BrCa. Previous studies have described different variants of in-vivo ^{1}H-MRS of the breast. Technical variables with direct influence on the quality of metabolite measurements have been summarized in an overview article by Stanwell and Mountford. [27] As the technical aspects of in-vivo MRS are evolving, standard practice protocols will be necessary to facilitate the adoption of ^{1}H-MRS into clinical routine.[27, 173, 174]

Metabolite concentrations are objective measures, and are thus not susceptible to errors in interpretation, unlike an MR image. If established as a routine diagnostic marker, they could potentially aid less experienced radiologists in the evaluation of MRIs of suspicious breast lesions. When DCE-MRI is performed on a patient, simultaneous metabolite quantification using in-vivo ^{1}H-MRS can have a decisive impact on the result of the diagnosis, without causing further distress to the patient. The prolongation of scan time by a few minutes that is required for an in-vivo ^{1}H-MRS exam will certainly be compensated by the possible benefit of avoiding unnecessary invasive procedures or wrong diagnoses.

While holding the potential to improve the quality of BrCa diagnostics, metabolite measurements have also contributed to the ongoing efforts to unravel the molecular alterations responsible for the development of BrCa. The Kennedy pathway was initially discovered as altered in in-vivo 1H-MRS in BrCa, and proved to be a molecular route for novel diagnostic and possibly even therapeutic potential. Thus, metabolite measurements not only offer valuable in-

formation for the individual patient, they can also open up new routes for research and clinical development.

5.7 Future Outlook

Advances during the past two decades indicate that ^{1}H-MRS could be of increasing importance as an adjunct tool to MRI in the future clinical care of BrCa. At the same time, the results of this study point to some of the inherent challenges within tumor biology associated with technological developments. If deeper insights into tumor metabolism can be achieved, advances in in-vivo tissue metabolite quantification might be able to substantially improve BrCa care.[175]

This experimental study used HRMAS ^{1}H-MRS, an ex-vivo high-resolution ^{1}H-MRS technique, to quantify metabolites in BrCa and normal benign breast tissue in order to get a deeper understanding of basic metabolic characteristics of tumors. Metabolite measurements were able to differentiate between different types of tumors, and between tumor and benign tissue. Meanwhile, tissue metabolite concentrations were highly variable, which could pose a challenge for the interpretation of high-resolution in-vivo metabolite data. Furthermore, one of the main hypotheses in this study, a correlation between tumor tissue Volume% and elevated tissue metabolite concentrations did not hold true. The answer to the question, of whether this result is irregular, or how strong this association might be, remains a prerequisite for the future clinical adoption of in-vivo ^{1}H-MRS. In conclusion, a better understanding of the basic mechanisms at work in tumor metabolism is needed to make sense of the information provided by technological advances.

As MRI technology advances, new possibilities in diagnostics and care are expected to evolve.[173] With increases in magnetic field strengths in clinical MR scanners, the availability of standardized and optimized receiving coils for breast MRI, improved pulse sequences and optimized shimming techniques, the SNR of in-vivo ^{1}H-MRS will likely increase in the future. Consequently, spectral and spatial resolutions of ^{1}H-MRS will grow, allowing for more detailed information.[27,176] Smaller lesions, such as lymph nodes and foci of a volume of $<5cm^3$ will be a possible subject of metabolite measurement in ^{1}H-MRS.[177] Metabolite measurements are also being discussed as the basis of individualized treatments for BrCa patients in the era of personalized medicine.[178,179] Further advances in metabolite measurements will consecutively require larger studies to evaluate the associated increases in diagnostic performance.

The hypotheses formulated in this study are a starting point in the development of a deeper understanding of tumor biology that could lead to potential improvements in the clinical care of BrCa. The question of whether and how these technological advances, which are yielding ever more detailed information about changes in tumor cells, will lead to improved patient care is the subject of ongoing research and remains to be answered in the future.

6 Bibliography

1. Jemal A, Siegel R, Ward E, et al. Cancer statistics, 2008. *CA: A Cancer Journal for Clinicians*. 2010;58(2):71-96. Available at: http://www.ncbi.nlm.nih.gov/pubmed/18287387.

2. Husmann G, Kaatsch P, Katalinic A, et al. *Krebs in Deutschland 2005/2006. Häufigkeiten und Trends.* 7th ed. Berlin: Robert Koch-Institut (Hrsg) und die Gesellschaft der epidemiologischen Krebsregister in Deutschland e.V. (Hrsg); 2010.

3. Haberland J, Bertz J, Wolf U. German cancer statistics 2004. *BMC Cancer*. 2010;10(52):1-10. Available at: http://www.biomedcentral.com/1471-2407/10/52.

4. Gøtzsche P, Nielsen M. Screening for breast cancer with mammography (Review). *The Cochrane Library*. 2009;(4).

5. Olivotto IA, Kan L, Coldman AJ. False positive rate of screening mammography. *The New England journal of medicine*. 1998;339(8):560, ff. Available at: http://www.ncbi.nlm.nih.gov/pubmed/9714619.

6. Nelson HD, Tyne K, Naik A, et al. Screening for Breast Cancer: An Update for the U.S. Preventive Services Task Force. *Annals of Internal Medicine Clinical Guidelines*. 2009;151(10):727 - 737.

7. Elmore JG, Barton MB, Moceri VM, et al. Ten-year risk of false positive screening mammograms and clinical breast examinations. *The New England journal of medicine*. 1998;338(16):1089-96. Available at: http://www.ncbi.nlm.nih.gov/pubmed/9545356.

8. Hofvind S, Thoresen S, Tretli S. The cumulative risk of a false-positive recall in the Norwegian Breast Cancer Screening Program. *Cancer*. 2004;101(7):1501-7. Available at: http://www.ncbi.nlm.nih.gov/pubmed/15378474.

9. Nelson HD, Tyne K, Naik A, et al. Screening for Breast Cancer: An Update for the U.S. Preventive Services Task Force. *Annals of Internal Medicine Clinical Guidelines*. 2009;151(10):727-37, W237-42. Available at: http://www.annals.org/cgi/content/abstract/151/10/727.

10. Rimer BK, Bluman LG. The psychosocial consequences of mammography. *Journal of the National Cancer Institute. Monographs*. 1997;(22):131-8. Available at: http://www.ncbi.nlm.nih.gov/pubmed/9709289.

11. Welch HG, Black WC. Overdiagnosis in cancer. *Journal of the National Cancer Institute*. 2010;102(9):605-13. Available at: http://www.ncbi.nlm.nih.gov/pubmed/20413742.

12. Kuhl CK. Breast MR imaging at 3T. *Magnetic Resonance Imaging Clinics of North America*. 2007;15(3):315-320.

13. Orel SG, Schnall MD. Imaging of the Breast for the Detection, Diagnosis, and Staging of Breast Cancer. *Radiology*. 2001;220:13-30.

14. Tozaki M. 1H MR Spectroscopy and Diffusion- Weighted Imaging of the Breast: Are They Useful Tools for Characterizing Breast Lesions Before Biopsy? *AJR Women's Imaging*. 2009;(September):840-849.

15. Sherif H. Peripheral washout sign on contrast-enhanced MR images of the breast. *Radiology*. 1997;205(1):209-13. Available at: http://www.ncbi.nlm.nih.gov/pubmed.

16. Orel SG, Schnall MD. MR Imaging of the Breast for the Detection, Diagnosis, and Staging of Breast Cancer. *Radiology*. 2001;220(1):13-30. Available at: http://www.ncbi.nlm.nih.gov/pubmed/11425968.

17. Daniel BL, Yen YF, Glover GH, et al. Breast disease: Dynamic spiral MR imaging. *Radiology*. 1998;209(2):499-509. Available at: http://www.ncbi.nlm.nih.gov/pubmed/9807580.

18. Heywang-Köbrunner SH. Contrast-enhanced MRI of the breast: accuracy, value, controversies, solutions. *European Journal of Radiology*. 1997;24(2):94-108. Available at: http://dx.doi.org/10.1016/S0720-048X(96)01142-4.

19. Kuhl CK, Mielcareck P, Klaschik S, et al. Dynamic breast MR imaging: are signal intensity time course data useful for differential diagnosis of enhancing lesions? *Radiology*. 1999;211(1):101-10. Available at: http://www.ncbi.nlm.nih.gov/pubmed/10189459.

20. Liberman L, Morris EA, Lee MJ-Y, et al. Breast Lesions Detected on MR Imaging: Features and Positive Predictive Value. *Am. J. Roentgenol.* 2002;179(1):171-178. Available at: http://www.ajronline.org/cgi/content/abstract/179/1/171.

21. Saslow D, Boetes C, Burke W, et al., for the American Cancer Society Breast Cancer Advisory Group,. American Cancer Society Guidelines for Breast Screening with MRI as an Adjunct to Mammography. *CA: A Cancer Journal for Clinicians*. 2007;57(2):75-89. Available at: http://caonline.amcancersoc.org/cgi/content/abstract/57/2/75.

22. Kriege M, Brekelmans CTM, Boetes C, et al. Efficacy of MRI and mammography for breast-cancer screening in women with a familial or genetic predisposition. *The New England journal of medicine*. 2004;351(5):427-37. Available at: http://www.ncbi.nlm.nih.gov/pubmed/15282350.

23. Warner E, Plewes DB, Hill K a, et al. Surveillance of BRCA1 and BRCA2 mutation carriers with magnetic resonance imaging, ultrasound, mammography, and clinical breast examination. *JAMA : the journal of the American Medical Association*. 2004;292(11):1317-25. Available at: http://www.ncbi.nlm.nih.gov/pubmed/15367553.

24. Jagannathan NR. Breast MR. *NMR in biomedicine*. 2009;22(1):1-2. Available at: http://www.ncbi.nlm.nih.gov/pubmed/19137539.

25. Sinha S, Sinha U. Recent advances in breast MRI and MRS. *NMR in biomedicine*. 2009;22(1):3-16. Available at: http://www.ncbi.nlm.nih.gov/pubmed/18654998.

26. Cecil KM, Schnall MD, Siegelman ES, et al. The evaluation of human breast lesions with magnetic resonance imaging and proton magnetic resonance spectroscopy. *Breast Cancer Res Treat*. 2001;68(1):45-54. Available at: http://www.ncbi.nlm.nih.gov/entrez/query.fcgi?cmd=Retrieve&db=PubMed&dopt=Citation&list_uids=11678308.

27. Stanwell P, Mountford CE. In vivo proton MR spectroscopy of the breast. *Radiographics : a review publication of the Radiological Society of North America, Inc*. 2007;27 Suppl 1:S253-66. Available at: http://www.ncbi.nlm.nih.gov/pubmed/18180231.

28. Sardanelli F, Fausto A, Di Leo G, et al. In vivo proton MR spectroscopy of the breast using the total choline peak integral as a marker of malignancy. *AJR Am J Roentgenol*. 2009;192(6):1608-1617. Available at: http://www.ncbi.nlm.nih.gov/entrez/query.fcgi?cmd=Retrieve&db=PubMed&dopt=Citation&list_uids=19457825.

29. Bolan PJ, Nelson MT, Yee D, et al Imaging in breast cancer: Magnetic resonance spectroscopy. *Breast Cancer Res*. 2005;7(4):149-152. Available at: http://www.ncbi.nlm.nih.gov/entrez/query.fcgi?cmd=Retrieve&db=PubMed&dopt=Citation&list_uids=15987466.

30. Roebuck JR, Cecil KM, Schnall MD, et al. Human breast lesions: characterization with proton MR spectroscopy. *Radiology*. 1998;209(1):269-75. Available at: http://www.ncbi.nlm.nih.gov/pubmed/9769842.

31. Yeung DK, Cheung HS, Tse GM. Human breast lesions: characterization with contrast-enhanced in vivo proton MR spectroscopy--initial results. *Radiology*. 2001;220(1):40-46. Available at: http://www.ncbi.nlm.nih.gov/entrez/query.fcgi?cmd=Retrieve&db=PubMed&dopt=Citation&list_uids=11425970.

32. Tse GM, Cheung HS, Pang L-M, et al. Characterization of lesions of the breast with proton MR spectroscopy: comparison of carcinomas, benign lesions, and phyllodes tumors. *AJR. American Journal of Roentgenology*. 2003;181(5):1267-72. Available at: http://www.ncbi.nlm.nih.gov/pubmed/14573418.

33. Kvistad KA, Bakken IJ, Gribbestad IS, et al. Characterization of neoplastic and normal human breast tissues with in vivo (1)H MR spectroscopy. *J Magn Reson Imaging*. 1999;10(2):159-164. Available at: http://www.ncbi.nlm.nih.gov/entrez/query.fcgi?cmd=Retrieve&db=PubMed&dopt=Citation&list_uids=10441019.

34. Stanwell P, Gluch L, Clark D, et al., Mountford CE. Specificity of choline metabolites for in vivo diagnosis of breast cancer using 1H MRS at 1.5 T. *European radiology*. 2005;15(5):1037-43. Available at: http://www.ncbi.nlm.nih.gov/pubmed/15351906.

35. Bartella L, Morris EA, Dershaw DD, et al. Proton MR Spectroscopy with Choline Peak as Malignancy Marker Improves Positive Predictive Value for Breast Cancer Diagnosis. 2006;239(3).

36. Bartella L, Thakur SB, Morris EA, et al. Enhancing nonmass lesions in the breast: evaluation with proton (1H) MR spectroscopy. *Radiology*. 2007;245(1):80-87. Available at: http://www.ncbi.nlm.nih.gov/entrez/query.fcgi?cmd=Retrieve&db=PubMed&dopt=Citation&list_uids=17885182.

37. Podo F. Tumour phospholipid metabolism. *NMR in biomedicine*. 1999;12(7):413-39. Available at: http://www.ncbi.nlm.nih.gov/pubmed/10654290.

38. Gibellini F, Smith TK. The Kennedy pathway-De novo synthesis of phosphatidylethanolamine and phosphatidylcholine. *IUBMB life*. 2010;62(6):414-28. Available at: http://www.ncbi.nlm.nih.gov/pubmed/20503434.

39. Aoyama C, Yamazaki N, Terada H, et al. Structure and characterization of the genes for murine choline/ethanolamine kinase isozymes alpha and beta. *J Lipid Res*. 2000;41(3):452-464. Available at: http://www.ncbi.nlm.nih.gov/entrez/query.fcgi?cmd=Retrieve&db=PubMed&dopt=Citation&list_uids=10706593.

40. Aoyama C, Liao H, Ishidate K. Structure and function of choline kinase isoforms in mammalian cells. *Prog Lipid Res*. 2004;43(3):266-281. Available at: http://www.ncbi.nlm.nih.gov/entrez/query.fcgi?cmd=Retrieve&db=PubMed&dopt=Citation&list_uids=15003397.

41. Cheng LL, Chang IW, Louis DN, et al. Correlation of high-resolution magic angle spinning proton magnetic resonance spectroscopy with histopathology of intact human brain tumor specimens. *Cancer Res*. 1998;58(9):1825-1832. Available at: http://www.ncbi.nlm.nih.gov/entrez/query.fcgi?cmd=Retrieve&db=PubMed&dopt=Citation&list_uids=9581820.

42. Eliyahu G, Kreizman T, Degani H. Phosphocholine as a biomarker of breast cancer: molecular and biochemical studies. *Int J Cancer*. 2007;120(8):1721-1730. Available at: http://www.ncbi.nlm.nih.gov/entrez/query.fcgi?cmd=Retrieve&db=PubMed&dopt=Citation&list_uids=17236204.

43. Glunde K, Jie C, Bhujwalla ZM. Molecular causes of the aberrant choline phospholipid metabolism in breast cancer. *Cancer Res*. 2004;64(12):4270-4276. Available at: http://www.ncbi.nlm.nih.gov/entrez/query.fcgi?cmd=Retrieve&db=PubMed&dopt=Citation&list_uids=15205341.

44. Bray F SR, Ferlay J, Parkin DM. Estimates of cancer incidence and mortality in Europe in 1995. *Eur J Cancer*. 2002;38(1):99-166. Available at: http://www.ncbi.nlm.nih.gov/pubmed.

45. Weiss JR, Moysich KB, Swede H. Epidemiology of Male Breast Cancer. *Biomarkers*. 2005;14(January):20-26.

46. Morimoto T, Komaki K, Inui K, et al. Involvement of nipple and areola in early breast cancer. *Cancer*. 1985;55(10):2459-2463. Available at: http://onlinelibrary.wiley.com/doi/10.1002/1097-0142(19850515)55:10<2459::AID-CNCR2820551025>3.0.CO;2-L/abstract.

47. Sakorafas GH, Blanchard K, Sarr MG, et al. Paget's disease of the breast. *Cancer treatment reviews*. 2001;27(1):9-18. Available at: http://www.ncbi.nlm.nih.gov/pubmed/11237774.

48. Baxter N. Preventive health care, 2001 update: should women be routinely taught breast self-examination to screen for breast cancer? *CMAJ : Canadian Medical Association journal = journal de l'Association medicale canadienne*. 2001;164(13):1837-46. Available at: http://www.cmaj.ca/cgi/content/full/164/13/1837.

49. Hackshaw AK, Paul EA. Breast self-examination and death from breast cancer: a meta-analysis. *British journal of cancer*. 2003;88(7):1047-53. Available at: http://www.pubmedcentral.nih.gov/articlerender.fcgi?artid=2376382&tool=pmcentrez&rendertype=abstract.

50. Barton MB, Harris R, Fletcher SW. The rational clinical examination. Does this patient have breast cancer? The screening clinical breast examination: should it be done? How? *JAMA : the journal of the American Medical Association*. 1999;282(13):1270-80. Available at: http://www.ncbi.nlm.nih.gov/pubmed/10517431.

51. Bobo JK, Lee NC, Thames SF. Findings from 752,081 clinical breast examinations reported to a national screening program from 1995 through 1998. *Journal of the National Cancer Institute*. 2000;92(12):971-6. Available at: http://www.ncbi.nlm.nih.gov/pubmed/10861308.

52. Humphrey L, Chan B, Detlefsen S, et al. Screening for Breast Cancer. *U.S. Preventive Services Task Force Evidence Syntheses, formerly Systematic Evidence Reviews*. 2002. Available at: http://www.ncbi.nlm.nih.gov/bookshelf/br.fcgi?book=es15.

53. Michaelson JS, Silverstein M, Sgroi D, et al. The effect of tumor size and lymph node status on breast carcinoma lethality. *Cancer*. 2003;98(10):2133-43. Available at: http://www.ncbi.nlm.nih.gov/pubmed/14601082.

54. Heywang-Köbrunner SH, Bock K, Mairs A, et al. Effect of population based screening on breast cancer mortality. *The Lancet*. 2011;378(9805):1775-1776.

55. Kerlikowske K, Grady D, Barclay J, et al. Positive predictive value of screening mammography by age and family history of breast cancer. *JAMA : the journal of the American Medical Association*. 1993;270(20):2444-50. Available at: http://www.ncbi.nlm.nih.gov/pubmed/8230621.

56. Fletcher SW, Black W, Harris R, et al. Report of the International Workshop on Screening for Breast Cancer. *Journal of the National Cancer Institute*. 1993;85(20):1644-56. Available at: http://www.ncbi.nlm.nih.gov/pubmed/8105098.

57. Mushlin AI, Kouides RW, Shapiro DE. Estimating the accuracy of screening mammography: a meta-analysis. *American journal of preventive medicine*. 1998;14(2):143-53. Available at: http://www.ncbi.nlm.nih.gov/pubmed/9631167.

58. Bick U. [Mammography screening in Germany: how, when and why?]. *RöFo : Fortschritte auf dem Gebiete der Röntgenstrahlen und der Nuklearmedizin*. 2006;178(10):957-69. Available at: http://www.ncbi.nlm.nih.gov/pubmed/17021975.

59. Diekmann S, Diekmann F. [Mammography screening in Germany]. *Der Radiologe*. 2008;48(1):17-25. Available at: http://www.ncbi.nlm.nih.gov/pubmed/18030441.

60. Nystrom L, Andersson I, Bjurstam N, et al. Long-term effects of mammography screening: updated overview of the Swedish randomised trials. *The Lancet*. 2002;359(9310):909-919. Available at: http://www.ncbi.nlm.nih.gov/pubmed/11918907.

61. Tabar L, Yen M, Vitak B, et al. Mammography service screening and mortality in breast cancer patients: 20-year follow-up before and after introduction of screening. *The Lancet*. 2003;361(9367):1405-1410. Available at: http://www.ncbi.nlm.nih.gov/pubmed/12727392.

62. Schulz-Wendtland R, Becker N, Bock K, et al. [Mammography screening]. *Der Radiologe*. 2007;47(4):359-69. Available at: http://www.ncbi.nlm.nih.gov/pubmed/17375277.

63. Silverstein MJ, Recht A, Lagios MD, et al. Special report: Consensus conference III. Image-detected breast cancer: state-of-the-art diagnosis and treatment. *Journal of the American*

College of Surgeons. 2009;209(4):504-20. Available at: http://www.ncbi.nlm.nih.gov/pubmed/19801324.

64. Moore SG, Shenoy PJ, Fanucchi L, et al. Cost-effectiveness of MRI compared to mammography for breast cancer screening in a high risk population. *BMC health services research*. 2009;9:9. Available at: http://www.pubmedcentral.nih.gov/articlerender.fcgi?artid=2630922&tool=pmcentrez&rendertype=abstract.

65. Sardanelli F, Boetes C, Borisch B, et al. Magnetic resonance imaging of the breast : Recommendations from the EUSOMA working group. *European Journal of Cancer*. 2010;6.

66. Mann RM, Kuhl CK, Kinkel K. Breast MRI: Guidelines from the European Society of Breast Imaging. *European radiology*. 2008;(18):1307-1318.

67. Lopez JK, Bassett LW. Invasive lobular carcinoma of the breast: spectrum of mammographic, US, and MR imaging findings. *Radiographics : a review publication of the Radiological Society of North America, Inc*. 2009;29(1):165-76. Available at: http://www.ncbi.nlm.nih.gov/pubmed/19168843.

68. Olson JA, Morris EA, Van Zee KJ, et al. Magnetic resonance imaging facilitates breast conservation for occult breast cancer. *Annals of surgical oncology*. 2000;7(6):411-5. Available at: http://www.ncbi.nlm.nih.gov/pubmed/10894136.

69. Dietzel M, Baltzer P, Vag T, et al. Magnetic Resonance Mammography of Invasive Lobular Versus Ductal Carcinoma: Systematic Comparison of 811 Patients Reveals High Diagnostic Accuracy Irrespective of Typing. *Journal of Computer Assisted Tomography*. 2010;34(4):587 - 595.

70. Dietzel M, Baltzer P, Vag T, et al. Differential diagnosis of breast lesions 5 mm or less: is there a role for magnetic resonance imaging? *Journal of Computer Assisted Tomography*. 2010;34(3):456 - 464.

71. Glunde K, Jacobs MA, Bhujwalla ZM. Choline metabolism in cancer: implications for diagnosis and therapy. *Expert Rev Mol Diagn*. 2006;6(6):821-829. Available at: http://www.ncbi.nlm.nih.gov/entrez/query.fcgi?cmd=Retrieve&db=PubMed&dopt=Citation&list_uids=17140369.

72. Huang W, Fisher PR, Dulaimy K, et al. Detection of breast malignancy: diagnostic MR protocol for improved specificity. *Radiology*. 2004;232(2):585-591. Available at: http://www.ncbi.nlm.nih.gov/entrez/query.fcgi?cmd=Retrieve&db=PubMed&dopt=Citation&list_uids=15205478.

73. Meisamy S, Bolan PJ, Baker EH, et al. Adding in vivo quantitative 1H MR spectroscopy to improve diagnostic accuracy of breast MR imaging: preliminary results of observer performance study at 4.0 T. *Radiology*. 2005;236(2):465-75. Available at: http://www.ncbi.nlm.nih.gov/pubmed/16040903.

74. Kumar M, Jagannathan NR, Seenu V, et al. Monitoring the therapeutic response of locally advanced breast cancer patients: sequential in vivo proton MR spectroscopy study. *J Magn Reson Imaging*. 2006;24(2):325-332. Available at: http://www.ncbi.nlm.nih.gov/entrez/query.fcgi?cmd=Retrieve&db=PubMed&dopt=Citation&list_uids=16786567.

75. Meisamy S, Bolan PJ, Baker EH, et al. Neoadjuvant chemotherapy of locally advanced breast cancer: predicting response with in vivo (1)H MR spectroscopy--a pilot study at 4 T. *Radiology*. 2004;233(2):424-431. Available at: http://www.ncbi.nlm.nih.gov/entrez/query.fcgi?cmd=Retrieve&db=PubMed&dopt=Citation&list_uids=15516615.

76. Manton DJ, Chaturvedi A, Hubbard A, et al. Neoadjuvant chemotherapy in breast cancer: early response prediction with quantitative MR imaging and spectroscopy. *Br J Cancer*. 2006;94(3):427-435. Available at: http://www.ncbi.nlm.nih.gov/entrez/query.fcgi?cmd=Retrieve&db=PubMed&dopt=Citation&list_uids=16465174.

77. Lenkinski RE, Wang X, Elian M, et al. Interaction of gadolinium-based MR contrast agents with choline: implications for MR spectroscopy (MRS) of the breast. *Magn Reson Med*. 2009;61(6):1286-1292. Available at: http://www.ncbi.nlm.nih.gov/entrez/query.fcgi?cmd=Retrieve&db=PubMed&dopt=Citation&list_uids=19365855.

78. Geraghty PR, Den Bosch MAAJ van, Spielman DM, et al. MRI and (1)H MRS of the breast: presence of a choline peak as malignancy marker is related to K21 value of the tumor in patients with invasive ductal carcinoma. *The breast journal*. 2008;14(6):574-80. Available at: http://www.ncbi.nlm.nih.gov/pubmed/19000051.

79. Zeisel SH. Choline: an essential nutrient for humans. *Nutrition*. 2000;16(7-8):669-71. Available at: http://www.ncbi.nlm.nih.gov/pubmed/10906592.

80. Zeisel SH, Costa KA. Choline: an essential nutrient for public health. *Nutr Rev*. 2009;67(11):615-623. Available at: http://www.ncbi.nlm.nih.gov/entrez/query.fcgi?cmd=Retrieve&db=PubMed&dopt=Citation&list_uids=19906248.

81. Koepsell H, Endou H. The SLC22 drug transporter family. *Pflügers Archiv*. 2004;447(5):666-76. Available at: http://www.ncbi.nlm.nih.gov/pubmed/12883891.

82. Koepsell H, Schmitt BM, Gorboulev V. Organic cation transporters. *Reviews of physiology, biochemistry and pharmacology*. 2003;150:36-90. Available at: http://www.ncbi.nlm.nih.gov/pubmed/12827517.

83. Vance JE, Vance DE. Phospholipid biosynthesis in mammalian cells. *Biochemistry and cell biology = Biochimie et biologie cellulaire*. 2004;82(1):113-28. Available at: http://www.ncbi.nlm.nih.gov/pubmed/15052332.

84. NCBI. CHKA choline kinase alpha [Homo sapiens]. *NCBI Entrez Gene Bank*. 2010. Available at: http://www.ncbi.nlm.nih.gov/gene/1119.

85. NCBI. CHKB choline kinase beta [Homo sapiens]. *NCBI Entrez Gene Bank*. 2010. Available at: http://www.ncbi.nlm.nih.gov/gene/1120.

86. Yamazaki N, Shinohara Y, Kajimoto K, et al. Novel expression of equivocal messages containing both regions of choline/ethanolamine kinase and muscle type carnitine palmitoyltransferase I. *J Biol Chem*. 2000;275(41):31739-31746. Available at: http://www.ncbi.nlm.nih.gov/entrez/query.fcgi?cmd=Retrieve&db=PubMed&dopt=Citation&list_uids=10918069.

87. Glunde K, Bhujwalla ZM. Choline kinase alpha in cancer prognosis and treatment. *The lancet oncology*. 2007;8(10):855-7. Available at: http://www.ncbi.nlm.nih.gov/pubmed/17913651.

88. Rohlfs EM, Garner SC, Mar M-H, et al. Glycerophosphocholine and Phosphocholine Are the Major Choline Metabolites in Rat Milk. *J. Nutr.* 1993;123(10):1762-1768. Available at: http://jn.nutrition.org/cgi/content/abstract/123/10/1762.

89. Gribbestad IS, Fjösne HE, Haugen OA, et al. In vitro proton NMR spectroscopy of extracts from human breast tumours and non-involved breast tissue. *Anticancer research*. 1993;13(6A):1973-80. Available at: http://www.ncbi.nlm.nih.gov/pubmed/8297103.

90. Katz-Brull R, Lavin PT, Lenkinski RE. Clinical utility of proton magnetic resonance spectroscopy in characterizing breast lesions. *J Natl Cancer Inst*. 2002;94(16):1197-1203. Available at: http://www.ncbi.nlm.nih.gov/entrez/query.fcgi?cmd=Retrieve&db=PubMed&dopt=Citation&list_uids=12189222.

91. Lean C, Doran S, Somorjai RL, et al., Mountford CE. Determination of grade and receptor status from the primary breast lesion by magnetic resonance spectroscopy. *Technology in cancer research & treatment*. 2004;3(6):551-6. Available at: http://www.ncbi.nlm.nih.gov/pubmed/15560712.

92. Mountford CE. Diagnosis and prognosis of breast cancer by magnetic resonance spectroscopy of fine-needle aspirates analysed using a statistical classification strategy. *The british journal of surgery*. 2009;22(1):114-127. Available at: http://www.ncbi.nlm.nih.gov/pubmed.

93. Mackinnon WB, Barry PA, Malycha PL, et al., Mountford CE. Fine-needle biopsy specimens of benign breast lesions distinguished from invasive cancer ex vivo with proton MR spectroscopy. *Radiology*. 1997;204(3):661-6. Available at: http://www.ncbi.nlm.nih.gov/pubmed/9280241.

94. Ramirez de Molina A, Gutiérrez R, Ramos MA, et al. Increased choline kinase activity in human breast carcinomas: clinical evidence for a potential novel antitumor strategy. *Oncogene*. 2002;21(27):4317-22. Available at: http://www.ncbi.nlm.nih.gov/pubmed/12082619.

95. Cheng LL, Chang IW, Smith BL,et al. Evaluating human breast ductal carcinomas with high-resolution magic-angle spinning proton magnetic resonance spectroscopy. *J Magn Reson*. 1998;135(1):194-202. Available at: http://www.ncbi.nlm.nih.gov/entrez/query.fcgi?cmd=Retrieve&db=PubMed&dopt=Citation&list_uids=9799694.

96. Sitter B, Sonnewald U, Spraul M, et al. High-resolution magic angle spinning MRS of breast cancer tissue. *NMR in biomedicine*. 2002;15(5):327-37. Available at: http://www.ncbi.nlm.nih.gov/pubmed/12203224.

97. Sitter B, Lundgren S, Bathen TF, et al. Comparison of HR MAS MR spectroscopic profiles of breast cancer tissue with clinical parameters. *NMR in biomedicine*. 2006;19(1):30-40. Available at: http://www.ncbi.nlm.nih.gov/pubmed/16229059.

98. Sitter B, Bathen TF, Singstad TE, et al. Quantification of metabolites in breast cancer patients with different clinical prognosis using HR MAS MR spectroscopy. *NMR in biomedicine*. 2010;(June 2009). Available at: http://www.ncbi.nlm.nih.gov/pubmed/20101607.

99. Aboagye EO, Bhujwalla ZM. Malignant transformation alters membrane choline phospholipid metabolism of human mammary epithelial cells. *Cancer Res*. 1999;59(1):80-84. Available at: http://www.ncbi.nlm.nih.gov/entrez/query.fcgi?cmd=Retrieve&db=PubMed&dopt=Citation&list_uids=9892190.

100. Ronen SM, Jackson LE, Beloueche M, et al. Magnetic resonance detects changes in phosphocholine associated with Ras activation and inhibition in NIH 3T3 cells. *British journal of cancer*. 2001;84(5):691-6. Available at: http://www.pubmedcentral.nih.gov/articlerender.fcgi?artid=2363797&tool=pmcentrez&rendertype=abstract.

101. Bhujwalla ZM, Aboagye EO, Gillies RJ, et al. Nm23-transfected MDA-mB-435 human breast carcinoma cells form tumors with altered phospholipid metabolism and pH: A31P nuclear magnetic resonance study in vivo and in vitro. *Magnetic Resonance in Medicine*. 1999;41(5):897-903. Available at: http://onlinelibrary.wiley.com/doi/10.1002/(SICI)1522-2594(199905)41:5<897::AID-MRM7>3.0.CO;2-T/abstract.

102. Ronen SM, Rushkin E, Degani H. Lipid metabolism in large T47D human breast cancer spheroids: 31P- and 13C-NMR studies of choline and ethanolamine uptake. *Biochimica et biophysica acta*. 1992;1138(3):203-12. Available at: http://www.ncbi.nlm.nih.gov/pubmed/1547282.

103. Katz-Brull R, Degani H. Kinetics of choline transport and phosphorylation in human breast cancer cells; NMR application of the zero trans method. *Anticancer Research*. 1996;16(3B):1375-80. Available at: http://www.ncbi.nlm.nih.gov/pubmed.

104. Glunde K, Raman V, Mori N, et al. RNA interference-mediated choline kinase suppression in breast cancer cells induces differentiation and reduces proliferation. *Cancer research*. 2005;65(23):11034-43. Available at: http://www.ncbi.nlm.nih.gov/pubmed/16322253.

105. Ramirez De Molina A, Banez-Coronel M, Gutierrez R, et al. Choline kinase activation is a critical requirement for the proliferation of primary human mammary epithelial cells and breast tumor progression. *Cancer Res*. 2004;64(18):6732-6739. Available at: http://www.ncbi.nlm.nih.gov/entrez/query.fcgi?cmd=Retrieve&db=PubMed&dopt=Citation&list_uids=15374991.

106. Glunde K, Ackerstaff E, Mori N, et al. Choline phospholipid metabolism in cancer: consequences for molecular pharmaceutical interventions. *Mol Pharm*. 2006;3(5):496-506. Available at: http://www.ncbi.nlm.nih.gov/entrez/query.fcgi?cmd=Retrieve&db=PubMed&dopt=Citation&list_uids=17009848.

107. Rodriguez-Gonzalez A, Ramirez de Molina A, Benitez-Rajal J, et al. Phospholipase D and choline kinase: their role in cancer development and their potential as drug targets. *Prog Cell Cycle Res*. 2003;5:191-201. Available at: http://www.ncbi.nlm.nih.gov/entrez/query.fcgi?cmd=Retrieve&db=PubMed&dopt=Citation&list_uids=14593713.

108. Hernandez-Alcoceba R, Fernandez F, Lacal JC. In vivo antitumor activity of choline kinase inhibitors: a novel target for anticancer drug discovery. *Cancer Res*. 1999;59(13):3112-3118. Available at:

http://www.ncbi.nlm.nih.gov/entrez/query.fcgi?cmd=Retrieve&db=PubMed&dopt=Citation&list_uids=10397253.

109. Ramirez De Molina A, Gallego-Ortega D, Sarmentero-Estrada J, et al. Choline kinase as a link connecting phospholipid metabolism and cell cycle regulation: implications in cancer therapy. *The international journal of biochemistry & cell biology*. 2008;40(9):1753-63. Available at: http://www.ncbi.nlm.nih.gov/pubmed/18296102.

110. Janardhan S, Srivani P, Sastry GN. Choline kinase: an important target for cancer. *Curr Med Chem*. 2006;13(10):1169-1186. Available at: http://www.ncbi.nlm.nih.gov/entrez/query.fcgi?cmd=Retrieve&db=PubMed&dopt=Citation&list_uids=16719778.

111. Mori N, Glunde K, Takagi T, et al. Choline kinase down-regulation increases the effect of 5-fluorouracil in breast cancer cells. *Cancer research*. 2007;67(23):11284-90. Available at: http://www.ncbi.nlm.nih.gov/pubmed/18056454.

112. Bernhard Blümich. *Essential NMR*. 1st ed. Berlin: Springer; 2005:1-15.

113. Mazzola EP, Joseph BL, Holland LN. *Nuclear Magnetic Resonance Spectroscopy: An Introduction to Principles, Applications, and Experimental Methods.* 1st ed. Upper Saddle River: Prentice Hall; 2003.

114. Hendee WR, Ritenour ER. Medical imaging physics. In: *Medical imaging physics*. 4th ed. John Wiley & Sons; 2002:355 - 365.

115. Hesse M, Meier H, Zeeh B. *Spektroskopische Methoden in der organischen Chemie*. 7th ed. Stuttgart: Thieme; 2007:74 - 293.

116. Govindaraju V, Young K, Maudsley AA. Proton NMR chemical shifts and coupling constants for brain metabolites. *NMR in biomedicine*. 2000;13(3):129-53. Available at: http://www.ncbi.nlm.nih.gov/pubmed/10861994.

117. Cheng LL, Chang IW, Smith BL, et al. Evaluating human breast ductal carcinomas with high-resolution magic-angle spinning proton magnetic resonance spectroscopy. *J Magn Reson*. 1998;135(1):194-202. Available at: http://www.ncbi.nlm.nih.gov/entrez/query.fcgi?cmd=Retrieve&db=PubMed&dopt=Citation&list_uids=9799694.

118. Ratai EM, Pilkenton S, Lentz MR, et al. Comparisons of brain metabolites observed by HRMAS 1H NMR of intact tissue and solution 1H NMR of tissue extracts in SIV-infected macaques. *NMR Biomed*. 2005;18(4):242-251. Available at: http://www.ncbi.nlm.nih.gov/entrez/query.fcgi?cmd=Retrieve&db=PubMed&dopt=Citation&list_uids=15759297.

119. Cheng LL, Burns MA, Taylor JL, et al. Metabolic characterization of human prostate cancer with tissue magnetic resonance spectroscopy. *Cancer Res*. 2005;65(8):3030-3034. Available at: http://www.ncbi.nlm.nih.gov/entrez/query.fcgi?cmd=Retrieve&db=PubMed&dopt=Citation&list_uids=15833828.

120. Jordan KW, Adkins CB, Su L, et al. Comparison of squamous cell carcinoma and adenocarcinoma of the lung by metabolomic analysis of tissue-serum pairs. *Lung cancer (Amsterdam, Netherlands)*. 2009. Available at: http://www.ncbi.nlm.nih.gov/pubmed/19559498.

121. Cheng LL, Newell K, Mallory AE. Quantification of neurons in Alzheimer and control brains with ex vivo high resolution magic angle spinning proton magnetic resonance spectroscopy and stereology. *Magn Reson Imaging*. 2002;20(7):527-533. Available at: http://www.ncbi.nlm.nih.gov/entrez/query.fcgi?cmd=Retrieve&db=PubMed&dopt=Citation&list_uids=12413598.

122. Cheng LL, Ma MJ, Becerra L, et al. Quantitative neuropathology by high resolution magic angle spinning proton magnetic resonance spectroscopy. *Proceedings of the National Academy of Sciences of the United States of America*. 1997;94(12):6408-13. Available at: http://www.pubmedcentral.nih.gov/articlerender.fcgi?artid=21063&tool=pmcentrez&rendertype=abstract.

123. Johnson MC. Anatomy and Physiology of the Breast. In: *Management of Breast Disease*. 1st ed. Berlin: Springer; 2010:1-26.

124. Bae YK, Gabrielson EW. Premalignant and Malignant Breast Pathology. In: *Management of Breast Disease*. 1st ed. New York: Springer; 2010:169 - 180.

125. Newman LA, Hayes DF. Evidence-Based Management of Breast Cancer. In: *Oncology: An Evidence-Based Approach*. 1st ed. Berlin: Springer; 2006:951-982.

126. Newcomb PA, Wernli KJ. Risk Factors. In: *Breast Cancer Risk Reduction and Early Detection*. Vol 1. 1st ed. Berlin: Springer; 2010:3 - 23.

127. Hall JM, Lee MK, Newman B, et al. Linkage of early-onset familial breast cancer to chromosome 17q21. *Science (New York, N.Y.)*. 1990;250(4988):1684-9. Available at: http://www.ncbi.nlm.nih.gov/pubmed/2270482.

128. Yang X, Lippman ME. BRCA1 and BRCA2 in breast cancer. *Breast cancer research and treatment*. 1999;54(1):1-10. Available at: http://www.ncbi.nlm.nih.gov/pubmed/10369075.

129. Suter R, Marcum JA. The molecular genetics of breast cancer and targeted therapy. *Biologics : targets & therapy*. 2007;1(3):241-58. Available at: http://www.pubmedcentral.nih.gov/articlerender.fcgi?artid=2721311&tool=pmcentrez&rendertype=abstract.

130. Ferretti G, Felici A, Papaldo P, et al. HER2/neu role in breast cancer: from a prognostic foe to a predictive friend. *Current opinion in obstetrics & gynecology*. 2007;19(1):56-62. Available at: http://www.ncbi.nlm.nih.gov/pubmed/17218853.

131. Barros FFT, Powe DG, Ellis IO, et al. Understanding the HER family in breast cancer: interaction with ligands, dimerization and treatments. *Histopathology*. 2010;56(5):560-72. Available at: http://www.ncbi.nlm.nih.gov/pubmed/20459566.

132. Lurje G, Lenz H-J. EGFR signaling and drug discovery. *Oncology*. 2009;77(6):400-410. Available at: http://www.ncbi.nlm.nih.gov/pubmed/20130423.

133. Chen Y, Olopade OI. MYC in breast tumor progression. *Expert review of anticancer therapy*. 2008;8(10):1689-98. Available at: http://www.ncbi.nlm.nih.gov/pubmed/18925859.

134. Berx G, Van Roy F. The E-cadherin/catenin complex: an important gatekeeper in breast cancer tumorigenesis and malignant progression. *Breast cancer research : BCR*. 2001;3(5):289-93. Available at:

http://www.pubmedcentral.nih.gov/articlerender.fcgi?artid=138690&tool=pmcentrez&rendertype=abstract.

135. Caldeira JRF, Prando EC, Quevedo FC, et al. CDH1 promoter hypermethylation and E-cadherin protein expression in infiltrating breast cancer. *BMC cancer*. 2006;6:48. Available at: http://www.pubmedcentral.nih.gov/articlerender.fcgi?artid=1523210&tool=pmcentrez&rendertype=abstract.

136. Cuny M, Kramar A, Courjal F, et al. Relating genotype and phenotype in breast cancer: an analysis of the prognostic significance of amplification at eight different genes or loci and of p53 mutations. *Cancer research*. 2000;60(4):1077-83. Available at: http://www.ncbi.nlm.nih.gov/pubmed/10706127.

137. Sommer S, Fuqua SA. Estrogen receptor and breast cancer. *Seminars in cancer biology*. 2001;11(5):339-52. Available at: http://www.ncbi.nlm.nih.gov/pubmed/11562176.

138. Anon F. The world Health Organization Histological Typing of Breast Tumors--Second Edition. The World Organization. *American journal of clinical pathology*. 1982;78(6):806-16. Available at: http://www.ncbi.nlm.nih.gov/pubmed/7148748.

139. Stenkvist B, Bengtsson E, Eriksson O, et al. Histopathological systems of breast cancer classification: reproducibility and clinical significance. *Journal of clinical pathology*. 1983;36(4):392-8. Available at: http://www.pubmedcentral.nih.gov/articlerender.fcgi?artid=498233&tool=pmcentrez&rendertype=abstract.

140. Singletary SE. Revision of the American Joint Committee on Cancer Staging System for Breast Cancer. *Journal of Clinical Oncology*. 2002;20(17):3628-3636. Available at: http://jco.ascopubs.org/cgi/content/abstract/20/17/3628.

141. Fu KL, Fu YS, Basett LW, et al. Invasive Malignancies. In: *Diagnosis of Diseases of the Breast*. 2nd ed. Philadelphia: Elsevier Saunders; 2005:438 - 518.

142. Sobin LH, Gospodarowicz M, Wittekind C (eds). Breast Tumors. In: *TNM Classification of Malignant Tumours*. 7th ed. Hoboken: Blackwell-Wiley; 2010:181 - 193.

143. Lee AHS, Ellis IO. The Nottingham prognostic index for invasive carcinoma of the breast. *Pathology oncology research*. 2008;14(2):113-5. Available at: http://www.ncbi.nlm.nih.gov/pubmed/18543079.

144. Mansel RE. Surgical Management of Patients with Metastatic Breast Cancer. In: *Metastasis of Breast Cancer*. 1st ed. Dordrecht: Springer; 2008:355-362. Available at: http://books.google.com/books?id=14pb5b6gT-oC&pgis=1.

145. Molina R. Tumor Markers in Bresast Cancer. In: *Tumor Markers: Physiology, Pathobiology, Technology, and Clinical Applications*. 1st ed. Wahington, DC: Amer. Assoc. for Clinical Chemistry; 2002:165-177. Available at: http://books.google.com/books?id=qwJHDfXMozUC&pgis=1.

146. Fisher B, Anderson S, Bryant J, et al. Twenty-year follow-up of a randomized trial comparing total mastectomy, lumpectomy, and lumpectomy plus irradiation for the treatment of invasive breast cancer. *The New England journal of medicine*. 2002;347(16):1233-41. Available at: http://www.ncbi.nlm.nih.gov/pubmed/12393820.

147. Fisher B, Jeong J-H, Anderson S, et al. Twenty-five-year follow-up of a randomized trial comparing radical mastectomy, total mastectomy, and total mastectomy followed by irradiation. *The New England journal of medicine*. 2002;347(8):567-75. Available at: http://www.ncbi.nlm.nih.gov/pubmed/12192016.

148. Krag D, Weaver D, Ashikaga T, et al. The sentinel node in breast cancer--a multicenter validation study. *The New England journal of medicine*. 1998;339(14):941-6. Available at: http://www.ncbi.nlm.nih.gov/pubmed/9753708.

149. Veronesi U, Paganelli G, Viale G, et al. A randomized comparison of sentinel-node biopsy with routine axillary dissection in breast cancer. *The New England journal of medicine*. 2003;349(6):546-53. Available at: http://www.ncbi.nlm.nih.gov/pubmed/12904519.

150. Barone JE, Tucker JB, Perez JM, et al. Evidence-based medicine applied to sentinel lymph node biopsy in patients with breast cancer. *The American surgeon*. 2005;71(1):66-70. Available at: http://www.ncbi.nlm.nih.gov/pubmed/15757061.

151. Liu SV, Melstrom L, Yao K, et al. Neoadjuvant therapy for breast cancer. *Journal of surgical oncology*. 2010;101(4):283-91. Available at: http://www.ncbi.nlm.nih.gov/pubmed/20187061.

152. Jordan KW, He W, Halpern EF, et al. Evaluation of Tissue Metabolites with High Resolution Magic Angle Spinning MR Spectroscopy Human Prostate Samples After Three-Year Storage at -80 degrees C. *Biomark Insights*. 2007;2:147-154. Available at: http://www.ncbi.nlm.nih.gov/entrez/query.fcgi?cmd=Retrieve&db=PubMed&dopt=Citation&list_uids=19662199.

153. Bourne R, Dzendrowskyj T, Mountford C. Leakage of metabolites from tissue biopsies can result in large errors in quantitation by MRS. *NMR in biomedicine*. 2003;16(2):96-101. Available at: http://www.ncbi.nlm.nih.gov/pubmed/12730950.

154. Middleton DA, Bradley DP, Connor SC, et al. The effect of sample freezing on proton magic-angle spinning NMR spectra of biological tissue. *Magnetic Resonance in Medicine.* 1998;40(1):166-9. Available at: http://www.ncbi.nlm.nih.gov/pubmed/9660567.

155. Cheng LL, Lean CL, Bogdanova A, et al. Enhanced resolution of proton NMR spectra of malignant lymph nodes using magic-angle spinning. *Magnetic Resonance in Medicine.* 1996;36(5):653-8. Available at: http://www.ncbi.nlm.nih.gov/pubmed/8916014.

156. Espina V, Wulfkuhle JD, Calvert VS, et al. Laser-capture microdissection. *Nature protocols*. 2006;1(2):586-603. Available at: http://www.ncbi.nlm.nih.gov/pubmed/17406286.

157. Rozen S, Skaletsky HJ. Primer3 on the WWW for general users and for biologist programmers. In: *Bioinformatics Methods and Protocols: Methods in Molecular Biology*. Totowa, NJ: Humana Press; 2000:365-386.

158. Untergasser A, Nijveen H, Rao X, et al. Primer3Plus, an enhanced web interface to Primer3. *Nucleic Acids Research*. 2007;35:W71-W74.

159. Livak KJ, Schmittgen TD. Analysis of relative gene expression data using real-time quantitative PCR and the 2(-Delta Delta C(T)) Method. *Methods*. 2001;25(4):402-8. Available at: http://www.ncbi.nlm.nih.gov/pubmed/11846609.

160. Lekanne Deprez R. Sensitivity and accuracy of quantitative real-time polymerase chain reaction using SYBR green I depends on cDNA synthesis conditions. *Analytical Biochemistry*. 2002;307(1):63-69. Available at: http://dx.doi.org/10.1016/S0003-2697(02)00021-0.

161. Schmittgen TD, Zakrajsek BA. Effect of experimental treatment on housekeeping gene expression: validation by real-time, quantitative RT-PCR. *J Biochem Biophys Methods*. 2000;46(1-2):69-81. Available at: http://www.ncbi.nlm.nih.gov/entrez/query.fcgi?cmd=Retrieve&db=PubMed&dopt=Citation&list_uids=11086195.

162. Rutledge RG. Sigmoidal curve-fitting redefines quantitative real-time PCR with the prospective of developing automated high-throughput applications. *Nucleic acids research*. 2004;32(22):e178. Available at: http://www.ncbi.nlm.nih.gov/pubmed/15601990.

163. Liu W, Saint DA. Validation of a quantitative method for real time PCR kinetics. *Biochemical and Biophysical Research Communications*. 2002;294:347-353.

164. Bolan PJ, Meisamy S, Baker EH, et al. In vivo quantification of choline compounds in the breast with 1H MR spectroscopy. *Magn Reson Med*. 2003;50(6):1134-1143. Available at: http://www.ncbi.nlm.nih.gov/entrez/query.fcgi?cmd=Retrieve&db=PubMed&dopt=Citation&list_uids=14648561.

165. Corum CA, McIntosh AD, Bolan PJ, et al. Feasibility of single-voxel MRS measurement of apparent diffusion coefficient of water in breast tumors. *Magn Reson Med*. 2009;61(5):1232-1237. Available at: http://www.ncbi.nlm.nih.gov/entrez/query.fcgi?cmd=Retrieve&db=PubMed&dopt=Citation&list_uids=19235916.

166. Krishnamachary B, Glunde K, Wildes F, et al. Noninvasive detection of lentiviral-mediated choline kinase targeting in a human breast cancer xenograft. *Cancer Res*. 2009;69(8):3464-3471. Available at: http://www.ncbi.nlm.nih.gov/entrez/query.fcgi?cmd=Retrieve&db=PubMed&dopt=Citation&list_uids=19336572.

167. Gutie R, Olmeda D, Lacal JC. Choline Kinase Activation Is a Critical Requirement for the Proliferation of Primary Human Mammary Epithelial Cells and Breast Tumor Progression. *Analysis*. 2004;5:6732- 6739.

168. Taylor JL, Wu CL, Cory D, et al. High-resolution magic angle spinning proton NMR analysis of human prostate tissue with slow spinning rates. *Magn Reson Med*. 2003;50(3):627-632. Available at: http://www.ncbi.nlm.nih.gov/entrez/query.fcgi?cmd=Retrieve&db=PubMed&dopt=Citation&list_uids=12939772.

169. Espina V, Heiby M, Pierobon M, et al. Laser capture microdissection technology. *Expert review of molecular diagnostics*. 2007;7(5):647-57. Available at: http://www.ncbi.nlm.nih.gov/pubmed/17892370.

170. Swillens S, Dessars B, Housni HE. Revisiting the sigmoidal curve fitting applied to quantitative real-time PCR data. *Analytical biochemistry*. 2008;373(2):370-6. Available at: http://www.ncbi.nlm.nih.gov/pubmed/17996715.

171. Ramirez de Molina A, Rodriguez-Gonzalez A, Lacal JC. From Ras signalling to ChoK inhibitors: a further advance in anticancer drug design. *Cancer Lett*. 2004;206(2):137-148. Available at: http://www.ncbi.nlm.nih.gov/entrez/query.fcgi?cmd=Retrieve&db=PubMed&dopt=Citation&list_uids=15013519.

172. Hernandez-Alcoceba R, Saniger L, Campos J, et al. Choline kinase inhibitors as a novel approach for antiproliferative drug design. *Oncogene*. 1997;15(19):2289-2301. Available at: http://www.ncbi.nlm.nih.gov/entrez/query.fcgi?cmd=Retrieve&db=PubMed&dopt=Citation&list_uids=9393874.

173. Haddadin IS, McIntosh A, Meisamy S, et al. Metabolite quantification and high-field MRS in breast cancer. *NMR Biomed*. 2009;22(1):65-76. Available at: http://www.ncbi.nlm.nih.gov/entrez/query.fcgi?cmd=Retrieve&db=PubMed&dopt=Citation&list_uids=17957820.

174. Ramadan S, Stanwell P, Malycha P, et al. Proton MRS of the breast in the clinical setting. *NMR Biomed*. 2009;22(1):54-64. Available at: http://www.ncbi.nlm.nih.gov/entrez/query.fcgi?cmd=Retrieve&db=PubMed&dopt=Citation&list_uids=19086012.

175. Karellas A, Vedantham S. Breast cancer imaging: A perspective for the next decade. *Medical Physics*. 2008;35(11):4878-97. Available at: http://link.aip.org/link/MPHYA6/v35/i11/p4878/s1&Agg=doi.

176. Klomp DWJ, De Bank B van, Raaijmakers A, et al. 31P MRSI and 1H MRS at 7T: Initial results in human breast cancer. *NMR in biomedicine*. 2011;24(10):1337-42.

177. Morse DL, Carroll D, Day S, et al. Characterization of breast cancers and therapy response by MRS and quantitative gene expression profiling in the choline pathway. *NMR Biomed*. 2009;22(1):114-127. Available at: http://www.ncbi.nlm.nih.gov/entrez/query.fcgi?cmd=Retrieve&db=PubMed&dopt=Citation&list_uids=19016452.

178. Bathen TF, Sitter B, Sjøbakk TE, et al. Magnetic Resonance Metabolomics of Intact Tissue : A Biotechnological Tool in Cancer Diagnostics and Treatment Evaluation. *Cancer Research*. 2010;70(17):6692-6696.

179. Sijens PE, Dorrius MD, Kappert P, et al. Quantitative multivoxel proton chemical shift imaging of the breast. *Magnetic resonance imaging*. 2010:1-6. Available at: http://www.ncbi.nlm.nih.gov/pubmed/20071119.

7 Acknowledgements

It is my great pleasure to thank everyone who supported me in writing this dissertation:

First of all, I would like to especially thank Prof. Dr. med. Matthias Taupitz from the Institute for Radiology at Charité - Universitätsmedizin Berlin for enabling this work. Next, I would like to express my special gratitude to Professor Leo L. Cheng, PhD, Massachusetts General Hospital, Harvard Medical School for supervising this project with good guidance and continuous encouragement. Moreover, I would like to thank Margaret Lentz, PhD for her excellent help in planning and troubleshooting experiments, as well as Hyun Kim, Vallent Lee, and Christen Adkins for their help in organization of experiments. Furthermore, I would like to thank Prof. Dr. med. Carsten Denkert from the Institute of Pathology at Charité – Universitätsmedizin Berlin, as well as Polly Dhond PhD, Randall Peterson, PhD, Zaver Bhujwalla, PhD, Kristine Glunde, PhD, and Hadassa Degani, PhD, for productive discussions.

Finally, I would like to express my special thanks to my family, who made this work possible supported me extraordinarily along the way.

8 Curriculum Vitae

Mein Lebenslauf wird aus datenschutzrechtlichen Gründen in der elektronischen Version meiner Arbeit nicht veröffentlicht.

Due to data privacy, my curriculum vitae will not be published in the electronic version of my work.

9 Eidesstattliche Erklärung

Eidesstattliche Versicherung

„Ich, Sebastian Herberger, versichere an Eides statt durch meine eigenhändige Unterschrift, dass ich die vorgelegte Dissertation mit dem Thema „Choline Metabolism and Choline Kinase Gene Expression in Human Breast Cancer“ selbstständig und ohne nicht offengelegte Hilfe Dritter verfasst und keine anderen als die angegebenen Quellen und Hilfsmittel genutzt habe.
Alle Stellen, die wörtlich oder dem Sinne nach auf Publikationen oder Vorträgen anderer Autoren beruhen, sind als solche in korrekter Zitierung (siehe „Uniform Requirements for Manuscripts (URM)“ des ICMJE -*www.**icmje**.org*) kenntlich gemacht. Die Abschnitte zu Methodik (insbesondere praktische Arbeiten, Laborbestimmungen, statistische Aufarbeitung) und Resultaten (insbesondere Abbildungen, Graphiken und Tabellen) entsprechen den URM (s.o) und werden von mir verantwortet.
Meine Anteile an etwaigen Publikationen zu dieser Dissertation entsprechen denen, die in der untenstehenden gemeinsamen Erklärung mit dem/der Betreuer/in, angegeben sind. Sämtliche Publikationen, die aus dieser Dissertation hervorgegangen sind und bei denen ich Autor bin, entsprechen den URM (s.o) und werden von mir verantwortet.

Die Bedeutung dieser eidesstattlichen Versicherung und die strafrechtlichen Folgen einer unwahren eidesstattlichen Versicherung (§156,161 des Strafgesetzbuches) sind mir bekannt und bewusst.

Datum Unterschrift

10 Publikationsliste

Anteilserklärung an etwaigen erfolgten Publikationen

Sebastian Herberger hatte folgenden Anteil an den folgenden Publikationen:

Herberger, S.D., Kaul D., Adkins, C.B., Smith B.L., Cheng, L.L., Lentz, M.R., Brachtel, E.F.
A Glimpse into Tumor Metabolism by Magnetic Resonance Spectroscopy: Choline Compounds and Choline Kinase Gene Expression in Human Breast Cancer. *Modern Pathology* 22 (S1): 46A, 2009

Beitrag im Einzelnen: Experimentelle Planung und Durchführung, Verfassung, Präsentation

Herberger, S.D., Taupitz, M., Cheng, L.L., Brachtel, E.F., Lentz, M.R.
A Glimpse into Tumor Metabolism: High Field-NMR-Spectroscopy of Choline Compounds and Choline Kinase-α Gene Expression in Human Breast Cancer. *Der Pathologe*; Supplement 1-2009

Beitrag im Einzelnen: Experimentelle Planung und Durchführung, Verfassung, Präsentation

Unterschrift, Datum und Stempel des betreuenden Hochschullehrers/der betreuenden Hochschullehrerin

Unterschrift des Doktoranden/der Doktorandin